

Budget of nitrous acid (HONO) ~~and its impacts on atmospheric oxidation capacity~~ at an urban site in the fall season of Guangzhou, China

5 Yihang Yu^{1,2,†}, Peng Cheng^{1,2,5,*}, Huirong Li^{1,2}, Wenda Yang^{1,2}, Baobin Han^{1,2}, Wei Song³, Weiwei Hu³, Xinming Wang³, Bin Yuan^{4,5}, Min Shao^{4,5}, Zhijiong Huang⁴, Zhen Li⁴, Junyu Zheng^{4,5}, Haichao Wang⁶ and Xiaofang Yu^{1,2}

¹Institute of Mass Spectrometry and Atmospheric Environment, Jinan University, Guangzhou 510632, China

²Guangdong Provincial Engineering Research Center for Online Source Apportionment System of Air Pollution, Guangzhou 510632, China

10 ³State Key Laboratory of Organic Geochemistry, Guangzhou Institute of Geochemistry, Chinese Academy of Sciences, Guangzhou 510640, China

⁴Institute for Environmental and Climate Research, Jinan University, Guangzhou 511443, China

⁵Guangdong-Hongkong-Macau Joint Laboratory of Collaborative Innovation for Environmental Quality, Guangzhou 511443, China

15 ⁶School of Atmospheric Sciences, Sun Yat-Sen University, Zhuhai, China.

~~†These authors contribute equally to this paper.~~

*Correspondence to: Peng Cheng (chengp@jnu.edu.cn)

Abstract. ~~Nitrous acid (HONO) can produce hydroxyl radicals (OH) by photolysis and plays an important role in atmospheric photochemistry. Over the years, high concentrations of HONO have been observed in the Pearl River Delta region (PRD) of China, which may be one reason for the elevated atmospheric oxidation capacity. A comprehensive atmospheric observation campaign was conducted at an urban site in Guangzhou from 27 September to 9 November 2018. During the period, HONO was measured from 0.02 to 4.43 ppbv with an average of 0.74 ± 0.70 ppbv. The emission ratios (HONO/NO_x) of $0.9 \pm 0.4\%$ were derived from 11 fresh plumes. The primary emission rates of HONO at night were calculated to be between 0.04 ± 0.02 ppbv h⁻¹ and 0.30 ± 0.15 ppbv h⁻¹ based on a high resolution emission inventory. The HONO formation rate by the homogeneous reaction of OH + NO at night was 0.26 ± 0.08 ppbv h⁻¹, which can be seen as secondary results from primary emission. They were both much higher than the increase rate of HONO (0.02 ppbv h⁻¹) during night. The soil emission rate of HONO at night was calculated to be 0.019 ± 0.001 ppbv h⁻¹. Assuming dry deposition as the dominant removal process of HONO at night, a deposition velocity of at least ~ 1.8 cm s⁻¹ is required to balance the direct emissions and OH + NO reaction. Correlation analysis shows that NH₃ and relative humidity (RH) may participate in the heterogeneous transformation from NO₂ to HONO at night. In the daytime, the average primary emission P_{emis} was 0.12 ± 0.01 ppbv h⁻¹, and the homogeneous reaction $P_{\text{OH+NO}}$ was 0.79 ± 0.61 ppbv h⁻¹, larger than the unknown sources P_{Unknown} (0.65 ± 0.46 ppbv h⁻¹). These results suggest primary emissions as a key factor affecting HONO at our site, both during daytime and nighttime. Similar to previous studies, the daytime unknown source of HONO, P_{Unknown} , appeared to be related~~

20
25
30

to the photo-enhanced conversion of NO_2 . The daytime average OH production rates by photolysis of HONO was 3.7×10^6
35 $\text{cm}^{-3}\text{-s}^{-1}$, lower than that from $\text{O}^1\text{D} + \text{H}_2\text{O}$ at $4.9 \times 10^6 \text{cm}^{-3}\text{-s}^{-1}$. Simulations of OH and O_3 with the Master Chemical
Mechanism (MCM) box model suggested strong enhancement effect of HONO on OH and O_3 by 59% and 68.8%,
respectively, showing a remarkable contribution of HONO to the atmospheric oxidation in the fall season of Guangzhou.
High concentrations of nitrous acid (HONO) have been observed in the Pearl River Delta (PRD) region of China in recent
years, contributing to elevated atmospheric oxidation capacity by producing OH through HONO photolysis. We have
40 investigated budget of HONO at an urban site in Guangzhou from 27 September to 9 November 2018 using data from a
comprehensive atmospheric observation campaign. During this period, HONO was measured from 0.02 to 4.43 ppbv with an
average of 0.74 ± 0.70 ppbv. Emission ratios (HONO/ NO_x) of $0.9 \pm 0.4\%$ were derived from 11 fresh plumes. The primary
emission rate of HONO at night was calculated to be between 0.04 ± 0.02 ppbv h^{-1} and 0.30 ± 0.15 ppbv h^{-1} based on a
high-resolution NO_x emission inventory. Heterogeneous conversion of NO_2 on ground surface (0.27 ± 0.13 ppbv h^{-1}),
45 primary emission from vehicle exhaust (between 0.04 ± 0.02 ppbv h^{-1} and 0.30 ± 0.15 ppbv h^{-1} with a middle value of 0.16
 ± 0.07 ppbv h^{-1}) and the homogeneous reaction of $\text{NO} + \text{OH}$ (0.14 ± 0.30 ppbv h^{-1}) were found to be the three largest
sources of HONO at night. Heterogeneous NO_2 conversion on the aerosol surfaces (0.03 ± 0.02 ppbv h^{-1}) and soil emission
(0.019 ± 0.009 ppbv h^{-1}) were two other minor sources. Correlation analysis shows that NH_3 and relative humidity (RH) may
have participated in the heterogeneous transformation from NO_2 to HONO at night. Dry deposition (0.41 ± 0.31 ppbv h^{-1})
50 was the largest removal process of HONO at night, followed by dilution (0.18 ± 0.16 ppbv h^{-1}), while HONO loss on aerosol
surfaces was much slower (0.008 ± 0.006 ppbv h^{-1}). In the daytime, the average primary emission P_{emis} was 0.12 ± 0.02 ppbv
 h^{-1} , and the homogeneous reaction $P_{\text{OH}+\text{NO}}$ was 0.79 ± 0.61 ppbv h^{-1} , larger than the unknown source P_{Unknown} (0.65 ± 0.46
ppbv h^{-1}). Similar to previous studies, P_{Unknown} appeared to be related to the photo-enhanced conversion of NO_2 .
Our results show that primary emissions and reaction of $\text{NO} + \text{OH}$ can significantly affect HONO at a site with intensive
55 emissions, both during daytime and nighttime. The impact of uncertain parameter values assumed in the calculation of
HONO sources can have strong impact on the relative importance of HONO sources at night, and could be reduced by
improving knowledge on key parameters such as the NO_2 uptake coefficient. The uncertainty with estimating direct emission
can be reduced by using emission data with higher resolution and quality. Our study highlights the importance of better
constraining both conventional and novel HONO sources by reducing uncertainties in their key parameters in advancing our
60 knowledge on this important source of atmospheric OH.

Keywords: HONO; Atmospheric oxidation capacity; Budget analysis; Heterogeneous reaction; Uncertainty

1 Introduction

As a primary source of hydroxyl radical (OH), HONO has attracted scientific researchers' great interest. The photolysis of
65 HONO (Reaction R1) can generate a substantial amount of OH, which is a primary atmosphere oxidant that is responsible

for oxidizing and removing of most natural and anthropogenic trace gases. Additionally, OH radicals can initiate the oxidation of the volatile organic compounds (VOC) to produce hydroperoxyl radicals (HO_2) and organic peroxy radicals (RO_2). These free radicals can further lead to the formation of ozone (O_3) in the presence of nitrogen oxides (NO_x) (Xue et al., 2016; Finlayson-Pitts and Pitts, 2000; Hofzumahaus et al., 2009; Lelieveld et al., 2016; Tan et al., 2018). Up to 33–92% OH formation can be attributed to HONO photolysis in both rural and urban sites (Kleffmann et al., 2005; Michoud et al., 2012; Tan et al., 2017; Xue et al., 2020; Hendrick et al., 2014). However, the detailed formation mechanisms of HONO are still not well understood and the observed HONO concentrations cannot be completely explained by current research (Sörgel et al., 2011a; Kleffmann et al., 2005; Sarwar et al., 2008; Liu et al., 2019a; Lee et al., 2016; Liu et al., 2020c).



HONO sources generally include direct emissions, homogeneous reactions and heterogeneous reactions. HONO can be directly emitted into the troposphere from combustion processes such as biomass burning, vehicle exhaust, domestic heating, and industrial exhaust (Liu et al., 2019b; Neuman et al., 2016; Nie et al., 2015; Kramer et al., 2020). The emission ratios of HONO/ NO_x of traffic sources have been estimated in the range of 0.3%–0.85% through tunnel experiments considering various engine types (Kirchstetter et al., 1996; Kurtenbach et al., 2001; Kramer et al., 2020). Soil nitrite formed through the processes of biological nitrification and denitrification, were proposed to be a prominent HONO source in the troposphere (Maljanen et al., 2013; Oswald et al., 2013; Wu et al., 2019; Su et al., 2011). Subsequently, biological soil crusts (biocrusts) were also found to release HONO (Weber et al., 2015; Porada et al., 2019; Meusel et al., 2018). In addition, an acid displacement mechanism has also been suggested to contribute substantial fraction of daytime HONO formation (VandenBoer et al., 2015). The reaction between NO and OH is considered an important pathway of HONO formation when OH and NO concentrations are relatively high (Alicke et al., 2002; Li et al., 2012; Pagsberg et al., 1997; Qin et al., 2009; Wong et al., 2011), whereas this pathway often cannot explain the observed HONO concentrations, especially during daytime (Tang et al., 2015; Li et al., 2010; Czader et al., 2012; Tong et al., 2016). Bejan et al. (2006) studied the HONO formation by the photolysis of different gaseous nitrophenols and proposed that the photolysis of nitrophenols can partly explain the observed HONO formation in the urban atmosphere. Zhang and Tao (2010) proposed that HONO can form through homogeneous nucleation of NH_3 , NO_2 and H_2O . However, this reaction has not yet been observed in field experiments nor tested by laboratory studies. Li et al. (2014b) proposed that the reaction of NO_2 with HO_2 - H_2O could be a gas phase source of HONO in the lower troposphere. But Ye et al. (2015) estimated the HONO yield of the reaction of NO_2 with HO_2 - H_2O was only 3%. Additionally, heterogeneous reactions on different kinds of surfaces have also been found to be possible significant HONO sources, including heterogeneous reactions of NO_2 on ground surfaces (Meusel et al., 2016; VandenBoer et al., 2013), building surfaces (Aeker et al., 2006; Indarto, 2012), ocean surfaces (Wen et al., 2019; Wojtal et al., 2011; Yang et al., 2021a), soil surfaces (Laufs et al., 2017; Kleffmann et al., 2003; Yang et al., 2021b) and vegetation surfaces (Stutz et al., 2002; Marion et al., 2021), etc. Photosensitized reduction reaction of NO_2 on organic surfaces (such as

100 humic acids and aromatics) has been considered as an effective pathway to generate HONO (George et al., 2005; Stemmler
et al., 2006; Liu et al., 2020a; Ammar et al., 2010; Brigante et al., 2008; Cazoir et al., 2014; Sosodova et al., 2011). The
heterogeneous conversion of NO₂ to HONO on humid surfaces have also been studied (Finlayson Pitts et al., 2003; Ammann
et al., 1998; Ndour et al., 2008) and this conversion can be further promoted by ambient NH₃ and SO₂ (Ge et al., 2019; Wang
105 et al., 2016; Xu et al., 2019; Li et al., 2018b; Wang et al., 2021a). In addition, HONO can also be formed by heterogeneous
conversion of NO₂ on secondary organic aerosols and fresh soot particles (Arens et al., 2001; Ziemba et al., 2010), but the
contributions and mechanisms are still under discussion (Arens et al., 2001; Aubin and Abbatt, 2007; Bröske et al., 2003;
Qin et al., 2009). Both field observations and laboratory studies found that the photolysis of adsorbed HNO₃ and particulate
nitrate (NO₃⁻) made an important contribution to HONO formation (Ye et al., 2016; Ye et al., 2017; Zhou et al., 2003; Zhou
110 et al., 2002b; Zhou et al., 2011; Ziemba et al., 2010). However, Laufs and Kleffmann (2016) obtained a very low HNO₃
photolysis frequency in laboratory, almost two orders of magnitude lower than the result by Zhou et al. (2003).

The Pearl River Delta (PRD) region is one of the biggest city clusters in the world with dense population and large
anthropogenic emissions. Rapid economic development and urbanization have led to severe deterioration of air quality in
this region, which was characterized by atmospheric "compound pollution" with concurrent high fine particulate matter
115 (PM_{2.5}) and ozone (O₃) (Tang, 2004; Chan and Yao, 2008; Yue et al., 2010; Wang et al., 2017b; Xue et al., 2014; Zheng et
al., 2010). While O₃ has been increasing along with reduced PM_{2.5} over recent years in the region (Li et al., 2014a; Liao et al.,
2020; Wang et al., 2009; Zhong et al., 2013; Lu et al., 2018), and has become the dominant factor of the air quality index
exceeding the national standard (Feng et al., 2019), indicating the enhancement of atmospheric oxidation capacity. By far
two comprehensive atmospheric observations were conducted in the PRD region to detect OH radicals. High concentrations
120 of OH radicals were observed both times, especially in the first time it was the highest ever reported, which cannot be
explained by the current knowledge of atmospheric chemistry (Hofzumahaus et al., 2009). Substantial level of HONO was
suggested to be the major source of the OH-HO₂-RO₂ radical system in above two campaigns (Lu et al., 2012; Tan et al.,
2019a). Moreover, high concentrations of HONO have also been confirmed in other observations in this area during last two
decades (Hu et al., 2002; Su et al., 2008b; Su et al., 2008a; Qin et al., 2009; Li et al., 2012; Shao et al., 2004). Fast OH
125 production through HONO photolysis may be a key factor for the increasing atmospheric oxidation capacity and ozone
concentration in this area.

In this work, we performed continuous measurements of HONO, along with trace gases, photolysis frequencies and
meteorological conditions at an urban site in Guangzhou from 27 September to 9 November 2018, as part of the field
130 campaign named "Particles, Radicals, Intermediates from oxidation of primary Emissions in Greater Bay Area" (PRIDE-
GBA2018). Benefiting from numerous prior field observational studies in the PRD region, our study stands in a strong
position to ensure high quality of data acquisition and analysis of HONO, along with a full suite of other chemical species,
providing a unique and valuable opportunity to refine our knowledge of HONO sources and sinks, as well as the role of

HONO in the photochemistry of O₃ and OH in such a region with extensive air pollution as well as rigorous emission control over recent years. A high resolution (3 km × 3 km) NO_x emission inventory for the Guangzhou city (Huang et al., 2021) was used to estimate the primary emission rates of NO_x and HONO, which would reduce the uncertainty of HONO primary emission rate. By analysing our observational data, both nighttime HONO formation pathways and daytime HONO budgets have been investigated in this study. The contribution of HONO photolysis to OH production has been calculated and compared with that of O₃ photolysis and ozonolysis of alkenes. The impact of HONO on atmospheric oxidation capacity and O₃ formation is further investigated using a chemical box model based on Master Chemical Mechanism (MCMv3.3.1). Nitrous acid (HONO) is an important primary source of hydroxyl radical (OH) through photolysis (Reaction R1), contributing up to 33–92% OH at rural and urban sites (Kleffmann et al., 2005; Michoud et al., 2012; Tan et al., 2017; Xue et al., 2020; Hendrick et al., 2014). OH is the principle atmospheric oxidant that is responsible for oxidizing and removing most natural and anthropogenic trace gases. OH initiates the oxidation of the volatile organic compounds (VOC) to produce hydroperoxyl radicals (HO₂) and organic peroxy radicals (RO₂), which further lead to the formation of ground-level ozone (O₃) in the presence of nitrogen oxides (NO_x = NO + NO₂) (Xue et al., 2016; Finlayson-Pitts and Pitts, 2000; Hofzumahaus et al., 2009; Lelieveld et al., 2016; Tan et al., 2018), as well as secondary organic aerosols (SOA). However, the detailed formation mechanisms of HONO are still not well understood and the observed HONO concentrations cannot be completely explained by current knowledge (Sörgel et al., 2011a; Kleffmann et al., 2005; Sarwar et al., 2008; Liu et al., 2019a; Lee et al., 2016; Liu et al., 2020c).



So far numerous HONO sources have been found, and they can be categorized as direct emissions, homogeneous reactions and heterogeneous reactions. Fossil fuel combustion is the most important direct emission source of HONO (Kurtenbach et al., 2001; Kirchstetter et al., 1996; Rappenglück et al., 2013; Kramer et al., 2020; Xu et al., 2015; Trinh et al., 2017). In general, the emission ratios of HONO/NO_x obtained from fresh air masses and vehicle exhaust (0.03%–1.7%) (Kurtenbach et al., 2001; Kirchstetter et al., 1996; Rappenglück et al., 2013; Trinh et al., 2017; Liu et al., 2017; Pitts et al., 1984; Nakashima and Kajii, 2017) are much smaller than the ratios of HONO/NO_x observed in the low boundary layer (2.3%–9%) (Yang et al., 2014; Zhou et al., 2002a; Hao et al., 2020; Gu et al., 2021; Li et al., 2018a; Yu et al., 2009; Acker et al., 2006), reflecting substantial secondary formation of HONO away from direct emissions. Recent studies found that soil emission might be another major direct emission source of HONO (Su et al., 2011; Oswald et al., 2013; Weber et al., 2015; Wu et al., 2019; Porada et al., 2019; Wang et al., 2021b), although the confirmation of its atmospheric significance requires further comparisons between laboratory and field measurements. It should be noted that direct emissions may surpass secondary sources at sampling sites with heavy emission impacts (Liu et al., 2019a; Tong et al., 2015; Zhang et al., 2019b; Tong et al., 2016; Meusel et al., 2016).

170 Homogeneous gas-phase reaction between NO and OH (R2) is the most well known secondary source of HONO (Perner and
Platt, 1979). HONO concentrations measured in the atmosphere cannot be explained by direct emission and this reaction
alone, especially during daytime (Kleffmann et al., 2005; Lee et al., 2016) when a large source of HONO is necessary to
sustain the measured level of HONO against fast photolysis. Numerous new homogeneous HONO formation mechanisms
have been proposed so far to explain the gap between observed and predicted HONO, including HONO formation by
photolysis of o-nitrophenol (Bejan et al., 2006; Yang et al., 2021c), homogeneous nucleation of NH₃, NO₂ and H₂O (Zhang
and Tao, 2010), and the homogeneous reaction between water vapor (H₂O) and electronically excited NO₂ ($\lambda > 420$ nm)
175 followed by the reaction of NO₂ with HO₂·H₂O (Li et al., 2008; Li et al., 2014b). These gas-phase reactions have yet to be
confirmed to occur in the atmosphere, and are unlikely to be the main HONO source.



Heterogeneous reactions of NO₂ on various surfaces have drawn substantial interest due to the observed correlation between
HONO and NO₂ during many field observations. Vertical gradient observations appear to suggest that HONO is more likely
produced from the ground surface (Wong et al., 2012; Kleffmann et al., 2003; Stutz et al., 2002; VandenBoer et al., 2013;
185 Wong et al., 2011; Villena et al., 2011), while some observations found a good correlation between HONO and aerosol
surface area (Reisinger, 2000; Su et al., 2008a; Jia et al., 2020; Zheng et al., 2020; Liu et al., 2014), which can be related to
the concentration and composition of particulate matter (Cui et al., 2018; Liu et al., 2014; Colussi et al., 2013; Yabushita et
al., 2009; Kinugawa et al., 2011). Both laboratory studies and field observations have found that hydrolysis of NO₂ on wet
surfaces can produce HONO (R3), and the uptake coefficient of NO₂ (γ) can vary by several orders of magnitude (Finlayson-
190 Pitts et al., 2003; Stutz et al., 2004; Acker et al., 2004). HONO can also be generated by NO₂ reduction on reductive surfaces
(soot, semivolatile organic compounds, humic acid, etc.) at a much faster rate than NO₂ hydrolysis, but the surfaces could be
inactivated in a short period of time (Ammann et al., 1998; Han et al., 2017a; Han et al., 2017b; Gerecke et al., 1998; Monge
et al., 2010; Gutzwiller et al., 2002; Wall and Harris, 2017; Stemmler et al., 2006). However, irradiation could enhance the
reaction and maintain the activity of the surfaces, making it possible to play an important role in HONO formation during
195 daytime. Both laboratory and field studies found that photolysis of adsorbed HNO₃ and particulate nitrate (NO₃⁻) could
produce HONO (Ye et al., 2016; Ye et al., 2017; Zhou et al., 2003; Zhou et al., 2002b; Zhou et al., 2011), which might be an
important HONO source, at least in remote areas and polar regions. Evidence of other new pathways and mechanisms has
also been found and their atmospheric relevance discussed (Ge et al., 2019; Wang et al., 2016; Xu et al., 2019; Li et al.,
2018b; Xia et al., 2021; Zhao et al., 2021; Gen et al., 2021).

200

The Pearl River Delta (PRD) region is one of the biggest city clusters in the world with dense population and large anthropogenic emissions. Rapid economic development and urbanization have led to severe air pollution in this region, which has been characterized by atmospheric "compound pollution" with concurrently high fine particulate matter (PM_{2.5}) and ozone (O₃) (Tang, 2004; Chan and Yao, 2008; Yue et al., 2010; Wang et al., 2017b; Xue et al., 2014; Zheng et al., 2010).
205 Over recent years, O₃ has been increasing along with reduced PM_{2.5} in the region (Li et al., 2014a; Liao et al., 2020; Wang et al., 2009; Zhong et al., 2013; Lu et al., 2018), and has become the dominant factor of the air quality index exceeding the national standard (Feng et al., 2019), indicating the enhancement of atmospheric oxidation capacity. So far, two comprehensive atmospheric observations have been conducted in the PRD region, focusing on the balance and dynamics of OH sources and sinks (Hofzumahaus et al., 2009; Tan et al., 2019a). Substantial amount of HONO was suggested to be a
210 major source of the OH–HO₂–RO₂ radical system in these two campaigns (Lu et al., 2012; Tan et al., 2019a) as well as in other previous campaigns (Hu et al., 2002; Su et al., 2008b; Su et al., 2008a; Qin et al., 2009; Li et al., 2012; Shao et al., 2004).

In this work, we performed continuous measurements of HONO, along with trace gases, photolysis frequencies and meteorological conditions at an urban site in Guangzhou from 27 September to 9 November 2018, as part of the field
215 campaign "Particles, Radicals, Intermediates from oxidation of primary Emissions in Greater Bay Area" (PRIDE-GBA2018). Benefiting from numerous prior field observational studies in the PRD region, our study stands in a strong position to ensure high quality of data acquisition and analysis of HONO, along with a full suite of other chemical species, providing a unique and valuable opportunity to refine our knowledge of HONO sources and sinks, as well as the role of HONO in the
220 photochemistry of O₃ and OH in such a region with extensive air pollution as well as rigorous emission control over recent years.

Departing from the valuable knowledge and experiences gained from numerous previous HONO studies in the PRD region and around the world, we aim to draw useful and unique insights from a detailed analysis of our dataset in the context of a
225 comprehensive review of previous data and findings, with special attention paid to reducing and/or characterizing the uncertainties in parameterizations and their implications on the relative importance of various HONO sources and sinks. Specifically, (1) a high resolution (3 km × 3 km) NO_x emission inventory for the Guangzhou city (Huang et al., 2021) was used to estimate the primary emission rates of NO_x and HONO, which would reduce the uncertainty of HONO primary emission rate; (2) a wide range of possible parameter values have been evaluated for each source to quantify their strengths
230 and rank their importance; (3) uncertainties associated with each source and other possible factors are discussed in detail.

2 Experiment

2.1 Observation site

235 The sampling site (23.14° N, 113.36° E) is located in the Guangzhou Institute of Geochemistry Chinese Academy of Sciences (GIGCAS). The instruments were deployed in the cabin on the rooftop of a seven-story building (~ 40 m above the ground). The site is surrounded by residential communities and schools, with no industrial manufacturers or power plants around, representing a typical urban environment in the PRD region. The south China Expressway and Guangyuan Expressway, both with heavy traffic loading, are located at west and south of the site, with distances of about 300 m. As a result, the site often experienced local emissions from traffic. The location and surroundings of the site are shown in Fig. S1.

240 2.2 Measurements

HONO was measured by a custom-built LOPAP (LOng Path Absorption Photometer) (Heland et al., 2001; Kleffmann et al., 2006). More information about our custom-built LOPAP (including principle, quality assurance/quality control, instrument parameters and intercomparison) are introduced in supplement information.

245 In addition to HONO, ambient VOCs were measured using a TH-300B On-Line VOCs Monitoring System involving detection technology of ultralow temperature preconcentration coupled with gas chromatography-mass spectrometry (GC/MS) with the time resolution of 1 h. NO_x (NO + NO₂) was measured by a nitrogen oxides analyzer (Thermo Scientific, Model 42i), which used a NO-NO_x chemiluminescence detector equipped with a molybdenum-based converter with the time resolution and detection limit of 1 min and 1 ppbv respectively. It should be noted that the molybdenum oxide (MoO)
250 converters may also convert some NO_z (= NO_y - NO_x) (e.g., HONO, peroxyacetyl nitrate (PAN), HNO₃, and so on.) species to NO and hence could overestimate the ambient NO₂ concentrations. The degree of overestimation depends on both air mass age and the composition of NO_y. At our site that was greatly affected by fresh emissions, the relative interferences of NO_z to NO₂ have been estimated to be around 10%, which is closed to the results of Xu et al. (2013) and negligible for our discussion of HONO budget. O₃ was measured by an O₃ analyzer (Thermo Scientific, Model 49i) via ultraviolet absorption
255 method with the time resolution and detection limit of 1 min and 1 ppbv respectively. SO₂ was measured by SO₂ analyzer (Thermo Scientific, Model 43i) via pulsed fluorescence method with the time resolution and detection limit of 1 min and 1 ppbv respectively. CO was measured by a CO analyzer (Thermo Scientific, Model 48i) with the time resolution and detection limit of 1 min and 0.1 ppmv respectively. NH₃ was measured by laser absorption spectroscopy (PICARRO, G2508) with the time resolution and detection limit of 1 min and 1 ppbv respectively. Gaseous HNO₃ was detected by a Time-Of-
260 Flight Chemical Ionization Mass Spectrometer (Aerodyne Research Inc., TOF-CIMS) with a time resolution of 1 min. And particulate nitrate (NO₃⁻) was measured by Time-Of-Flight Accelerator Mass Spectrometry (Aerodyne Research Inc., TOF-AMS) with a time resolution of 1 min. PM_{2.5} was measured by a Beta Attenuation Monitor (MET One Instruments Inc., BAM-1020) with the time resolution and detection limit of 1 h and 4.0 μg m⁻³ respectively. The meteorological data,

including temperature (T), relative humidity (RH) and wind speed and direction (WS, WD) were recorded by Vantage Pro2
265 Weather Station (Davis Instruments Inc., Vantage Pro2) with the time resolution of 1 min. Photolysis frequencies including
J(HONO), J(NO₂), J(H₂O₂) and J(O¹D) were measured by a filter radiometry (Focused Photonics Inc., PFS-100) with a time
resolution of 1 min.

~~2.3 Box model~~

~~To evaluate the influence of HONO chemistry on the atmospheric oxidation capacity, a zero dimensional box model
270 (Framework for 0-Dimensional Atmospheric Modeling FOAM) based on the Master Chemical Mechanism (MCMv3.3.1)
(Wolfe et al., 2016; Jenkin et al., 2003; Jenkin et al., 2015) was applied to calculate the concentrations of O₃ and OH radicals.
The Master Chemical Mechanism describes atmospheric gas phase organic chemistry in detail which has been widely used
in atmospheric chemistry modelling. Kinetic rate coefficients were derived from the MCM v3.3.1 website
(<http://mem.leeds.ac.uk/MCM>). The model was implemented in MATLAB 2012. In this work, the boundary layer diurnal
275 cycle has been modified and the dilution factor k_{dil} was set at 86400^{-1} s. The solar zenith angle was calculated based on
longitude, latitude and time of the observation. Photolysis rate correction coefficient j_{corr} was set to 1. The model simulation
was constrained by hourly averaged measurement data, including HONO, NO, NO₂, CO, SO₂, VOC species (listed in Table
S2), and temperature, water vapor, wind speed, wind direction, pressure and photolysis frequencies J(NO₂), J(HONO),
J(O¹D) and J(H₂O₂). Other non-measured photolysis frequencies were calculated according to Eq. (1) (Jenkin et al., 1997),
280 and then scaled by the measured J(NO₂):~~

$$J_i = L_i \cos(\chi)^{M_i} \exp(-N_i \sec(\chi)) \quad (1)$$

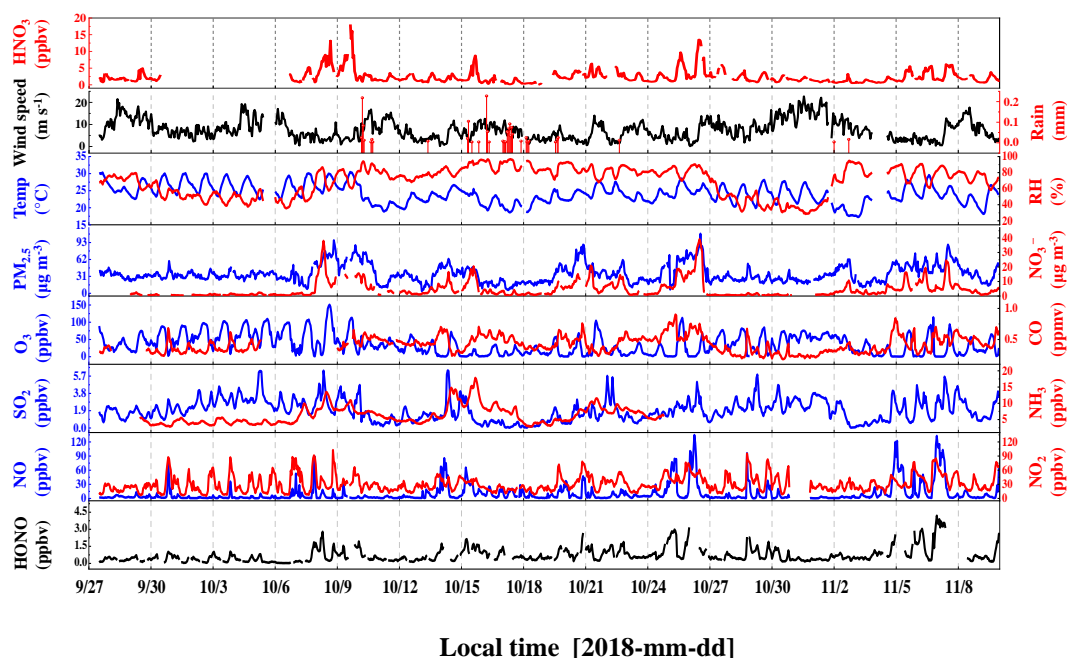
~~where χ represents the solar zenith angle (SZA); L_i , M_i and N_i are the photolysis parameters under clear sky conditions which
were taken from Jenkin et al. (1997). The heterogeneous processes as well as deposition of chemical species were not
considered in this model. The simulation results were evaluated by comparing against the measurements, and index of
285 agreement (IOA), a statistical parameter was employed for the evaluation (Jeon et al., 2018; Xing et al., 2019; Li et al., 2010).
Two simulations with and without HONO constrained by measured values were conducted to examine the impact of HONO
on OH and O₃ formation.~~

3 Results and discussion

3.1 Data overview

290 The time series of meteorological parameters and pollutants during the campaign are shown in Fig. 1. The HONO
concentrations ranged from 0.02 to 4.43 ppbv with an average of 0.74 ± 0.70 ppbv. Table 1 summarizes the HONO
observations reported in PRD region since 2002. HONO appears to have shown a decreasing trend in Guangzhou, as
improvement of air quality in Guangzhou was witnessed during the past decade. Spikes of NO occurred frequently, even up

to 134.8 ppbv, as a result of traffic emissions from two major roads near the site. The concentrations of NO₂, SO₂, NH₃ and PM_{2.5} ranged from 5.4–102.0 ppbv, 0–6.3 ppbv, 2.8–7.8 ppbv and 4–109 μg m⁻³ respectively with the average values of 50.8 ± 17.2 ppbv, 1.9 ± 1.2 ppbv, 6.3 ± 2.7 ppbv, and 36 ± 16 μg m⁻³ respectively. The O₃ concentrations ranged from 0.3–149.8 ppbv with an average peak concentration of 73.9 ± 28.4 ppbv. During the observation, the temperature ranged from 17 °C to 30 °C with an average of 24 ± 3 °C, and the relative humidity ranged from 28% to 97% with an average of 70 ± 17%. The average wind speed was 6.8 ± 4.5 m s⁻¹, while the maximum wind speed was 22.7 m s⁻¹. There was a pollution period from 8th to 10th October with elevated PM_{2.5} (60 ± 12 μg m⁻³) and HONO (0.94 ± 0.58 ppbv). By contrast, from 29 October to 3 November, efficient ventilation driven by strong winds (> 11 m s⁻¹) led to low levels of most pollutants in this period, with average concentrations of PM_{2.5} and HONO at 28 ± 11 μg m⁻³ and 0.56 ± 0.34 ppbv, respectively.



305 **Figure 1. Temporal variations of meteorological and pollutants during the observation period.**

Table 1. Overview of the ambient HONO, NO₂ and NO_x measurement, as well as the ratios of HONO/NO₂ in the PRD region ordered chronologically. Data from Guangzhou are in italic.

Location	Date	HONO (ppbv)	HONO (ppbv)		NO ₂ (ppbv)		NO _x (ppbv)		HONO/NO ₂		Reference
			Night	Day	Night	Day	Night	Day	Night	Day	
<i>Guangzhou</i>	<i>Jul 2002</i>	<i>1.89</i>	–	–	–	–	–	–	–	–	<i>1</i>
<i>(China)</i>	<i>Nov 2002</i>	<i>1.52</i>	–	–	–	–	–	–	–	–	
<i>Xinken</i>	<i>Oct–Nov 2004</i>	<i>1.20</i>	<i>1.30</i>	<i>0.80</i>	<i>34.8</i>	<i>30.0</i>	<i>37.8</i>	<i>40.0</i>	<i>0.037</i>	<i>0.027</i>	<i>2</i>
<i>Back Garden</i>	<i>Jul 2006</i>	<i>0.93</i>	<i>0.95</i>	<i>0.24</i>	<i>16.5</i>	<i>4.5</i>	<i>20.9</i>	<i>5.5</i>	<i>0.057</i>	<i>0.053</i>	<i>3</i>
<i>Guangzhou</i>	<i>Jul 2006</i>	<i>2.80</i>	<i>3.50</i>	<i>2.00</i>	<i>20.0</i>	<i>30.0</i>	–	–	<i>0.175</i>	<i>0.067</i>	<i>4</i>
<i>Guangzhou</i>	<i>Oct 2015</i>	<i>1.64</i>	<i>2.25</i>	<i>0.90</i>	<i>40.5</i>	<i>27.3</i>	<i>57.9</i>	<i>39.8</i>	<i>0.060</i>	<i>0.030</i>	<i>5</i>
<i>Guangzhou</i>	<i>Jul 2016</i>	<i>1.03</i>	<i>1.27</i>	<i>0.70</i>	<i>35.0</i>	<i>25.9</i>	<i>66.3</i>	<i>52.1</i>	<i>0.040</i>	<i>0.070</i>	<i>6</i>
<i>This work</i>	<i>Sep–Nov 2018</i>	<i>0.74</i>	<i>0.91</i>	<i>0.44</i>	<i>36.9</i>	<i>23.3</i>	<i>47.7</i>	<i>30.1</i>	<i>0.026</i>	<i>0.022</i>	
<i>Jiangmen</i>	<i>Oct–Nov 2008</i>	<i>0.60</i>	–	<i>0.48</i>	–	–	–	<i>9.1</i>	–	–	<i>7</i>
	<i>Aug 2011</i>	<i>0.66</i>	<i>0.66</i>	<i>0.70</i>	<i>21.8</i>	<i>18.1</i>	<i>29.3</i>	<i>29.3</i>	<i>0.031</i>	<i>0.042</i>	
<i>Hong Kong</i>	<i>Nov 2011</i>	<i>0.93</i>	<i>0.95</i>	<i>0.89</i>	<i>27.2</i>	<i>29.0</i>	<i>37.2</i>	<i>40.6</i>	<i>0.034</i>	<i>0.030</i>	<i>8</i>
<i>(China)</i>	<i>Feb 2012</i>	<i>0.91</i>	<i>0.88</i>	<i>0.92</i>	<i>22.2</i>	<i>25.8</i>	<i>37.8</i>	<i>48.3</i>	<i>0.036</i>	<i>0.035</i>	
	<i>May 2012</i>	<i>0.35</i>	<i>0.33</i>	<i>0.40</i>	<i>14.7</i>	<i>15.0</i>	<i>19.1</i>	<i>21.1</i>	<i>0.022</i>	<i>0.030</i>	
<i>Hong Kong</i>	<i>Sep–Dec 2012</i>	<i>0.13</i>	–	–	–	–	–	–	–	–	<i>9</i>
<i>Heshan</i>	<i>Oct 2013</i>	<i>1.57</i>	–	–	–	–	–	–	–	–	<i>10</i>
<i>Heshan</i>	<i>Oct–Nov 2014</i>	<i>1.40</i>	<i>1.78</i>	<i>0.77</i>	<i>19.3</i>	<i>17.9</i>	<i>21.5</i>	<i>22.7</i>	<i>0.093</i>	<i>0.055</i>	<i>11</i>
<i>Hong Kong</i>	<i>Mar–May 2015</i>	<i>3.30</i>	<i>2.86</i>	<i>3.91</i>	–	–	–	–	–	–	<i>12</i>
<i>Heshan</i>	<i>Jan 2017</i>	<i>2.70</i>	<i>3.10</i>	<i>2.30</i>	–	–	–	–	<i>0.116</i>	<i>0.089</i>	<i>13</i>

References: 1. Hu et al. (2002); 2. Su et al. (2008a) and Su et al. (2008b); 3. Su (2008) and Li et al. (2012); 4. Qin et al. (2009); 5. Tian et al. (2018); 6. Yang et al. (2017a); 7. Yang (2014); 8. Xu et al. (2015); 9. Zha et al. (2014); 10. Yue et al. (2016); 11. Liu (2017); 12. Yun et al. (2017). 13. Yun (2018).

The time series of photolysis frequencies $J(\text{HONO})$, $J(\text{O}^1\text{D})$ and $J(\text{NO}_2)$ in the whole observation period are shown in Fig. S3.
315 The maximum values of $J(\text{HONO})$, $J(\text{O}^1\text{D})$ and $J(\text{NO}_2)$ are $1.58 \times 10^{-3} \text{ s}^{-1}$, $2.54 \times 10^{-5} \text{ s}^{-1}$ and $9.31 \times 10^{-3} \text{ s}^{-1}$, respectively. These J values tracked a similar diurnal pattern, reaching a maximum at noon with high solar radiation and decreasing to zero at night.

The diurnal variations of HONO, NO_2 , HONO/ NO_2 , and NO are shown in Fig. 2. A daytime trough and a night-time peak of
320 HONO were observed, as typically seen in cities and rural sites (Lee et al., 2016; Xue et al., 2020; Villena et al., 2011; Yang et al., 2021d). The observed high HONO concentration around 0.5 ppbv at daytime implies strong HONO production to balance its rapid loss through photolysis. NO_2 showed a similar diurnal pattern. It is worth noting that the diurnal variation of NO was quite similar to that of HONO, implying the potential association between them. Additionally, the observed large amount of NO (10.8 ± 17.2 ppbv) at night indicates strong primary emission near the site. As an indicator of NO_2 to HONO
325 conversion, the ratio of HONO/ NO_2 rose at night and decreased after sunrise due to photolysis, ranging from 0.2% to 9.1% with an average of $2.3 \pm 1.3\%$, which is lower than most previous field observations in [the](#) PRD region (Li et al., 2012; Qin et al., 2009; Xu et al., 2015), and is typical for relatively fresh plumes. ~~Previous many field observations also reported low values of HONO/ NO_2 ranging from 2% to 10% in freshly polluted air masses~~ (Febo et al., 1996; Lammel and Cape, 1996; Sörgel et al., 2011b; Stutz et al., 2004; Zhou et al., 2007; Su et al., 2008a). ~~The relatively stable and low value of HONO/ NO_2 in nighttime seems to indicate the low contribution of heterogeneous reactions of NO_2 to HONO concentrations.~~
330

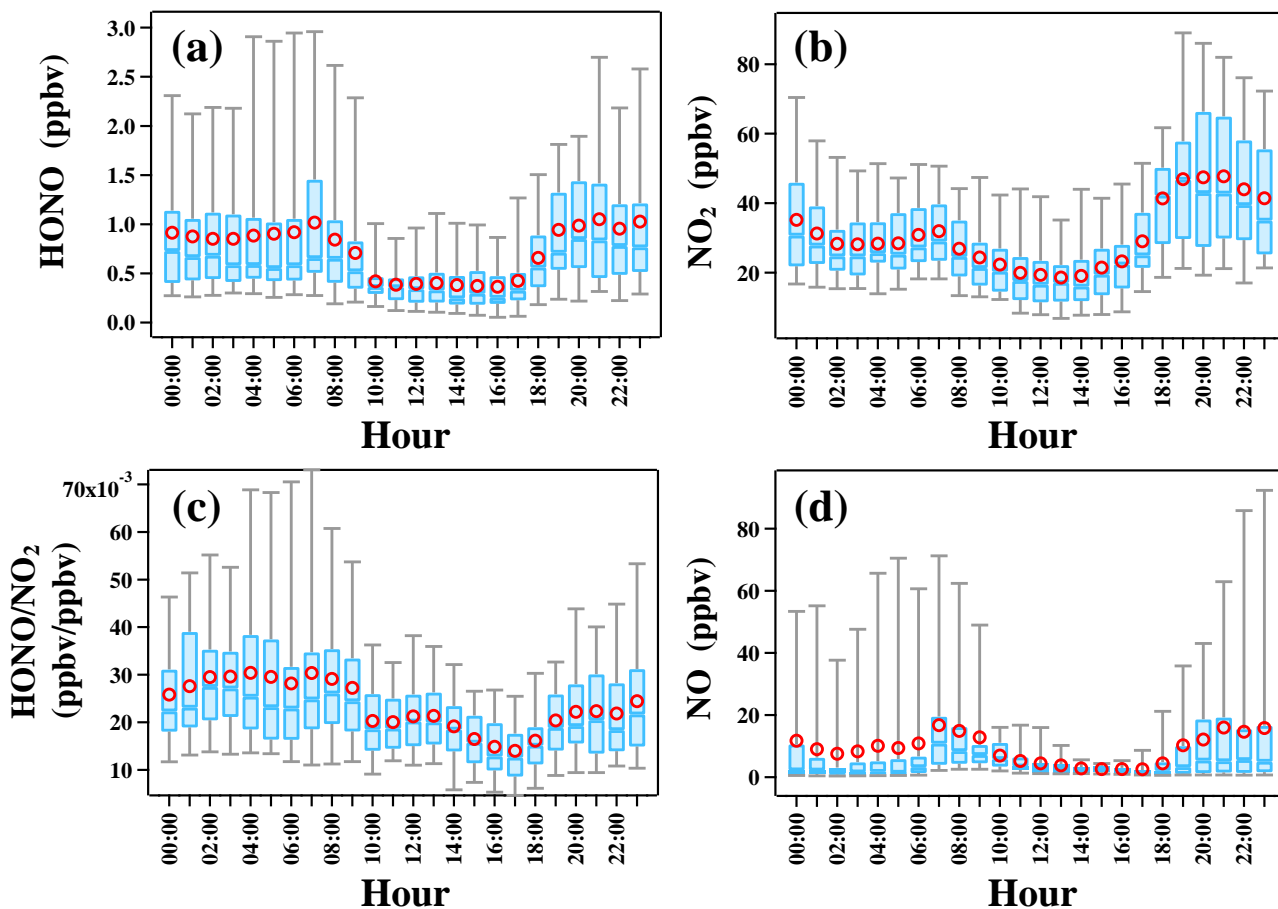


Figure 2. Diurnal profiles of HONO, NO₂, NO and HONO/NO₂ during the observation period. The blue line in the box and red circle refer to the median and mean, respectively. Boxes represent 25% to 75% of the data, and whiskers 95% of the data. The box plots presented in this study is generated by an Igor Pro-based computer program, Histbox (Wu et al., 2018).

335

3.2 Nocturnal HONO formation and sources

3.2.1 Direct emissions

As noted in Sect. 1, the site was expected to receive substantial direct emission of HONO from two major roads nearby. We obtained the emitted HONO/NO_x ratios in fresh plumes defined with the following criteria (Xu et al., 2015):

- 340 (a) NO_x > 49.7 ppbv (highest 25% of NO_x data);
 (b) NO/NO_x > 0.8;
 (c) good correlation between NO_x and HONO ($R^2 > 0.70$, $P < 0.05$);
 (d) short duration of plumes (< 2 h);

(e) global radiation $< 10 \text{ W m}^{-2}$ ($J(\text{NO}_2) < 0.25 \times 10^{-3} \text{ s}^{-1}$).

345

During the campaign, 11 fresh plumes were identified to satisfy criteria (a)–(e) (see Table S32). Two cases among them are shown in Fig. S4. The HONO/NO_x ratios in these selected plumes varied from 0.1% to 1.5% with an average value of $0.9 \pm 0.4\%$, which is comparable to the average value of 1.2% measured in Hong Kong (Xu et al., 2015), 1.0% observed in Hong Kong (Yun et al., 2017), 0.79% measured in Nanjing (Liu et al., 2019b) and 0.69% observed in Changzhou (Shi et al., 2020b). It should be noted that the emission factor derived in this study ~~is was~~ based on field observation and the screening criterion for fresh air mass ~~is was~~ $\text{NO}/\text{NO}_x > 0.8$, while the fresh air mass was characterized by $\text{NO}/\text{NO}_x > 0.9$ in the tunnel experiments conducted by Kurtenbach et al. (2001), so the air masses we selected were still slightly aged and the emission factor derived in this study is slightly overestimated.

355

To evaluate the primary emission, three methods have been used in previous studies (Liu et al., 2019b; Liu et al., 2020b; Meng et al., 2020). In method (1), ~~the observed NO_x concentration is simply assumed to represent the accumulation of emissions but ignore the sinks of NO_x and HONO, as well as transport and convection. On this basis,~~ $[\text{HONO}]_{\text{emis}}$ (the primary emission's contribution to HONO concentration) is ~~estimated as equal to~~ the product of emission coefficient K and observed NO_x concentration (Cui et al., 2018; Huang et al., 2017) (see Eq. (12)). ~~Since it is difficult to determine the time of~~

360

~~NO_x emissions, method (1) can not exclude the NO_x levels before emission begins. This method ignores the sink of NO_x and HONO, as well as transport and convection. On this basis, the observed NO_x is equal to the accumulation of NO_x emission, and HONO emission is linearly related to NO_x concentration. However, ubiquitous loss of NO_x would increase the uncertainty of this method, especially during daytime. With this in mind,~~ In method (2), primary emission rate P_{emis} is ~~estimated as equal to~~ the product of emission coefficient K and $[\Delta\text{NO}_x]/\Delta t$, ~~the increase of NO_x concentration during Δt~~

365

~~where $[\Delta\text{NO}_x]$ is the difference between observed NO_x at two time points~~ (Liu et al., 2019b; Zheng et al., 2020) (see Eq. (23)). ~~The promise of this method is similar to method (1), and it can only be used when NO_x is increasing. As expected, a decrease in NO_x would yield a negative HONO emission rate, which is unrealistic. Obviously, it can only be used when NO_x is increasing. It should be noted that any loss of NO_x and HONO can be a source of error for these two methods, especially during daytime.~~ In method (3), ~~primary emission rate~~ P_{emis} is equal to the product of emission coefficient K and

370

NO_x^{*}, the NO_x emission from source emission inventory (Michoud et al., 2014; Su et al., 2008b) (see Eq. (34)). This method adheres to the definition of HONO emission rate, assuming that the primary sources are evenly mixed in a specific area. It is desirable ~~to use~~ ~~that~~ emission inventory data with high spatial and temporal resolution ~~are used~~ to obtain an accurate estimate.

375

$$[\text{HONO}]_{\text{emis}} = K \times [\text{NO}_x] \tag{12}$$

$$P_{\text{emis}} = K \times [\Delta\text{NO}_x] \tag{23}$$

$$P_{\text{emis}} = K \times \text{NO}_x^* \tag{34}$$

$$P_{\text{HONO}} = \frac{[\text{HONO}]_{t_2} - [\text{HONO}]_{t_1}}{t_2 - t_1} \quad (45)$$

380 In this study, we first used NO_x emission rate from a high-resolution emission inventory (Huang et al., 2021) to calculate
 emission rate of HONO P_{emis} at night (18:00–6:00). The NO_x emission rate was extracted from a 3 km × 3 km grid cell
 centred around our site. As a comparison, we also used the 2017 NO_x emission inventory of Guangzhou city to repeat the
 calculation. The two inventories are primarily different in spatial resolution. The high-resolution 3 km × 3 km data is
 expected to better represent local traffic emissions, whereas the city-level emission inventory represents the total emission.
 385 Since we cannot quantify the relative contribution of the local and regional emissions to this site, two results are used to
 represent upper and lower limits of the contribution of primary emissions to HONO. The nighttime height of the boundary
 layer is assuming to 200 m according to the previous study by Fan et al. (2008).

The observed HONO ~~production/~~accumulation rate P_{HONO} is calculated by Eq. (45), where $[\text{HONO}]_{t_1}$ and $[\text{HONO}]_{t_2}$
 390 represent the HONO concentration at 18:00 and 6:00 Local Time, respectively. Then an average P_{HONO} of 0.02 ± 0.06 ppbv
 h^{-1} can be derived. Hourly HONO primary emission rates calculated with the two inventories are shown in Fig. 3-5 (a). P_{emis}
 calculated with the high-resolution emission data (3 km × 3 km) shows a steep downward trend from 18:00 (0.56 ppbv h^{-1})
 to 4:00 (0.14 ppbv h^{-1}), followed by an upward trend from 4:00 (0.14 ppbv h^{-1}) to 6:00 (0.25 ppbv h^{-1}), with the ~~The~~ average
 of P_{emis} is $0.30 \pm 0.15 \text{ ppbv h}^{-1}$, ~~far larger than the average accumulating rate of HONO at night (0.02 ppbv h^{-1}) derived from~~
 395 ~~observed HONO variation~~. By contrast, P_{emis} with the city level emission data (Guangzhou) is much lower ($0.04 \pm 0.02 \text{ ppbv}$
 h^{-1}) and varied smoothly throughout the night. Similar results have been obtained at urban sites (Liu et al., 2020b; Liu et al.,
 2020c; [Gu et al., 2021](#)) and a suburban site (Michoud et al., 2014), while the result at a rural site is much lower (Su et al.,
 2008b) [in the PRD region](#). ~~The lower limit of the calculated P_{emis} is still larger than the observed HONO accumulation rate.~~
~~Considering the uncertainty of the inventories (-25%–28%), P_{emis} may be overestimated or underestimated to the same extent.~~
 400 ~~The uncertainty of P_{emis} stems from the uncertainty of the inventories (-25%–28%) (Huang et al., 2021). Regardless,~~
~~Nevertheless,~~ direct emission of HONO is still a large HONO source at night along with other sources of HONO that remain
 to be considered. ~~Furthermore, a large sink of HONO was necessary to explain the observed trend of HONO.~~

405

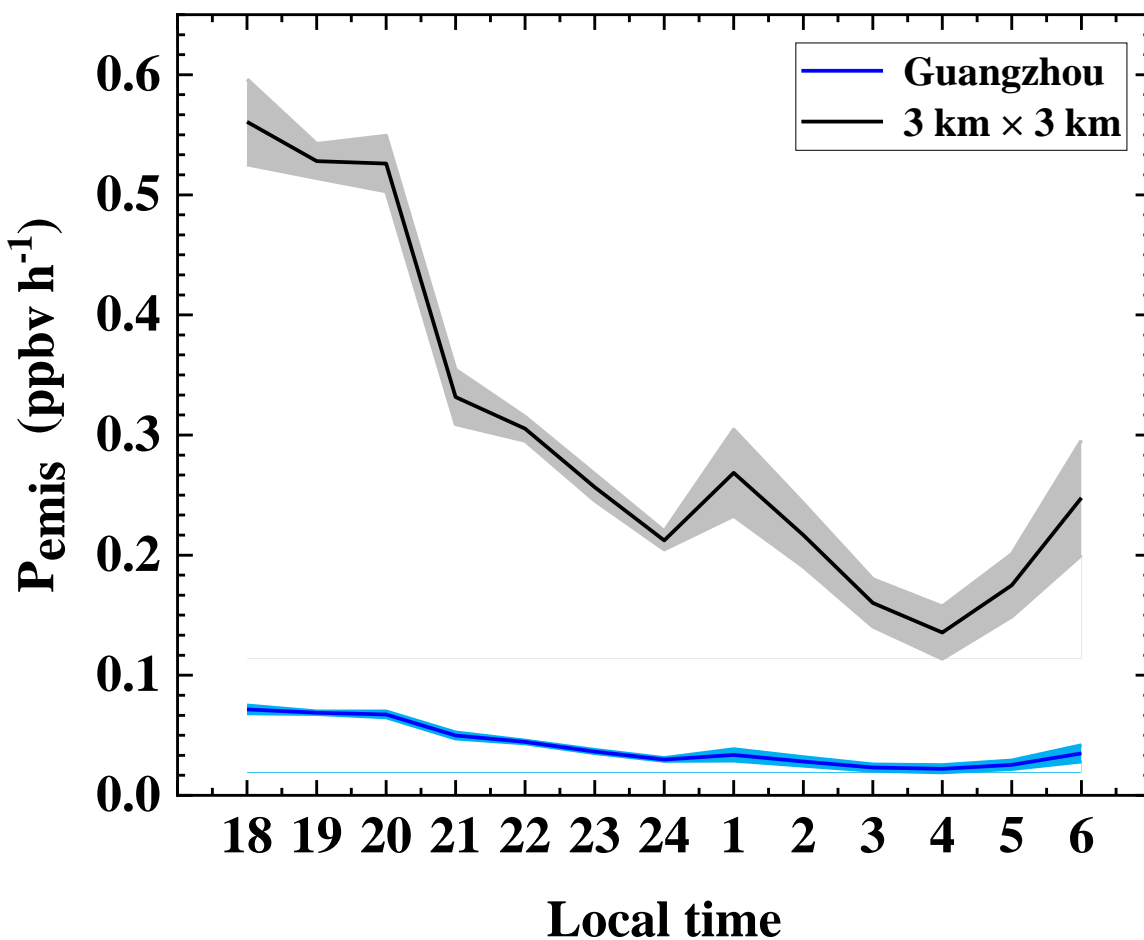


Figure 3. The nocturnal variation of HONO primary emission rates. The black and blue lines represent the HONO primary emission rates calculated by the 2017 NO_x emission source inventory of the 3 km × 3 km grid cell centred on the Guangzhou Institute of Geochemistry and the 2017 NO_x emission source inventory of Guangzhou city respectively. The coloured areas represent 1- σ standard deviations.

Method (1) is also adopted here to calculate $[\text{HONO}]_{\text{emis}}$, and $[\text{HONO}]_{\text{emis}}/[\text{HONO}]$ can simply represent the primary emission's contribution to HONO. We summarized $[\text{HONO}]_{\text{emis}}/[\text{HONO}]$ ratios obtained from urban sites in China (Table S4). We also calculated the primary emission's contribution to HONO ($[\text{HONO}]_{\text{emis}}/[\text{HONO}]$) using Method (1) and made comparisons against $[\text{HONO}]_{\text{emis}}/[\text{HONO}]$ ratios obtained previously from urban sites in China (Table S3). The values varied at a wide range from 12% to 52%, and the difference of 2 times or more existed in different seasons at the same site. These indicate the complexity of the impact of source emissions on observation site, with seasonal difference of more than a factor of 2 for the same site, reflecting large variability of HONO emissions spatially and temporally. The ratio of

~~[HONO]_{emis}/[HONO] at our site is at a high level of 47%, indicating that the site during the campaign is more strongly affected by primary emission from vehicle exhaust compared to most previous studies. In comparison, the ratio of [HONO]_{emis}/[HONO] at our site is relatively high at 47%, as can be expected from the relatively strong vehicle exhaust emissions near our site.~~

In addition to traffic emissions, we also estimated the HONO emission rate from soil P_{soil} (ppbv h⁻¹) according to Eq. (56):

$$P_{\text{soil}} = \frac{\alpha F_{\text{soil}}}{H} \quad (56)$$

where F_{soil} is the emission flux (g m⁻² s⁻¹); H is the height of boundary layer (H , m) and was assumed to be 200 m (Fan et al., 2008); α is the conversion factor ($\alpha = \frac{1 \times 10^9 \times 3600 \times R \times T}{M \times P} = \frac{2.99 \times 10^{13} \times T}{M \times P}$); T is the temperature (K); M is the molecular weight (g mol⁻¹) and P is the atmospheric pressure (Pa). HONO emission flux from soil depends on the temperature, water content and nitrogen nutrient content of soil, which have been considered according to the parameters reported in the literature (Oswald et al., 2013). Since grassland, coniferous forest and tropical rain forest are the typical plants in Guangzhou city area (Wu et al., 2015) and their emission fluxes are comparable (Oswald et al., 2013), emission flux from grassland was adopted to represent the soil HONO emission in Guangzhou. The average nighttime P_{soil} varied from 0.011 to 0.035 ppbv h⁻¹, with a mean value of $0.019 \pm 0.001-0.009$ ppbv h⁻¹. ~~It is comparable to the lower limit of primary emission rate of 0.04 ± 0.02 ppbv h⁻¹. The HONO emission rate from soil at our site is slightly larger than the result reported in Shijiazhuang urban area (Liu et al., 2020b) and comparable to that in Beijing urban area (Liu et al., 2020c). A caveat is that the calculation relies on laboratory results and is therefore prone to errors due to any possible inconsistency between laboratory simulations and field observations. Overall, soil emission is a minor source compared to other sources.~~

3.2.2 NO + OH homogeneous reaction

The reaction between NO and OH acts as the principle homogenous HONO source. It can contribute a substantial fraction to HONO formation when NO and OH concentrations are high (Alicke et al., 2003; Liu et al., 2019b; Wong et al., 2011; Tong et al., 2015; Zhang et al., 2019b). Taking the homogeneous Reactions R2 and R35 into account, the net HONO homogeneous production rate can be calculated by following Eq. (67):

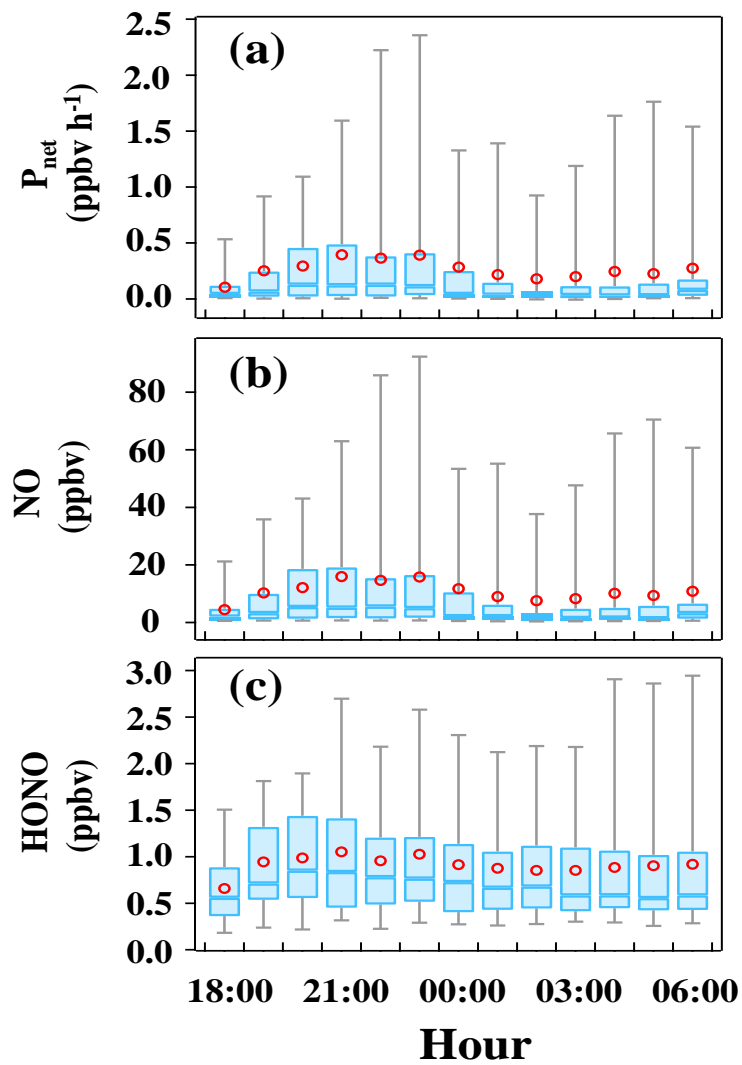


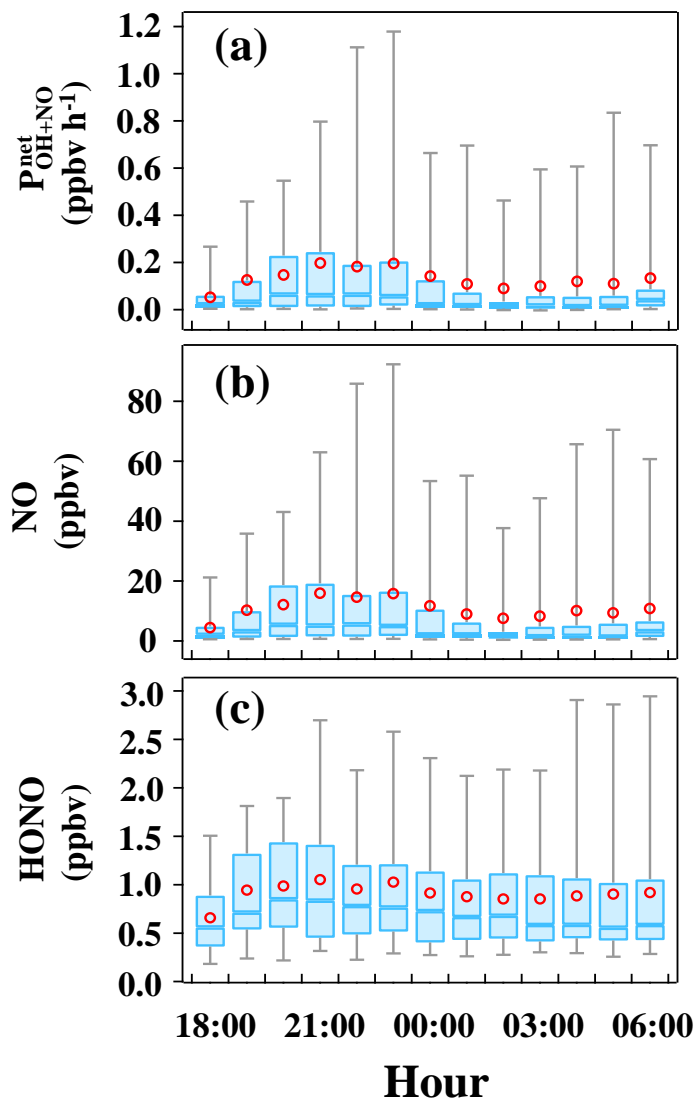
$$P_{\text{net}} P_{\text{OH+NO}}^{\text{net}} = k_{\text{NO+OH}} [\text{NO}][\text{OH}] - k_{\text{HONO+OH}} [\text{HONO}][\text{OH}] \quad (67)$$

In Eq. (67), $k_{\text{NO+OH}}$ (7.2×10^{-12} cm³ s⁻¹) and $k_{\text{HONO+OH}}$ (5.0×10^{-12} cm³ s⁻¹) are the reaction rate constants of the Reactions R2 and R35 at 298 K, respectively (Li et al., 2012). Since the OH concentration was not measured, an average nighttime value of $0.51 \pm 0 \times 10^6$ cm⁻³ measured in Heshan in the PRD region in autumn of 2014 was assumed (Tan et al., 2019) (Liu,

2017). As shown in Fig. 34, the variation of $P_{\text{OH}+\text{NO}}^{\text{net}}$ largely followed that of NO, since the variation of P_{net} is highly similar to NO, for the concentration of NO was 10 times larger than HONO. And the average value of $P_{\text{OH}+\text{NO}}^{\text{net}}$ is 0.26 ± 0.08 0.13 ± 0.30 ppbv h⁻¹, leading to a cumulative HONO contribution of 1.62 3.24 ppbv. The obtained $P_{\text{OH}+\text{NO}}^{\text{net}}$ is similar to previous studies, such as 0.12 ppbv h⁻¹ in Xianyang (Li et al., 2021), 0.13 ppbv h⁻¹ in Zhengzhou (Hao et al., 2020), 0.26 ppbv h⁻¹ in Xi'an (Huang et al., 2017) and 0.28 ppbv h⁻¹ in Guangzhou Back Garden (Li et al., 2012). However, We note that the measured HONO only increased 0.26 ppbv in this period, much smaller than the cumulative production of HONO by the reaction between NO and OH, indicating a large sink to balance this source and other sources that will be discussed below. It suggests that, (1) the reaction between NO and OH is adequate to explain the HONO increase in the whole night, even though other sources like NO₂ heterogeneous conversion might still exist; (2) except for HONO + OH, the strength of HONO sink should be at least 0.30 ppbv h⁻¹, 6 times larger than that obtained by Li et al. (2012) and comparable to that by Hao et al. (2020).

Since OH was not measured in our study, We carried out sensitivity tests using one fifth and tenth, twice and half of assumed OH concentration (1.0 0.5×10^6 cm⁻³) (Lou et al., 2010). As is shown in Table S54, within the range of nighttime OH concentration, the cumulative production of the homogeneous reaction of NO + OH in this study are always large enough to surpass all larger than the averaged measured accumulation of HONO, indicating that taking a value within the range of the observed nighttime OH concentration will not affect the conclusion of this study. the NO + OH source is a major source term regardless of uncertainties in OH concentrations.





470

Figure 34. The mean nocturnal variation of P_{OH+NO}^{net} , HONO and NO. The blue line in the box and red circle refer to the median and mean, respectively. Boxes represent 25% to 75% of the data, and whiskers 95 % of the data.

3.2.3 NO₂ to HONO heterogeneous conversion

Our analysis so far suggests that direct emissions and the homogeneous reaction between NO and OH are two major sources of HONO at night ~~more than sufficient to explain the growth of HONO concentration through the night. This finding is in line with the~~ The relatively high correlation ($R^2 = 0.5927$) between HONO and NO ~~is in line with this finding~~ (Fig. 45 (a)). ~~In addition, correlation analysis was conducted~~ In the following, we present results from correlation analysis to explore possible pathways of heterogeneous NO₂ to HONO conversion at night (18:00–6:00).

480 The ratio of HONO/NO₂ has often been used to indicate the heterogeneous conversion efficiency of NO₂ to HONO (Lammel and Cape, 1996; Stutz et al., 2002), for being less influenced by transport processes or convection. Figure 45 (c) shows a weak correlation ($R^2 = 0.0638$) between HONO/NO₂ and PM_{2.5}, suggesting that the formation of HONO on aerosol surfaces might not be the main pathway (Kalberer et al., 1999; Kleffmann et al., 2003; Wong et al., 2011; Zhang et al., 2009; Sörgel et al., 2011a; VandenBoer et al., 2013). Because the surface area of ground (including vegetation surface, building surface and soil, etc.) is generally larger than the surface area of aerosols (Zhang et al., 2016), some studies suggested that the heterogeneous reaction of NO₂ and water vapor on ground surfaces was the main source of HONO (Harrison and Kitto, 1994; Li et al., 2012; Wong et al., 2012). Furthermore, the correlations between HONO/NO₂ and NH₃ and RH are 0.3746 and 0.2381, respectively, and the correlation further improved between HONO/NO₂ and the product of NH₃ and RH ($R^2 = 0.4597$). Some studies proposed that NH₃ can decrease the free-energy barrier in hydrolysis of NO₂ thus enhance the HONO formation (Xu et al., 2019; Li et al., 2018b; Zhang and Tao, 2010; Wang et al., 2021a).

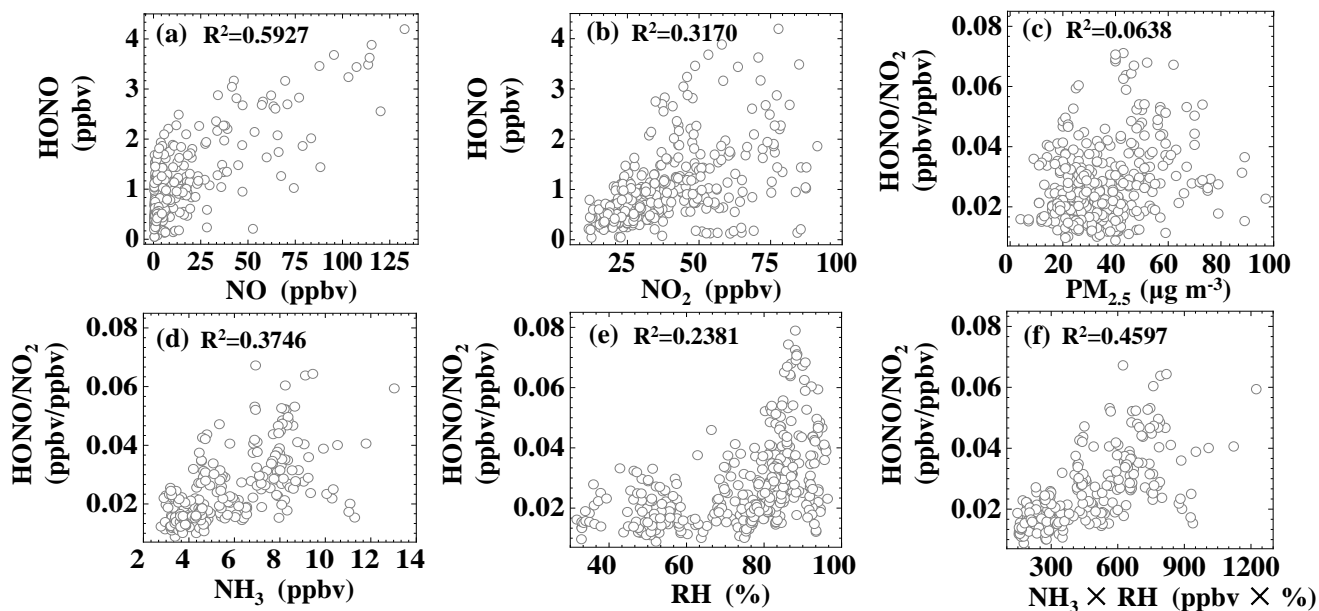
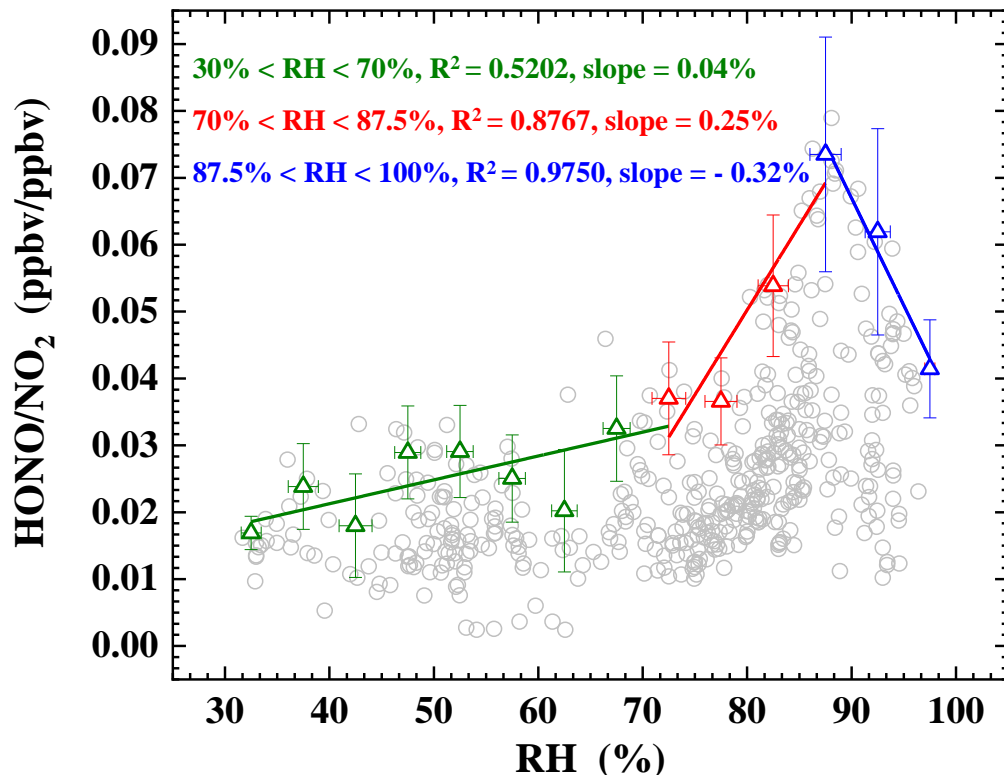


Figure 45. Correlations between HONO, HONO/NO₂ and various parameters during the time interval of 18:00–6:00.

In Fig. S56, we further explored the RH effect by focusing on high HONO/NO₂ values, i.e., the 5 highest HONO/NO₂ values for 5% RH intervals (Stutz et al., 2004). When RH was lower than 87.5%, HONO/NO₂ increased with RH, which is in accordance with the reaction kinetics of disproportionation reaction of NO₂ and H₂O. Furthermore, the slope of linear fitting between HONO/NO₂ and RH was much smaller for RH range of 30% ~ 70% (slope = 0.04%; $R^2 = 0.5202$) than for the RH range of 70% ~ 87.5% (slope = 0.25 %, $R^2 = 0.8767$). Similar piecewise correlations between HONO/NO₂ and RH have been found in previous studies (Qin et al., 2009; Zhang et al., 2019b), which have been interpreted as evidence for the non-linear dependence of NO₂-to-HONO conversion efficiency on RH. Once the relative humidity exceeded 87.5%, NO₂-to-HONO

500 conversion appeared to be inhibited by RH (slope = -0.32%; $R^2 = 0.9750$). A possible explanation is that the number of water layers formed on various surfaces increased rapidly with RH, resulting in effective uptake of HONO and making the surface inaccessible or less reactive to NO_2 . Previous studies also found fast growth of aqueous layers when RH over 70% for glass (Saliba et al., 2001) and over 80% for stone (Stutz et al., 2004). The tipping point inferred from ambient observations appear to vary across locales, likely reflecting the different composition of the ground surfaces, e.g., 60% for Chengdu (Yang et al., 2021d), 65–70% for Beijing (Wang et al., 2017a), 70% for Back Garden (Li et al., 2012), 75% for Shanghai (Wang et al., 2013), and 85% for Xi'an (Huang et al., 2017).

510 ~~In sum, our correlation analysis for HONO/ NO_2 suggests that nighttime heterogenous conversion of NO_2 into HONO at our site might be related to NH_3 and water vapor, whereas aerosol surfaces appeared unimportant.~~



~~Figure 6. Scatter plot of HONO/ NO_2 ratio against RH during nighttime from 18:00 to 6:00. Triangles are the average of top-5 HONO/ NO_2 values in each 5% RH interval.~~

We calculated the strength of the HONO formation from NO₂ heterogenous reaction on on ground surface (P_{ground}) and aerosol surface (P_{aerosol}) based on the empirical data derived from either experiments or observations.

$$P_{\text{ground}} = \frac{1}{8} \gamma_{\text{NO}_2 \rightarrow \text{ground}} \times [\text{NO}_2] \times C_{\text{NO}_2} \times \frac{S_g}{V} \quad (7)$$

$$P_{\text{aerosol}} = \frac{1}{4} \gamma_{\text{NO}_2 \rightarrow \text{aerosol}} \times [\text{NO}_2] \times C_{\text{NO}_2} \times \frac{S_a}{V} \quad (8)$$

$$\frac{S_g}{V} = \frac{2.2}{H} \quad (9)$$

Where C_{NO₂} is the mean molecular velocity of NO₂ (m s⁻¹), $\gamma_{\text{NO}_2 \rightarrow \text{ground}}$ and $\gamma_{\text{NO}_2 \rightarrow \text{aerosol}}$ represent the uptake coefficient of NO₂ on ground surface and aerosol surface, respectively. S_g/V and S_a/V are the surface area to volume ratio (m⁻¹) for both ground and aerosol, respectively. Considering the land use type of the study site, we treated the ground as an uneven surface, and a factor of 2.2 per unit ground surface measured by Voogt and Oke (1997) was adopted to calculate the total active surface. Hence, S_g/V can be calculated by Eq. (9), where H is the mixing layer height. The surface area-to-volume ratio S_a/V of PM₁₀ was not available in this study and was estimated according to PM_{2.5} and S_a/V value in Guangzhou Xinken by Su et al. (2008a). The uptake coefficients of NO₂ on ground surface and aerosol surface were assumed to be 4 × 10⁻⁶ following previous studies (Li et al., 2018a; Liu et al., 2019a; Zhang et al., 2021) (the summary of the parameterisations used for nighttime HONO budget calculation can be found in Table S5). With these assumptions, an average value of P_{ground} of 0.27 ± 0.13 ppbv h⁻¹ can be derived, which is far larger than P_{aerosol} (0.03 ± 0.02 ppbv h⁻¹) (Fig. 5 (c) and (d)).

In sum, our correlation analysis for HONO/NO₂ and parameterized calculations suggested that nighttime heterogenous conversion of NO₂ into HONO at our site mainly occurred on the ground rather than on aerosol sources, while the correlation analysis provides evidence for the role of NH₃ and water vapor in HONO formation. It should be noted that, unlike the NO + OH reaction or the primary emission, which turned out as major HONO sources even at their lower limit considering uncertainties, the magnitude of the heterogenous source as well as its contribution to overall HONO budget varied greatly with the assumed uptake coefficients of NO₂, which can span two orders of magnitude.

3.2.4 Removal of HONO through dry deposition

As discussed above, strong sinks are in Sect. 3.2.2, a sink of at least 0.30 ppbv h⁻¹ is required to balance the nighttime HONO production. Since the reactions of HONO + OH and HONO + HONO are negligible (Kaiser and Wu, 1977; Mebel et al., 1998), it is conceivable that HONO is mainly removed through deposition on the ground L_{Dep} (El Zein and Bedjanian, 2012; Li et al., 2012; Hao et al., 2020; Meng et al., 2020), transport processes, e.g. entrainment of background air L_{dilution} (Gall et al., 2016; Meng et al., 2020), and uptake on aerosols L_{aerosol}. These terms can be expressed as follows: HONO dry deposition velocity V_d can be estimated with Eq. (8):

$$\frac{d[\text{HONO}]}{dt} = P_{\text{emis}} + P_{\text{soil}} + P_{\text{net}} - \frac{V_d \times [\text{HONO}]}{H} \quad (8)$$

The average deposition velocity V_d between 18:00–6:00 was calculated to be 1.8 cm s^{-1} , which is within the range of prior researches ($0.077\text{--}3 \text{ cm s}^{-1}$) (Harrison and Kitto, 1994; Harrison et al., 1996; Stutz et al., 2002; Li et al., 2012; Spindler et al., 1999), and also consistent to the results derived from the HONO uptake coefficient on soil and ground (Donaldson et al., 2014; VandenBoer et al., 2013). It should be noted that heterogeneous conversion of NO_2 -HONO has not been taken into account, so 1.8 cm s^{-1} is the lower limit of dry deposition velocity. High RH at night probably increased the amount of adsorbed water on the ground surfaces and facilitates dry deposition of HONO.

In sum, primary emission from vehicle exhaust (between $0.04 \pm 0.02 \text{ ppbv h}^{-1}$ and $0.30 \pm 0.15 \text{ ppbv h}^{-1}$) and the homogeneous reaction of $\text{OH} + \text{NO}$ ($0.26 \pm 0.08 \text{ ppbv h}^{-1}$) were major sources of HONO at night. Nighttime soil emission rate was calculated to be $0.019 \pm 0.001 \text{ ppbv h}^{-1}$, which is comparable to the observed nocturnal increase rate of HONO (0.02 ppbv h^{-1}), further indicating the importance of direct emissions. Additionally, contribution from NO_2 -heterogeneous reactions on surfaces should not be ruled out. To balance the nighttime HONO budget by assuming dry deposition to be the principal loss process, a dry deposition rate of at least 1.8 cm s^{-1} is required.

$$L_{\text{Dep}} = \frac{V_d \times [\text{HONO}]}{H} \quad (10)$$

$$L_{\text{aerosol}} = \frac{1}{4} \gamma_{\text{HONO} \rightarrow \text{aerosol}} \times [\text{HONO}] \times C_{\text{HONO}} \times \frac{S_a}{V} \quad (11)$$

$$L_{\text{dilution}} = k_{(\text{dilution})} \times ([\text{HONO}] - [\text{HONO}]_{\text{background}}) \quad (12)$$

where V_d is the average deposition velocity, $\gamma_{\text{HONO} \rightarrow \text{aerosol}}$ is the uptake coefficient of HONO on aerosol surface, $k_{(\text{dilution})}$ is the dilution rate (including both vertical and horizontal transport) (Dillon et al., 2002), C_{HONO} is the mean molecular velocity of HONO (m s^{-1}), and $[\text{HONO}]$ and $[\text{HONO}]_{\text{background}}$ represents the HONO concentration at the observation site and the background site, respectively. In this work, the lowest nighttime HONO concentration was taken as the $[\text{HONO}]_{\text{background}}$.

The average loss rate of HONO by dilution was calculated to be $0.18 \pm 0.16 \text{ ppbv h}^{-1}$, which is in the range of prior results (Gall et al., 2016; Liu et al., 2020b; Liu et al., 2020c). The average value of L_{aerosol} and $L_{\text{OH+HONO}}$ was $0.008 \pm 0.006 \text{ ppbv h}^{-1}$ and $0.008 \pm 0.012 \text{ ppbv h}^{-1}$, respectively. In order to balance the nighttime HONO budget and assuming dry deposition to be responsible for the remaining amount of HONO loss, a dry deposition rate of $\sim 2.5 \text{ cm s}^{-1}$ was adopted accounting for an average loss rate of $0.41 \pm 0.31 \text{ ppbv h}^{-1}$ by deposition between 18:00–6:00, when using the median parameter values in Table S5 to calculate the HONO sources and sinks. This result is consistent with previous studies suggesting dry deposition as the dominant loss way for HONO during night (Li et al., 2012; Hao et al., 2020; Meng et al., 2020). The upper limit of L_{aerosol} is only $0.10 \pm 0.08 \text{ ppbv h}^{-1}$, suggesting that HONO loss on aerosols was not a major sink, as also suggested by prior studies (El Zein and Bedjanian, 2012; El Zein et al., 2013; Romanias et al., 2012).

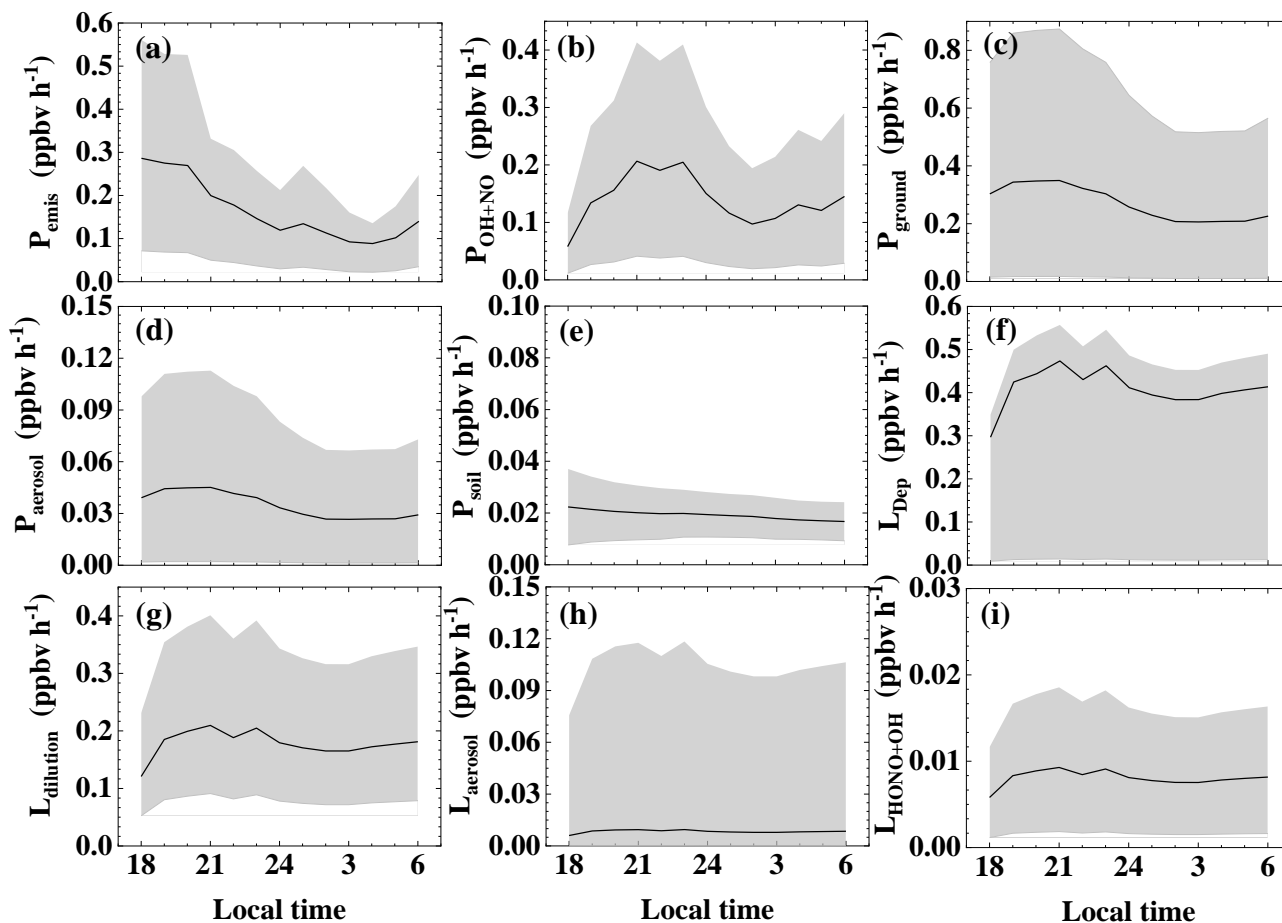
3.2.5 Nighttime HONO budget: relative importance of sources and their uncertainties

580 It is useful to evaluate the balance of HONO budget by evaluating calculated/parameterized sources and sinks against the observed HONO level and variability. The observed production rate of HONO P_{obs} can be defined as the sum of the total loss rates and change rates of HONO (Gu et al., 2021). When using the median values of parameters (Table S5) and taking an average throughout the night (18:00–6:00), all five sources are greater than or close to the average accumulating rate of HONO at night derived from observed HONO variation ($0.02 \pm 0.06 \text{ ppbv h}^{-1}$), indicating a balanced HONO budget
585 considering all uncertainties. Ranking the source strengths with their median estimates suggested that heterogeneous conversion of NO_2 on ground surface ($0.27 \pm 0.13 \text{ ppbv h}^{-1}$), primary emission from vehicle exhaust (between $0.04 \pm 0.02 \text{ ppbv h}^{-1}$ and $0.30 \pm 0.15 \text{ ppbv h}^{-1}$ with a middle value of $0.16 \pm 0.07 \text{ ppbv h}^{-1}$) and the homogeneous reaction of $\text{NO} + \text{OH}$ ($0.14 \pm 0.30 \text{ ppbv h}^{-1}$) were major sources of HONO at night. Nighttime soil emission rate ($0.019 \pm 0.009 \text{ ppbv h}^{-1}$) and heterogeneous NO_2 conversion on the aerosol surfaces ($0.03 \pm 0.02 \text{ ppbv h}^{-1}$) were two other minor sources. Dry deposition
590 ($0.41 \pm 0.31 \text{ ppbv h}^{-1}$) was the principal loss process of nighttime HONO, followed by dilution ($0.18 \pm 0.16 \text{ ppbv h}^{-1}$), while the homogeneous reaction of $\text{HONO} + \text{OH}$ ($0.008 \pm 0.012 \text{ ppbv h}^{-1}$) and HONO uptake on the aerosol surfaces ($0.008 \pm 0.006 \text{ ppbv h}^{-1}$) were insignificant.

We also made an attempt to obtain a time resolved HONO budget on an hourly basis, although the results are not satisfactory
595 for all the hours at night, with obvious differences between observed and calculated rates of HONO variation, e.g., at 22:00 and from 2:00 to 5:00 (Fig. S6). This is well expected considering much more amplified uncertainties associated with hourly variabilities of various quantities, which can be considerably reduced by averaging all hours. This is why subtle and careful data filtering is necessary when nighttime HONO chemistry is examined in detail (Wong et al., 2011). Such a granular analysis is more appropriate for the daytime when HONO lifetime is much shorter and uncertainties affecting the
600 interpretation of HONO chemistry (e.g., emission and transport) are much muted. As a matter of fact, because the rate of HONO change shown in Fig. S6 is a first order derivative of the HONO concentration itself, one can expect that HONO concentrations from each source would show greater variations, making it more difficult to compare on an hourly basis. Another challenge is that since those parameters used for calculating HONO source strengths have a range in their estimates (Table S5), the HONO source strengths also have a wide range individually, and therefore there are numerous possible
605 combinations of these sources with different strengths and rankings to close the budget.

The comparison and ranking of sources considering variability and uncertainty becomes less straightforward than ranking nighttime average source strengths (Fig. 5). Among the three largest sources, both primary (non-soil) emission and NO_2 heterogeneous source on ground showed an evening peak and decreased toward after midnight. The $\text{NO} + \text{OH}$ source showed a different trend with its lowest level in the evening, making it the smallest source among the three at that time. Although the
610

615 NO_2 heterogeneous source on ground appeared the largest with its median parameter value, it also had the largest range of estimate, suggesting that its importance is more uncertain compared to the other sources. On the other hand, the other two minor sources, i.e., the NO_2 heterogeneous source on aerosols and soil emission are unlikely more important than these three sources given their ranges of low estimates. The variability and uncertainty of dry deposition are largely dependant on other terms of sources and sinks since it is derived as a final term to balance the budget.



620 **Figure 5.** The nocturnal variation of the terms of HONO budget (a) primary emission from vehicle exhaust, (b) homogeneous reaction of $\text{NO} + \text{OH}$, (c) heterogeneous conversion of NO_2 on ground surfaces, (d) heterogeneous conversion of NO_2 on aerosol surfaces, (e) soil emission and HONO loss from (f) dry deposition, (g) dilution, (h) uptake on aerosols, (i) $\text{HONO} + \text{OH}$ during Sep. 27–Nov. 9 2018 in Guangzhou. The black line is the HONO production rates with the median values of parameters, and the grey shadow represents their lower and upper limits.

3.3 Daytime HONO budget and unknown sources analysis

625 3.3.1 Budget analysis

In this section, ~~we move on to a detailed budget analysis for HONO during the daytime, when chemistry is distinctly different from at night. Similar to the nighttime analysis by invoking different terms for the daytime chemistry, we concentrate on the daytime chemistry of HONO by a detailed budget analysis.~~ The time variation of HONO concentration at our site can be related to its sources and sinks as follows:

630

$$\frac{\partial[\text{HONO}]}{\partial t} = P_{\text{HONO}} - L_{\text{HONO}} = (P_{\text{OH}+\text{NO}} + P_{\text{Unknown}} + P_{\text{emis}} + P_{\text{soil}} + T_{\text{V}} + T_{\text{H}}) - (L_{\text{OH}+\text{HONO}} + L_{\text{Phot}} + L_{\text{Dep}}) \quad (139)$$

where $\partial[\text{HONO}]/\partial t$ represents the time variation of HONO; P_{HONO} and L_{HONO} are the sources and sinks of HONO, respectively; $P_{\text{OH}+\text{NO}}$ and $L_{\text{OH}+\text{HONO}}$ are the homogeneous HONO formation and loss rates in Reactions R2 and R3, respectively; P_{Unknown} is the HONO production rate from unknown sources; T_{V} and T_{H} are two terms representing vertical and horizontal transport processes, respectively; L_{Phot} denotes the photolysis loss rate of HONO, which can be calculated with $L_{\text{Phot}} = J(\text{HONO}) \times [\text{HONO}]$; ~~deposition loss rate of HONO~~ L_{Dep} ~~represents the deposition loss rate of HONO and can be calculated by Eq. (10), as $L_{\text{Dep}} = V_{\text{d}} \times [\text{HONO}]/H$, where V_{d} is the deposition velocity of HONO and H is the daytime mixing height.~~ Assuming a daytime V_{d} of 1.6 cm s^{-1} (Hou et al., 2016; Li et al., 2011) and an daytime mixing height (H) of 640 1000 m (Liao et al., 2018; Song et al., 2019), the average L_{Dep} is $0.003 \pm 0.001 \text{ ppbv h}^{-1}$, three orders of magnitude smaller than L_{Phot} and therefore can be ignored in the following discussion.

OH was not measured and was calculated with a parameterized approach based on strong correlation between observed OH radicals and $J(\text{O}^1\text{D})$. The parameterization was first proposed by Rohrer and Berresheim (2006) and has been applied by 645 several studies in China (Lu et al., 2013; Lu et al., 2012; Lu et al., 2014). In this study, OH was estimated with observed $J(\text{O}^1\text{D})$ along with parameters from fitting the observed OH radicals and $J(\text{O}^1\text{D})$ data in Guangzhou Back Garden by Lu et al. (2012). The daytime maximum OH concentration was estimated to be $1.3 \times 10^7 \text{ cm}^{-3}$, which is slightly smaller than the daily peak values of $1.5\text{--}2.6 \times 10^7 \text{ cm}^{-3}$ observed in summer of Guangzhou by Lu et al. (2012). And the estimated daily average OH concentration is $6.7 \times 10^6 \text{ cm}^{-3}$, close to $7.5 \times 10^6 \text{ cm}^{-3}$ measured in the PRD region in autumn of 2014 by Yang et al. 650 (2017b). Daytime P_{emis} was calculated based on the method (3) (mentioned in Sect. 3.2.1). Because the HONO lifetime was in the order of 20 min under typical daytime conditions (Stutz et al., 2000) and the transport distance is only a few kilometers, the NO_x emission rate extracted from the $3 \text{ km} \times 3 \text{ km}$ grid cell centred around sampling site is used to calculate the impact of primary emission on HONO.

655 To minimize interferences, we choose a period from 9:00 to 15:00 with intense solar radiation and a short HONO lifetime. Horizontal transport T_H was assumed negligible by selecting the cases with low wind speed (Su et al., 2008b; Yang et al., 2014). The magnitude of vertical transport T_V can be estimated by using a parameterization for dilution by background air according to Dillon et al. (2002), i.e. $T_V = k_{(\text{dilution})} \times ([\text{HONO}] - [\text{HONO}]_{\text{background}})$. Where $k_{(\text{dilution})}$ is the dilution rate, $[\text{HONO}]_{\text{background}}$ represents the background HONO concentration. Assuming a $k_{(\text{dilution})}$ of 0.23 h^{-1} (Dillon et al., 2002; Sörgel et al., 2011a), a $[\text{HONO}]_{\text{background}}$ value of 10 pptv (Zhang et al., 2009), and taking the mean noontime $[\text{HONO}]$ value of 400 pptv in this study, a value of about 0.09 ppbv h^{-1} can be derived, which is much smaller than L_{Phot} and can be ignored in the following discussion. The average daytime HONO emission rate from soil P_{soil} varied from 0.002 to 0.007 with a mean value of 0.004 ± 0.002 ppbv h^{-1} , which is three orders of magnitude smaller than L_{Phot} , and can also be ignored in the following discussion. As a result, P_{Unknown} can be expressed by Eq. (149), in which $\partial[\text{HONO}]/\partial t$ is substituted by

665 $\Delta[\text{HONO}]/\Delta t$.

$$\frac{\Delta[\text{HONO}]}{\Delta t} = (P_{\text{OH+NO}} + P_{\text{emis}} + P_{\text{Unknown}}) - (L_{\text{OH+HONO}} + L_{\text{Phot}}) \quad (149)$$

Figure 67 shows the budget of HONO from 9:00 to 15:00. As expected, photolysis HONO L_{Phot} ($1.58 \pm 0.82 \text{ ppbv h}^{-1}$) is the main loss pathway in the day, followed by a small contribution by the homogeneous reaction of $\text{HONO} + \text{OH}$ ($L_{\text{OH+HONO}}$, $0.07 \pm 0.03 \text{ ppbv h}^{-1}$). Among the sources, $P_{\text{OH+NO}}$ and P_{Unknown} were comparable in magnitudes, with an average of $0.79 \pm 0.61 \text{ ppbv h}^{-1}$ and $0.65 \pm 0.46 \text{ ppbv h}^{-1}$, respectively. P_{Unknown} showed a photo-enhanced feature, reaching its maximum at 12:00 at 0.97 ppbv h^{-1} , similar to the observations in Xinken (Su et al., 2008b), Beijing (Yang et al., 2014), Wangdu (Liu et al., 2019a), Changzhou (Zheng et al., 2020) and Cyprus (Meusel et al., 2016). The average of P_{Unknown} is comparable to the observation in Back Garden (0.77 ppbv h^{-1}) by Li et al. (2012), but smaller than those in Xinken ($\approx 2.0 \text{ ppbv h}^{-1}$) by Su et al. (2008b) and Guangzhou city area (1.25 ppbv h^{-1}) by Yang et al. (2017a). Homogeneous reaction of $\text{NO} + \text{OH}$ reached its maximum in the early morning, and contributed the most fraction in the whole day. Apparently, high NO concentrations at our site made $P_{\text{OH+NO}}$ the biggest daytime source of HONO, exceeding P_{Unknown} , similar to other high-NOx sites such as Santiago de Chile (Elshorbany et al., 2009), London (Heard et al., 2004), Paris (Michoud et al., 2014), Beijing (Liu et al., 2021; Slater et al., 2020; Zhang et al., 2019b; Liu et al., 2020c), Taiwan (Lin et al., 2006) and Hebei (Xue et al., 2020). Next, we investigate possible factors relating to P_{Unknown} .

670
675
680

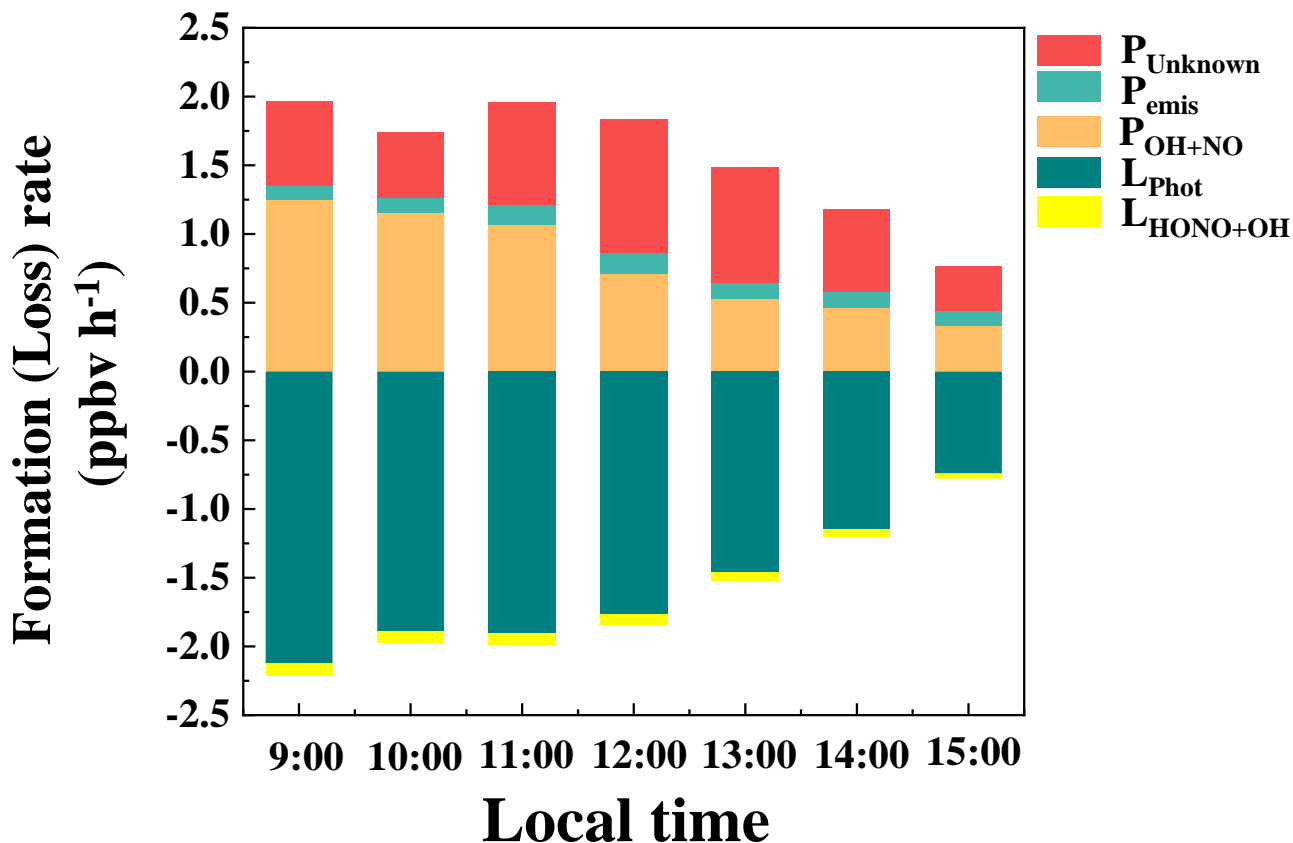


Figure 67. Items of the HONO budget (Eq. (14)) in Guangzhou during the observation period.

Figure 78 shows the correlation between P_{Unknown} and NO_2 and $J(\text{NO}_2)$ was 0.0681 and 0.2713, respectively. The correlation between P_{Unknown} and $\text{NO}_2 \times J(\text{NO}_2)$ further improved to 0.4116, indicating that P_{Unknown} may be related to the photo-enhanced reaction of NO_2 (Jiang et al., 2020; Li et al., 2018a; Liu et al., 2019a; Liu et al., 2019b; Su et al., 2008b; Zheng et al., 2020; Huang et al., 2017).

3.3.2 Possible mechanisms for daytime HONO production

No correlation was found between P_{Unknown} and $\text{PM}_{2.5}$ ($R^2 = 0.00014$), indicating that particulate matters may not be a key factor in daytime HONO production (Wong et al., 2012; Li et al., 2018a; Sörgel et al., 2011a; Wang et al., 2017a; Zheng et al., 2020). Meanwhile, the correlations between P_{Unknown} and nitrate in PM_1 and the sum of gaseous nitric acid and nitrate in PM_1 were very low, with R^2 of 0.0348 and 0.0062 respectively. And the correlation between P_{Unknown} and the product of nitrate and $J(\text{NO}_2)$ was also poor $R^2 = 0.0007$, which does not relate P_{Unknown} to the photolysis of nitrate or gaseous nitric acid. Wang et al. (2016) and Ge et al. (2019) suggested that NH_3 can efficiently promote the reaction of NO_2 and SO_2 to form

695 HONO and sulfate. However, we did not find good correlations for P_{Unknown} vs. NH_3 , P_{Unknown} vs. SO_2 , or P_{Unknown} vs. $\text{NH}_3 \times \text{SO}_2$.

In summary, at our site with relatively strong traffic impact and high NO , $\text{NO} + \text{OH}$ appears to be the largest daytime HONO source followed by an unknown photolytic source, which does not seem to be related to aerosols, nor the photolysis of
 700 nitrate/nitric acid, nor the reaction between NO_2 , SO_2 and NH_3 .

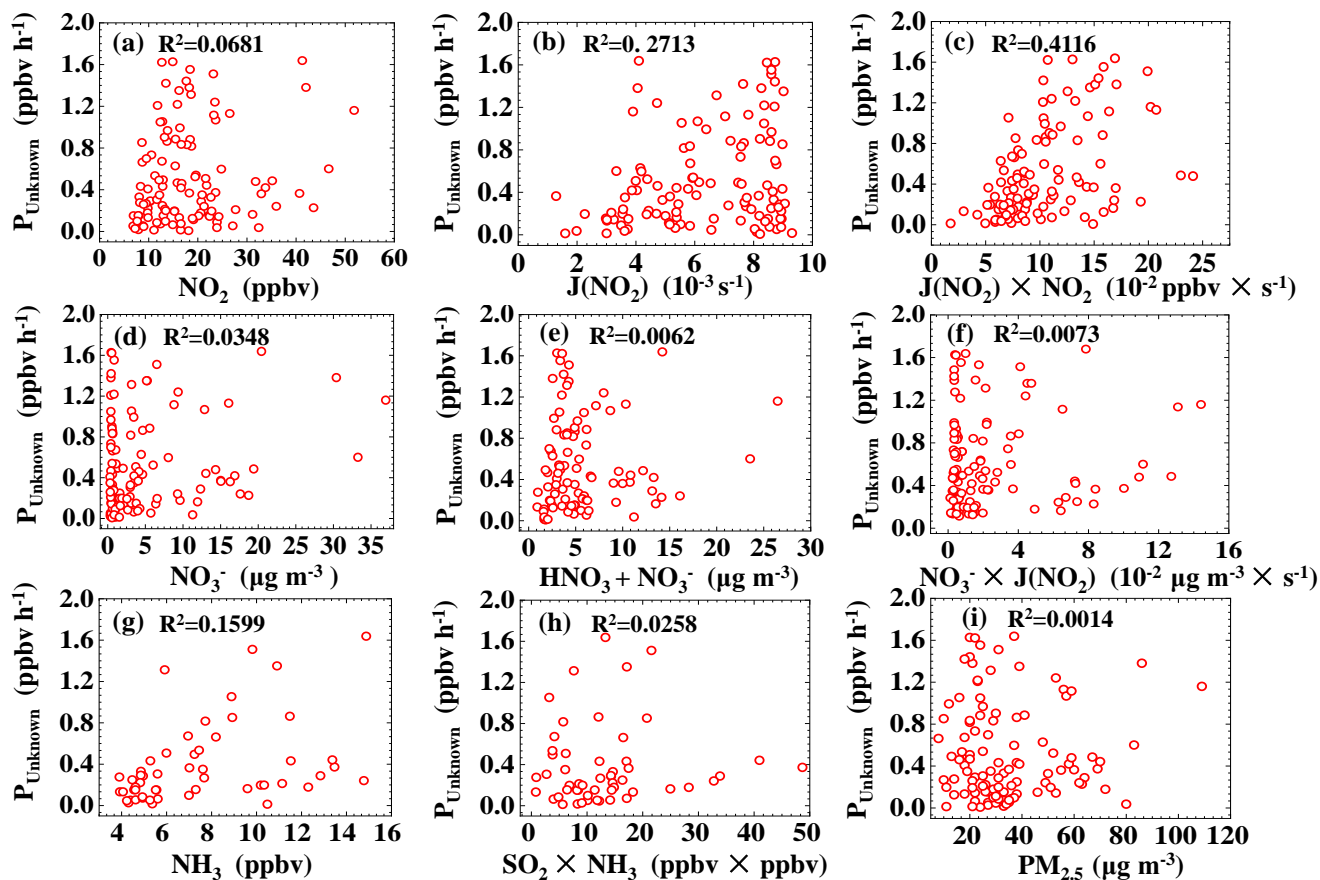


Figure 78. Correlations between daytime HONO unknown sources P_{Unknown} and related parameters.

3.4 The contribution of HONO, O_3 and ozonolysis of alkenes to OH

705 Photolysis of HONO and O_3 contribute dominant the primary source of OH radicals. Ozonolysis of alkenes was found to be important source of OH (Heard et al., 2004; Elshorbany et al., 2009; Tan et al., 2019b). Here we evaluated and compared the contribution of the three pathways. Other sources such as the photolysis of peroxides, is usually not very significant in urban areas, especially during daytime, thus was not considered in this study (Li et al., 2018a; Shi et al., 2020b). The contribution

of HCHO photolysis to OH was also not considered due to the lack of measurement for HCHO. The OH radicals' production rate from HONO photolysis $P_{\text{OH(HONO)}}$ can be calculated from the measured photolysis frequencies and the mixing ratios of HONO using Eq. (11). The net OH radicals' production from HONO $P_{\text{(HONO-OH)}}$ can be calculated by subtracting the OH loss caused by Reactions R1 and R2 from $P_{\text{OH(HONO)}}$ (Eq. (12)). The OH radicals' production rate from O_3 photolysis $P_{\text{(O}_3\text{-OH)}}$ can be calculated from Eq. (13). Only part of $\text{O}(^1\text{D})$ atoms, formed through the photolysis of O_3 at solar radiation below 320 nm (Reaction R4), can generate OH radicals by reacting with water vapor (Reaction R5) in the atmosphere, so we used the absolute mixing ratio of water vapor, which can be derived from the temperature and relative humidity data, to calculate the fraction of OH (Φ_{OH}) between Reactions R5 and R6. The reaction rate of $\text{O}(^1\text{D})$ with N_2 and O_2 is $3.1 \times 10^{-11} \text{ cm}^3 \cdot \text{s}^{-1}$ and $4.0 \times 10^{-11} \text{ cm}^3 \cdot \text{s}^{-1}$ respectively (Seinfeld and Pandis, 2016). In Eq. (15), $k_{\text{alkenes(i)+O}_3}$ represents the reaction rate constant for the reaction of O_3 with alkene (i), and Y_{OH_i} represents the yield of OH from the gas phase reaction of O_3 and alkene (i). Table S6 summarized the reaction rate constant of O_3 with alkenes at 298 K and the yields of OH.

$$P_{\text{OH(HONO)}} = J(\text{HONO})[\text{HONO}] \quad (11)$$

$$P_{\text{(HONO-OH)}} = P_{\text{OH(HONO)}} - k_{\text{NO+OH}}[\text{NO}][\text{OH}] - k_{\text{HONO+OH}}[\text{HONO}][\text{OH}] \quad (12)$$

$$P_{\text{(O}_3\text{-OH)}} = 2\Phi_{\text{OH}}[\text{O}_3]J(\text{O}^1\text{D}) \quad (13)$$

$$\Phi_{\text{OH}} = k_5[\text{H}_2\text{O}] / (k_5[\text{H}_2\text{O}] + k_6[\text{M}]) \quad (14)$$

$$P_{\text{(O}_3\text{+alkenes)-OH}} = \sum k_{\text{alkenes(i)+O}_3}[\text{alkenes(i)}][\text{O}_3] Y_{\text{OH}_i} \quad (15)$$



Figure 9 shows that $P_{\text{(HONO-OH)}}$ was larger than $P_{\text{(O}_3\text{-OH)}}$ before 10:00, while the latter became always higher with the solar radiation enhanced after 10:00. Both the two sources of OH reached their maximum around 12:00, while $P_{\text{(O}_3\text{-OH)}}$ was approximately two times of that of $P_{\text{(HONO-OH)}}$. On average, the OH production rates by photolysis of HONO and O_3 were $3.7 \times 10^6 \text{ cm}^3 \cdot \text{s}^{-1}$ and $4.9 \times 10^6 \text{ cm}^3 \cdot \text{s}^{-1}$, respectively. In daytime, the sum of OH production rates by ozonolysis of alkenes was $3 \times 10^5 \text{ cm}^3 \cdot \text{s}^{-1}$, which is much smaller than that of HONO and O_3 . This value ($3 \times 10^5 \text{ cm}^3 \cdot \text{s}^{-1}$) was comparable to the results in previous studies (Kim et al., 2014; Ge et al., 2021; Martinez et al., 2003; Ren et al., 2003; Lee et al., 2016; Aliche et al., 2002; Kleffmann et al., 2005; Ren et al., 2013), but smaller than some other studies (Shi et al., 2020b; Zheng et al., 2020; Heard et al., 2004). Table 2 summarizes the OH production rate from HONO and O_3 photolysis from previous studies worldwide. It can be seen that $P_{\text{(HONO-OH)}}$ are larger than $P_{\text{(O}_3\text{-OH)}}$ in most of the observations, but sometimes the opposite is reported. Apparently, the relative importance of $P_{\text{(HONO-OH)}}$ and $P_{\text{(O}_3\text{-OH)}}$ strongly depends on the ratio of HONO/ O_3 .

740 Especially in winter, photolysis of HONO tends to be the predominant OH source due to the low concentration of O₃ and water vapor.

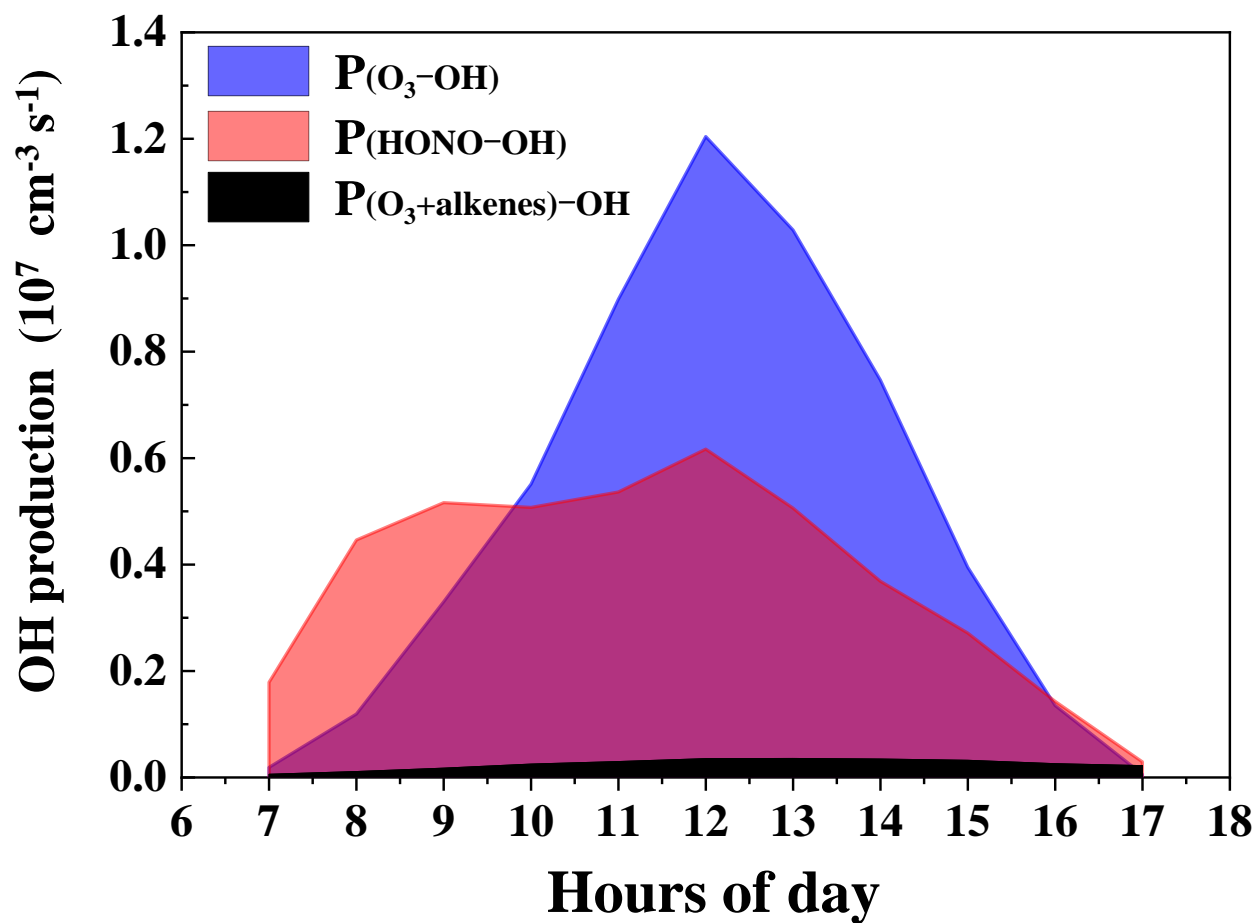


Figure 9. The yield and comparison of OH radicals by HONO, O₃ and ozonolysis of alkenes.

Location	Date	—Season	$P_{(\text{HONO-OH})}$ (ppbv h ⁻¹)	$P_{(\text{O}_3\text{-OH})}$ (ppbv h ⁻¹)	Reference
New York, USA	Jun–Jul 1998	Summer	0.10	0.22	1
Nashville, USA	Jun–Jul 1999	Summer	0.29	0.33	2
Birmingham, UK	Jan–Feb 2000	Winter	0.45	0.01	3
New York, USA	Jun–Aug 2001	Summer	0.81	0.19	4
Santiago, Chile	May–Jun 2005	Winter	2.90	0.01	5
	Mar 2005	Summer	1.70	0.13	
El Arenosillo, Spain	Dec 2008	Winter	0.11	0.09	6
Colorado, USA	Feb–Mar 2011	Winter	0.45	0.04	7
Beijing, China	Sep–Oct 2004	Autumn	1.31	0.18	8
Xinken, China	Oct–Nov 2004	Autumn	3.66	0.88	9
Back Garden, China	Jul 2006	Summer	1.32	2.20	10
Yufa, China	Aug 2006	Summer	1.68	0.38	11
Tung Chung, China	Aug 2011	Summer	1.50	0.90	12
Wangdu, China	Jun 2014	Summer	1.68	1.20	13
Hong Kong, China	Mar–May 2015	Spring	6.40	a	14
Changzhou, China	Dec 2015	Winter	1.04	0.36	15
	Oct 2015	Autumn	1.24	0.41	
Guangzhou, China	Jul 2016	Summer	0.71	0.44	16
	Aug 2016	Summer	1.88	0.63	
Jinan, China	Apr 2017	Spring	1.66	2.78	18
Changzhou, China	Dec 2017	Winter	0.52	0.02	19
	Mar–Apr 2018	Spring	0.51	0.18	
Nanjing, China	Nov–Nov 2017/2018	A year	1.16	0.41	20
Gucheng, China	Jan–Feb 2018	Winter	1.40	0.01	21
Guangzhou, China	Sep–Nov 2018	Autumn	0.54	0.72	22

a: far less than $P_{(\text{HONO-OH})}$

Reference: 1. Zhou et al. (2002a); 2. Martinez et al. (2003); 3. Heard et al. (2004); 4. Ren et al. (2003); 5. Elshorbany et al. (2010); 6. Sörgel et al. (2011a); 7. Kim et al. (2014); 8. An et al. (2009); 9. Su et al. (2008b); 10. Su (2008); 11. Yang et al. (2014); 12. Xue et al. (2016); 13. Liu et al. (2019a); 14. Yun et al. (2017); 15. Zheng et al. (2020); 16. Yang et al. (2017a); 17. Li et al. (2018a); 18. Shi et al. (2020a); 19. Jiang et al. (2020); 20. Liu et al. (2019b); 21. (Li in preparation); 22. This study

3.5 Box model simulation of HONO impact on atmospheric oxidation capacity

755 Atmospheric oxidation capacity refers to the total removal rates of CO and VOCs by major oxidants (e.g., OH, NO₃ and O₃) (Elshorbany et al., 2010; Xue et al., 2016; Tan et al., 2019b). As the primary oxidant in the atmosphere, the OH concentration is widely used to quantitatively describe the atmospheric oxidation capacity (Zheng et al., 2020; Liu et al., 2021; Shi et al., 2020b; Zhang et al., 2019a). And ozone is another indicator of atmospheric oxidation capacity. A box model (MCMv3.3.1) was conducted to simulate OH and O₃ concentrations with and without HONO constrained with observational data. Figure S5 shows the time series of measured and simulated O₃ concentrations. The model performance was evaluated to be good by the index of agreement (IOA) (see Supplementary information). It should be noted that the box model ignores the influence of transport and convection, so the simulated O₃ concentration does not represent the actual O₃ concentration in
760 the atmosphere.

The time series of simulation results of O₃ and OH can be found in Fig. S6. Figure 10 shows diurnal variations of simulated O₃ and OH with and without HONO constrained. Daytime maximum OH concentration with HONO ($6.1 \times 10^6 \text{ cm}^{-3}$) was simulated to be 59% higher than the simulation without HONO ($3.9 \times 10^6 \text{ cm}^{-3}$), and the daily maximum concentration of O₃ with HONO (43.2 ppbv) was simulated to be 68.8% higher than the simulation without HONO (25.6 ppbv). These results are
765 both within the range of prior studies (Elshorbany et al., 2012; Fu et al., 2019; Gil et al., 2021; Liu et al., 2021; Malkin et al., 2016; Xue et al., 2020; Yang et al., 2021a; Yun et al., 2017; Zhang et al., 2016), suggesting a strong HONO enhancement effect on atmospheric oxidation capacity. In addition, the impact of HONO on O₃ appeared two hours later than on OH, likely reflecting that HO₂ and RO₂, which are key proxy radicals in O₃ production were not significantly higher during early
770 morning hours, despite higher HONO and OH.

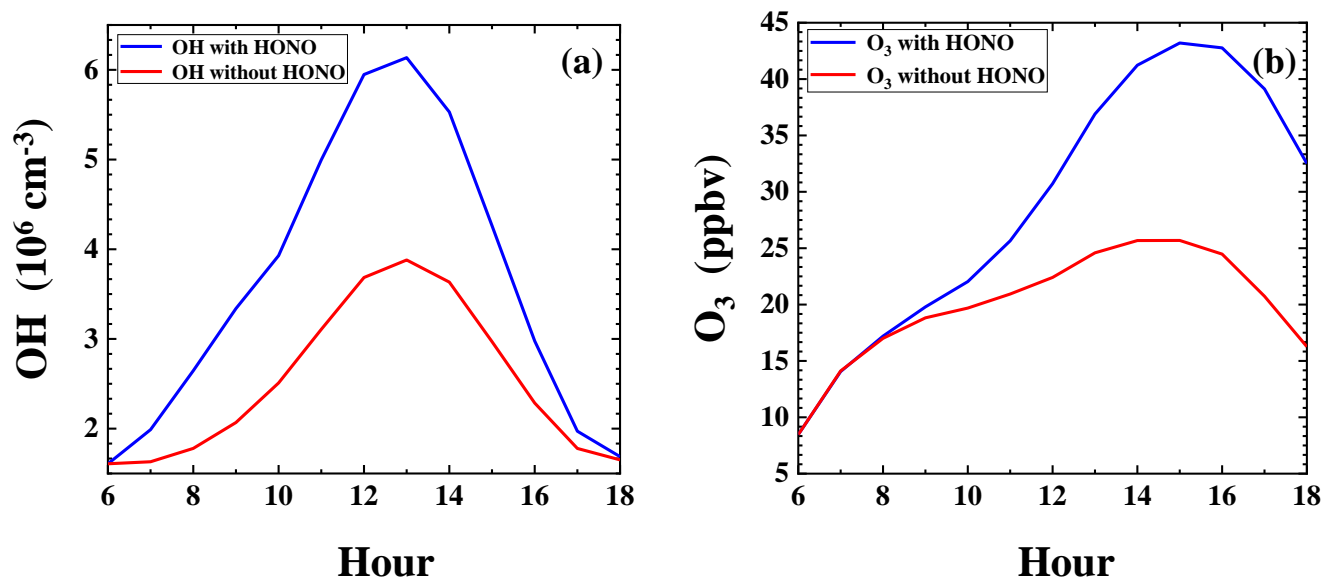


Figure 10. The diurnal variations of simulated O_3 and OH output with and without the HONO constrained in model.

4 Conclusions

775 Nitrous acid (HONO) was measured with a custom built LOPAP instrument, along with meteorological parameters and
 other atmospheric constituents at an urban site in Guangzhou in Pearl River Delta from 27 September to 9 November 2018.
 The HONO concentrations varied from 0.02 to 4.43 ppbv with an average of 0.74 ± 0.70 ppbv. Compared to prior
 measurements in Guangzhou, a decreasing trend of HONO can be seen along with improved air quality in the city over the
 past decade. The emission ratios (HONO/NO_x) were derived from an analysis of 11 fresh plumes, varying from 0.1% to 1.5%
 780 with an average value of $0.9\% \pm 0.4\%$. Using this estimated emission ratio and an estimate of NO_x emission rate extracted
 from a grid cell around our site in a high resolution (3 km × 3 km) NO_x emission inventory, we estimated a primary HONO
 emission rate of 0.30 ± 0.15 ppbv h⁻¹, which turned out far larger (almost by an order of magnitude) than what would be
 estimated with a city level NO_x emission estimate, which does not adequately represent NO_x emission rate specifically for
 the observation site. Thus, for future analysis of HONO data to properly estimate direct emission of HONO, we suggest that
 785 high quality emission data be used to reduce uncertainty. This is especially crucial for a site that receives nearby traffic
 emissions like ours. HONO produced by the homogeneous reaction of OH + NO at night was 0.26 ± 0.08 ppbv h⁻¹, which
 can be seen as secondary results from primary emission. They were both much higher than the observed increase rate of
 HONO (0.02 ppbv h⁻¹) during the night. Nighttime soil emission rate was calculated to be 0.019 ± 0.001 ppbv h⁻¹, which is
 comparable to the observed increase rate of HONO during night, thus further demonstrating the importance of direct
 790 emissions. In order to balance the nighttime HONO budget and assuming dry deposition to be the principle loss process, a
 dry deposition rate of at least 1.8 cm s^{-1} is required. Correlation analysis shows that the heterogeneous reaction of NO₂

795 related to NH_3 and RH may contribute to the nighttime HONO formation. Daytime HONO budget analysis revealed that in order to sustain the observed HONO concentration around 450 pptv despite fast photolysis of HONO, an additional unknown source production rate (P_{Unknown}) of 0.65 ± 0.46 ppbv h^{-1} was needed, in addition to the primary emission P_{emis} at 0.12 ± 0.01 ppbv h^{-1} , and the homogenous reaction source $P_{\text{OH+NO}}$ at 0.79 ± 0.61 ppbv h^{-1} . It is worth noting that the homogenous HONO source by $\text{NO} + \text{OH}$ appeared to be a stronger source of HONO than the unknown source (P_{Unknown}), because of high levels of NO at our site. Correlation analysis between P_{Unknown} and proxies of different mechanisms showed that P_{Unknown} appeared to be photo-enhanced, and yet the mechanism remains unclear. Aerosols should not be as important as ground as a heterogeneous reaction media, as very weak correlation between P_{Unknown} and $\text{PM}_{2.5}$. Moreover, no correlations were found
800 between P_{Unknown} and nitrate/ HNO_3 , NH_3 , SO_2 . We assessed the role of HONO in the production of OH and O_3 by calculating OH production rate as well as by simulating the chemistry with a box model (MCMv3.3.1). The average net formation rate of OH attributed to HONO, O_3 and ozonolysis of alkenes was $3.7 \times 10^6 \text{ cm}^{-3} \text{ s}^{-1}$, $4.9 \times 10^6 \text{ cm}^{-3} \text{ s}^{-1}$ and $3 \times 10^5 \text{ cm}^{-3} \text{ s}^{-1}$, respectively. Box model simulations confirmed strong HONO enhancement effect on OH and O_3 by 59% and 68.8%, respectively.

805 Nitrous acid (HONO) was measured with a custom-built LOPAP instrument, along with meteorological parameters and other atmospheric constituents at an urban site in Guangzhou in Pearl River Delta from 27 September to 9 November 2018. The HONO concentrations varied from 0.02 to 4.43 ppbv with an average of 0.74 ± 0.70 ppbv. Compared to prior measurements in Guangzhou, a decreasing trend of HONO can be seen along with improved air quality in the city over the past decade.

810

We have investigated budget of HONO at this site using these data and our key findings are summarized as follows.

We found that the emission ratios (HONO/NO_x) derived from an analysis of 11 fresh plumes varied from 0.1% to 1.5% with an average value of $0.9\% \pm 0.4\%$. Using this estimated emission ratio and an estimate of NO_x emission rate extracted from a grid cell around our site in a high-resolution (3 km \times 3 km) NO_x emission inventory, we estimated a primary HONO emission rate of 0.30 ± 0.15 ppbv h^{-1} , which turned out far larger (almost by an order of magnitude) than what would be estimated with a city-level NO_x emission estimate, which does not adequately represent NO_x emission rate specifically for the observation site. Thus, for future analysis of HONO data to properly estimate direct emission of HONO, we suggest that high quality emission data be used to reduce uncertainty. This is especially crucial for a site that receives nearby traffic emissions like ours.

820

HONO produced by the homogeneous reaction of $\text{NO} + \text{OH}$ at night was 0.14 ± 0.30 ppbv h^{-1} , which represents a secondary HONO source. Another major secondary HONO source at night is heterogeneous conversion of NO_2 on ground surface (0.27 ± 0.13 ppbv h^{-1}). Correlation analysis shows that the heterogeneous reaction of NO_2 related to NH_3 and RH may contribute to the nighttime HONO formation. These two secondary sources and the primary emission from vehicle exhaust (between

825

830 0.04 ± 0.02 ppbv h^{-1} and 0.30 ± 0.15 ppbv h^{-1} with a median value of 0.16 ± 0.07 ppbv h^{-1} were found to be the three largest sources of HONO at night. Because of the large range of those parameter values assumed in their calculations (e.g., the NO_2 uptake coefficient that spans two orders of magnitude), the relative importance of the three major sources depend on these assumptions. Soil emission (0.019 ± 0.009 ppbv h^{-1}) and heterogeneous NO_2 conversion on the aerosol surfaces (0.03 ± 0.02 ppbv h^{-1}) were two other minor sources. Our calculations suggested that dilution acted as a major sink (0.18 ± 0.16 ppbv h^{-1}), while loss of HONO on the aerosol surfaces played a much less important role. In order to balance the nighttime HONO budget and assuming dry deposition to be responsible for the remaining amount of HONO loss, a dry deposition rate of 2.5 cm s^{-1} is required, equivalent to a loss rate of 0.41 ± 0.31 ppbv h^{-1} .

835 Daytime HONO budget analysis revealed that in order to sustain the observed HONO concentration around 450 pptv despite fast photolysis of HONO, an additional unknown source production rate (P_{Unknown}) of 0.65 ± 0.46 ppbv h^{-1} was needed, in addition to primary emission P_{emis} at 0.12 ± 0.02 ppbv h^{-1} , and the homogenous reaction source $P_{\text{OH+NO}}$ at 0.79 ± 0.61 ppbv h^{-1} . It is worth noting that the homogenous HONO source by $\text{NO} + \text{OH}$ appeared to be a stronger source of HONO than the unknown source (P_{Unknown}), because of high levels of NO at our site. Correlation analysis between P_{Unknown} and proxies of different mechanisms showed that P_{Unknown} appeared to be photo-enhanced, and yet the mechanism remains unclear. Aerosols did not appear to be as important as ground as a heterogenous reaction media, as suggested by the weak correlation between P_{Unknown} and $\text{PM}_{2.5}$. No correlations were found between P_{Unknown} and nitrate/ HNO_3 , NH_3 , SO_2 .

845 Overall, these results from our study offer a unique perspective on HONO at an urban site receiving heavy traffic emissions in the PRD region. Our budget calculations and comprehensive uncertainty analysis suggest that at such locations as ours, HONO direct emissions and $\text{NO} + \text{OH}$ can become comparable or even surpass other HONO sources that typically receive greater attention and interest, such as the NO_2 heterogenous source and the unknown daytime photolytic source. Our findings emphasize the need to reduce the uncertainties of both conventional and novel HONO sources and sinks to advance our understanding of this important source of atmospheric OH.

850

Data availability

~~HONO data, other trace gases data and meteorological data are available upon request from the corresponding author.~~ The data used in this study are available from the corresponding author upon request (chengp@jnu.edu.cn).

Contribution

- 855 ~~Yihang Yu: Validation, Formal analysis, Writing—Original Draft, Visualization. Peng Cheng: Conceptualization, Methodology, Writing—Review & Editing, Supervision, Project administration, Funding acquisition. Huirong Li: Validation, Formal analysis, Investigation, Data Curation. Wenda Yang: Software, Investigation, Data Curation. Baobin Han: Investigation. Wei Song: Resources. Weiwei Hu: Resources. Xinming Wang: Resources. Bin Yuan: Resources. Min Shao: Resources. Zhijiong Huang: Resources. Zhen Li: Resources. Junyu Zheng: Resources. Haichao Wang: Writing—~~
860 ~~Review & Editing. Xiaofang Yu: Investigation. Peng Cheng organized the field campaign. Yihang Yu and Huirong Li analyzed the data and wrote the paper. All authors contributed to measurements, discussing results, and commenting on the paper. Yihang Yu and Peng Cheng contributed equally to this work.~~

Competing interests

- 865 The authors declare that they have no conflict of interest.

Acknowledgments

- This work was funded by the National Key Research and Development Program of China (grant nos. 2018YFC0213904, 2017YFC0210104), Science and Technology Plan Projects in Guangzhou (grant no. 201804010115), the Guangdong Natural Science Funds for Distinguished Young Scholar (grant no. 2018B030306037), the Guangdong Innovative and
870 Entrepreneurial Research Team Program (grant no. 2016ZT06N263), and the Special Fund Project for Science and Technology Innovation Strategy of Guangdong Province (grant no. 2019B121205004).

References

- Acker, K., Spindler, G., and Brüggemann, E.: Nitrous and nitric acid measurements during the INTERCOMP2000 campaign in Melpitz, Atmospheric Environment, 38, 6497-6505, <https://doi.org/10.1016/j.atmosenv.2004.08.030>, 2004.
- 875 Acker, K., Febo, A., Trick, S., Perrino, C., Bruno, P., Wiesen, P., Möller, D., Wierprecht, W., Auel, R., Giusto, M., Geyer, A., Platt, U., and Allegrini, I.: Nitrous acid in the urban area of Rome, Atmospheric Environment, 40, 3123-3133, <https://doi.org/10.1016/j.atmosenv.2006.01.028>, 2006.
- Alicke, B., Platt, U., and Stutz, J.: Impact of nitrous acid photolysis on the total hydroxyl radical budget during the Limitation of Oxidant Production/Pianura Padana Produzione di Ozono study in Milan, Journal of Geophysical Research: Atmospheres, 107, 8196, <https://doi.org/10.1029/2000JD000075>, 2002.
- 880 Alicke, B., Geyer, A., Hofzumahaus, A., Holland, F., Konrad, S., Pätz, H. W., Schäfer, J., Stutz, J., Volz-Thomas, A., and Platt, U.: OH formation by HONO photolysis during the BERLIOZ experiment, Journal of Geophysical Research: Atmospheres, 108, 8247, <https://doi.org/10.1029/2001JD000579>, 2003.

- 885 Ammann, M., Kalberer, M., Jost, D. T., Tobler, L., Rössler, E., Piguet, D., Gäggeler, H. W., and Baltensperger, U.: Heterogeneous production of nitrous acid on soot in polluted air masses, *Nature*, 395, 157-160, <https://doi.org/10.1038/25965>, 1998.
- Ammar, R., Monge, M. E., George, C., and D'Anna, B.: Photoenhanced NO₂ Loss on Simulated Urban Grime, *ChemPhysChem*, 11, 3956-3961, <https://doi.org/10.1002/cphc.201000540>, 2010.
- 890 An, J., Zhang, W., and Qu, Y.: Impacts of a strong cold front on concentrations of HONO, HCHO, O₃, and NO₂ in the heavy traffic urban area of Beijing, *Atmospheric Environment*, 43, 3454-3459, <https://doi.org/10.1016/j.atmosenv.2009.04.052>, 2009.
- Arens, F., Gutzwiller, L., Baltensperger, U., Gäggeler, H. W., and Ammann, M.: Heterogeneous Reaction of NO₂ on Diesel Soot Particles, *Environmental Science & Technology*, 35, 2191-2199, <https://doi.org/10.1021/es000207s>, 2001.
- 895 Aubin, D. G., and Abbatt, J. P. D.: Interaction of NO₂ with Hydrocarbon Soot: Focus on HONO Yield, Surface Modification, and Mechanism, *The Journal of Physical Chemistry A*, 111, 6263-6273, <https://doi.org/10.1021/jp068884h>, 2007.
- Bejan, I., Abd-el-Aal, Y., Barnes, I., Benter, T., Bohn, B., Wiesen, P., and Kleffmann, J.: The photolysis of ortho-nitrophenols: a new gas phase source of HONO, *Phys Chem Chem Phys*, 8, 2028-2035, <http://dx.doi.org/10.1039/B516590C>, 2006.
- 900 Brigante, M., Cazor, D., D'Anna, B., George, C., and Donaldson, D. J.: Photoenhanced Uptake of NO₂ by Pyrene Solid Films, *The Journal of Physical Chemistry A*, 112, 9503-9508, <https://doi.org/10.1021/jp802324g>, 2008.
- Bröske, R., Kleffmann, J., and Wiesen, P.: Heterogeneous conversion of NO₂ on secondary organic aerosol surfaces: A possible source of nitrous acid (HONO) in the atmosphere?, *Atmos. Chem. Phys.*, 3, 469-474, <https://doi.org/10.5194/acp-3-469-2003>, 2003.
- 905 Cazor, D., Brigante, M., Ammar, R., D'Anna, B., and George, C.: Heterogeneous photochemistry of gaseous NO₂ on solid fluoranthene films: A source of gaseous nitrous acid (HONO) in the urban environment, *Journal of Photochemistry and Photobiology A: Chemistry*, 273, 23-28, <https://doi.org/10.1016/j.jphotochem.2013.07.016>, 2014.
- Chan, C. K., and Yao, X.: Air pollution in mega cities in China, *Atmospheric Environment*, 42, 1-42, <https://doi.org/10.1016/j.atmosenv.2007.09.003>, 2008.
- 910 Colussi, A. J., Enami, S., Yabushita, A., Hoffmann, M. R., Liu, W.-G., Mishra, H., and Goddard, I. I. W. A.: Tropospheric aerosol as a reactive intermediate, *Faraday Discussions*, 165, 407-420, <http://dx.doi.org/10.1039/C3FD00040K>, 2013.
- Cui, L., Li, R., Zhang, Y., Meng, Y., Fu, H., and Chen, J.: An observational study of nitrous acid (HONO) in Shanghai, China: The aerosol impact on HONO formation during the haze episodes, *Science of The Total Environment*, 630, 1057-1070, <https://doi.org/10.1016/j.scitotenv.2018.02.063>, 2018.
- 915 Czader, B. H., Rappenglück, B., Percell, P., Byun, D. W., Ngan, F., and Kim, S.: Modeling nitrous acid and its impact on ozone and hydroxyl radical during the Texas Air Quality Study 2006, *Atmos. Chem. Phys.*, 12, 6939-6951, <https://doi.org/10.5194/acp-12-6939-2012>, 2012.
- Dillon, M. B., Lamanna, M. S., Schade, G. W., Goldstein, A. H., and Cohen, R. C.: Chemical evolution of the Sacramento urban plume: Transport and oxidation, *Journal of Geophysical Research: Atmospheres*, 107, ACH 3-1-ACH 3-15, <https://doi.org/10.1029/2001JD000969>, 2002.
- Donaldson, M. A., Berke, A. E., and Raff, J. D.: Uptake of Gas Phase Nitrous Acid onto Boundary Layer Soil Surfaces, *Environmental Science & Technology*, 48, 375-383, <https://doi.org/10.1021/es404156a>, 2014.
- 925 El Zein, A., and Bedjanian, Y.: Reactive Uptake of HONO to TiO₂ Surface: "Dark" Reaction, *The Journal of Physical Chemistry A*, 116, 3665-3672, <https://doi.org/10.1021/jp300859w>, 2012.
- El Zein, A., Romanias, M. N., and Bedjanian, Y.: Kinetics and Products of Heterogeneous Reaction of HONO with Fe₂O₃ and Arizona Test Dust, *Environmental Science & Technology*, 47, 6325-6331, <https://doi.org/10.1021/es400794c>, 2013.
- 930 Elshorbany, Y. F., Kurtenbach, R., Wiesen, P., Lissi, E., Rubio, M., Villena, G., Gramsch, E., Rickard, A. R., Pilling, M. J., and Kleffmann, J.: Oxidation capacity of the city air of Santiago, Chile, *Atmos. Chem. Phys.*, 9, 2257-2273, <https://doi.org/10.5194/acp-9-2257-2009>, 2009.

- Elshorbany, Y. F., Kleffmann, J., Kurtenbach, R., Lissi, E., Rubio, M., Villena, G., Gramsch, E., Rickard, A. R., Pilling, M. J., and Wiesen, P.: Seasonal dependence of the oxidation capacity of the city of Santiago de Chile, *Atmospheric Environment*, 44, 5383-5394, <https://doi.org/10.1016/j.atmosenv.2009.08.036>, 2010.
- 935 Elshorbany, Y. F., Steil, B., Brühl, C., and Lelieveld, J.: Impact of HONO on global atmospheric chemistry calculated with an empirical parameterization in the EMAC model, *Atmos. Chem. Phys.*, 12, 9977-10000, <https://doi.org/10.5194/acp-12-9977-2012>, 2012.
- Fan, S., Wang, B., Tesche, M., Engelmann, R., Althausen, A., Liu, J., Zhu, W., Fan, Q., Li, M., Ta, N., Song, L., and Leong, K.: Meteorological conditions and structures of atmospheric boundary layer in October 2004 over Pearl River Delta area, *Atmospheric Environment*, 42, 6174-6186, <https://doi.org/10.1016/j.atmosenv.2008.01.067>, 2008.
- 940 Febo, A., Perrino, C., and Allegrini, I.: Measurement of nitrous acid in milan, italy, by doas and diffusion denuders, *Atmospheric Environment*, 30, 3599-3609, [https://doi.org/10.1016/1352-2310\(96\)00069-6](https://doi.org/10.1016/1352-2310(96)00069-6), 1996.
- Feng, Y., Ning, M., Lei, Y., Sun, Y., Liu, W., and Wang, J.: Defending blue sky in China: Effectiveness of the “Air Pollution Prevention and Control Action Plan” on air quality improvements from 2013 to 2017, *Journal of Environmental Management*, 252, 109603, <https://doi.org/10.1016/j.jenvman.2019.109603>, 2019.
- 945 Finlayson-Pitts, B. J., and Pitts, J. N.: CHAPTER 4 - Photochemistry of Important Atmospheric Species, in: *Chemistry of the Upper and Lower Atmosphere*, edited by: Finlayson-Pitts, B. J., and Pitts, J. N., Academic Press, San Diego, 86-129, 2000.
- Finlayson-Pitts, B. J., Wingen, L. M., Sumner, A. L., Syomin, D., and Ramazan, K. A.: The heterogeneous hydrolysis of NO₂ in laboratory systems and in outdoor and indoor atmospheres: An integrated mechanism, *Physical Chemistry Chemical Physics*, 5, 223-242, <https://doi.org/10.1039/B208564J>, 2003.
- 950 Fu, X., Wang, T., Zhang, L., Li, Q., Wang, Z., Xia, M., Yun, H., Wang, W., Yu, C., Yue, D., Zhou, Y., Zheng, J., and Han, R.: The significant contribution of HONO to secondary pollutants during a severe winter pollution event in southern China, *Atmos. Chem. Phys.*, 19, 1-14, <https://doi.org/10.5194/acp-19-1-2019>, 2019.
- 955 Gall, E. T., Griffin, R. J., Steiner, A. L., Dibb, J., Scheuer, E., Gong, L., Rutter, A. P., Cevik, B. K., Kim, S., Lefter, B., and Flynn, J.: Evaluation of nitrous acid sources and sinks in urban outflow, *Atmospheric Environment*, 127, 272-282, <https://doi.org/10.1016/j.atmosenv.2015.12.044>, 2016.
- Ge, S., Wang, G., Zhang, S., Li, D., Xie, Y., Wu, C., Yuan, Q., Chen, J., and Zhang, H.: Abundant NH₃ in China Enhances Atmospheric HONO Production by Promoting the Heterogeneous Reaction of SO₂ with NO₂, *Environ Sci Technol*, 53, 14339-14347, <https://doi.org/10.1021/acs.est.9b04196>, 2019.
- 960 Ge, Y., Shi, X., Ma, Y., Zhang, W., Ren, X., Zheng, J., and Zhang, Y.: Seasonality of nitrous acid near an industry zone in the Yangtze River Delta region of China: Formation mechanisms and contribution to the atmospheric oxidation capacity, *Atmospheric Environment*, 254, 118420, <https://doi.org/10.1016/j.atmosenv.2021.118420>, 2021.
- Gen, M., Zhang, R., and Chan, C. K.: Nitrite/Nitrous Acid Generation from the Reaction of Nitrate and Fe(II) Promoted by Photolysis of Iron–Organic Complexes, *Environmental Science & Technology*, 55, 15715-15723, <https://doi.org/10.1021/acs.est.1c05641>, 2021.
- 965 George, C., Strekowski, R. S., Kleffmann, J., Stemmler, K., and Ammann, M.: Photoenhanced uptake of gaseous NO₂ on solid organic compounds: a photochemical source of HONO?, *Faraday Discuss*, 130, 195-210; discussion 241-164, 519-124, <http://dx.doi.org/10.1039/B417888M>, 2005.
- 970 Gerecke, A., Thielmann, A., Gutzwiller, L., and Rossi, M. J.: The chemical kinetics of HONO formation resulting from heterogeneous interaction of NO₂ with flame soot, *Geophysical Research Letters*, 25, 2453-2456, <https://doi.org/10.1029/98GL01796>, 1998.
- Gil, J., Kim, J., Lee, M., Lee, G., Ahn, J., Lee, D. S., Jung, J., Cho, S., Whitehill, A., Szykman, J., and Lee, J.: Characteristics of HONO and its impact on O₃ formation in the Seoul Metropolitan Area during the Korea-US Air Quality study, *Atmospheric Environment*, 247, 118182, <https://doi.org/10.1016/j.atmosenv.2020.118182>, 2021.
- 975 Gu, R., Shen, H., Xue, L., Wang, T., Gao, J., Li, H., Liang, Y., Xia, M., Yu, C., Liu, Y., and Wang, W.: Investigating the sources of atmospheric nitrous acid (HONO) in the megacity of Beijing, China, *Science of The Total Environment*, 152270, 10.1016/j.scitotenv.2021.152270, 2021.
- 980 Gutzwiller, L., Arens, F., Baltensperger, U., Gäggeler, H. W., and Ammann, M.: Significance of Semivolatile Diesel Exhaust Organics for Secondary HONO Formation, *Environmental Science & Technology*, 36, 677-682, <https://doi.org/10.1021/es015673b>, 2002.

- Han, C., Liu, Y., and He, H.: Heterogeneous reaction of NO₂ with soot at different relative humidity, *Environmental Science and Pollution Research*, 24, 21248-21255, <https://doi.org/10.1007/s11356-017-9766-y>, 2017a.
- 985 Han, C., Yang, W., Yang, H., and Xue, X.: Enhanced photochemical conversion of NO₂ to HONO on humic acids in the presence of benzophenone, *Environmental Pollution*, 231, 979-986, <https://doi.org/10.1016/j.envpol.2017.08.107>, 2017b.
- Hao, Q., Jiang, N., Zhang, R., Yang, L., and Li, S.: Characteristics, sources, and reactions of nitrous acid during winter at an urban site in the Central Plains Economic Region in China, *Atmos. Chem. Phys.*, 20, 7087-7102, <https://doi.org/10.5194/acp-20-7087-2020>, 2020.
- 990 Harrison, R. M., and Kitto, A.-M. N.: Evidence for a surface source of atmospheric nitrous acid, *Atmospheric Environment*, 28, 1089-1094, [https://doi.org/10.1016/1352-2310\(94\)90286-0](https://doi.org/10.1016/1352-2310(94)90286-0), 1994.
- Harrison, R. M., Peak, J. D., and Collins, G. M.: Tropospheric cycle of nitrous acid, *Journal of Geophysical Research: Atmospheres*, 101, 14429-14439, <https://doi.org/10.1029/96JD00341>, 1996.
- 995 Heard, D. E., Carpenter, L. J., Creasey, D. J., Hopkins, J. R., Lee, J. D., Lewis, A. C., Pilling, M. J., Seakins, P. W., Carslaw, N., and Emmerson, K. M.: High levels of the hydroxyl radical in the winter urban troposphere, *Geophysical Research Letters*, 31, <https://doi.org/10.1029/2004GL020544>, 2004.
- Heland, J., Kleffmann, J., Kurtenbach, R., and Wiesen, P.: A New Instrument To Measure Gaseous Nitrous Acid (HONO) in the Atmosphere, *Environmental Science & Technology*, 35, 3207-3212, <https://doi.org/10.1021/es000303t>, 2001.
- 1000 Hendrick, F., Müller, J. F., Clémer, K., Wang, P., De Mazière, M., Fayt, C., Gielen, C., Hermans, C., Ma, J. Z., Pinardi, G., Stavrou, T., Vlemmix, T., and Van Roozendael, M.: Four years of ground-based MAX-DOAS observations of HONO and NO₂ in the Beijing area, *Atmos. Chem. Phys.*, 14, 765-781, <https://doi.org/10.5194/acp-14-765-2014>, 2014.
- Hofzumahaus, A., Rohrer, F., Lu, K., Bohn, B., Brauers, T., Chang, C.-C., Fuchs, H., Holland, F., Kita, K., Kondo, Y., Li, X., Lou, S., Shao, M., Zeng, L., Wahner, A., and Zhang, Y.: Amplified Trace Gas Removal in the Troposphere, *Science*, 324, 1702-1704, <https://doi.org/10.1126/science.1164566>, 2009.
- 1005 Hou, S., Tong, S., Ge, M., and An, J.: Comparison of atmospheric nitrous acid during severe haze and clean periods in Beijing, China, *Atmospheric Environment*, 124, 199-206, <https://doi.org/10.1016/j.atmosenv.2015.06.023>, 2016.
- Hu, M., Zhou, F., Shao, K., Zhang, Y., Tang, X., and Slanina, J.: Diurnal variations of aerosol chemical compositions and related gaseous pollutants in Beijing and Guangzhou, *J Environ Sci Health A Tox Hazard Subst Environ Eng*, 37, 479-488, <https://doi.org/10.1081/ESE-120003229>, 2002.
- 1010 Huang, R. J., Yang, L., Cao, J., Wang, Q., Tie, X., Ho, K. F., Shen, Z., Zhang, R., Li, G., Zhu, C., Zhang, N., Dai, W., Zhou, J., Liu, S., Chen, Y., Chen, J., and O'Dowd, C. D.: Concentration and sources of atmospheric nitrous acid (HONO) at an urban site in Western China, *Science of The Total Environment*, 593-594, 165-172, <https://doi.org/10.1016/j.scitotenv.2017.02.166>, 2017.
- 1015 Huang, Z., Zhong, Z., Sha, Q., Xu, Y., Zhang, Z., Wu, L., Wang, Y., Zhang, L., Cui, X., Tang, M., Shi, B., Zheng, C., Li, Z., Hu, M., Bi, L., Zheng, J., and Yan, M.: An updated model-ready emission inventory for Guangdong Province by incorporating big data and mapping onto multiple chemical mechanisms, *Science of The Total Environment*, 769, 144535, <https://doi.org/10.1016/j.scitotenv.2020.144535>, 2021.
- Indarto, A.: Heterogeneous reactions of HONO formation from NO₂ and HNO₃: a review, *Research on Chemical Intermediates*, 38, 1029-1041, <https://doi.org/10.1007/s11164-011-0439-z>, 2012.
- 1020 Jenkin, M. E., Saunders, S. M., and Pilling, M. J.: The tropospheric degradation of volatile organic compounds: a protocol for mechanism development, *Atmospheric Environment*, 31, 81-104, [https://doi.org/10.1016/S1352-2310\(96\)00105-7](https://doi.org/10.1016/S1352-2310(96)00105-7), 1997.
- Jenkin, M. E., Saunders, S. M., Wagner, V., and Pilling, M. J.: Protocol for the development of the Master Chemical Mechanism, MCM v3 (Part B): tropospheric degradation of aromatic volatile organic compounds, *Atmos. Chem. Phys.*, 3, 181-193, <https://doi.org/10.5194/acp-3-181-2003>, 2003.
- 1025 Jenkin, M. E., Young, J. C., and Rickard, A. R.: The MCM v3.3.1 degradation scheme for isoprene, *Atmos. Chem. Phys.*, 15, 11433-11459, <https://doi.org/10.5194/acp-15-11433-2015>, 2015.
- Jeon, W., Choi, Y., Souri, A. H., Roy, A., Diao, L., Pan, S., Lee, H. W., and Lee, S. H.: Identification of chemical fingerprints in long-range transport of burning induced upper tropospheric ozone from Colorado to the North Atlantic Ocean, *Science of The Total Environment*, 613-614, 820-828, <https://doi.org/10.1016/j.scitotenv.2017.09.177>, 2018.

- 1030 Jia, C., Tong, S., Zhang, W., Zhang, X., Li, W., Wang, Z., Wang, L., Liu, Z., Hu, B., Zhao, P., and Ge, M.: Pollution characteristics and potential sources of nitrous acid (HONO) in early autumn 2018 of Beijing, *Science of The Total Environment*, 735, 139317, <https://doi.org/10.1016/j.scitotenv.2020.139317>, 2020.
- Jiang, Y., Xue, L., Gu, R., Jia, M., Zhang, Y., Wen, L., Zheng, P., Chen, T., Li, H., Shan, Y., Zhao, Y., Guo, Z., Bi, Y., Liu, H., Ding, A., Zhang, Q., and Wang, W.: Sources of nitrous acid (HONO) in the upper boundary layer and lower free troposphere of the North China Plain: insights from the Mount Tai Observatory, *Atmos. Chem. Phys.*, 20, 12115-12131, <https://doi.org/10.5194/acp-20-12115-2020>, 2020.
- 1035 Kaiser, E. W., and Wu, C. H.: A kinetic study of the gas phase formation and decomposition reactions of nitrous acid, *The Journal of Physical Chemistry*, 81, 1701-1706, <https://doi.org/10.1021/j100533a001>, 1977.
- Kalberer, M., Ammann, M., Arens, F., Gäggeler, H. W., and Baltensperger, U.: Heterogeneous formation of nitrous acid (HONO) on soot aerosol particles, *Journal of Geophysical Research: Atmospheres*, 104, 13825-13832, <https://doi.org/10.1029/1999JD900141>, 1999.
- 1040 Kim, S., VandenBoer, T. C., Young, C. J., Riedel, T. P., Thornton, J. A., Swarthout, B., Sive, B., Lerner, B., Gilman, J. B., Warneke, C., Roberts, J. M., Guenther, A., Wagner, N. L., Dubé, W. P., Williams, E., and Brown, S. S.: The primary and recycling sources of OH during the NACHTT-2011 campaign: HONO as an important OH primary source in the wintertime, *Journal of Geophysical Research: Atmospheres*, 119, 6886-6896, <https://doi.org/10.1002/2013JD019784>, 2014.
- 1045 Kinugawa, T., Enami, S., Yabushita, A., Kawasaki, M., Hoffmann, M. R., and Colussi, A. J.: Conversion of gaseous nitrogen dioxide to nitrate and nitrite on aqueous surfactants, *Physical Chemistry Chemical Physics*, 13, 5144-5149, <http://dx.doi.org/10.1039/C0CP01497D>, 2011.
- Kirchstetter, T. W., Harley, R. A., and Littlejohn, D.: Measurement of Nitrous Acid in Motor Vehicle Exhaust, *Environmental Science & Technology*, 30, 2843-2849, <https://doi.org/10.1021/es960135y>, 1996.
- 1050 Kleffmann, J., Kurtenbach, R., Lörzer, J., Wiesen, P., Kalthoff, N., Vogel, B., and Vogel, H.: Measured and simulated vertical profiles of nitrous acid—Part I: Field measurements, *Atmospheric Environment*, 37, 2949-2955, [https://doi.org/10.1016/S1352-2310\(03\)00242-5](https://doi.org/10.1016/S1352-2310(03)00242-5), 2003.
- Kleffmann, J., Gavriloaiei, T., Hofzumahaus, A., Holland, F., Koppmann, R., Rupp, L., Schlosser, E., Siese, M., and Wahner, A.: Daytime formation of nitrous acid: A major source of OH radicals in a forest, *Geophysical Research Letters*, 32, <https://doi.org/10.1029/2005GL022524>, 2005.
- 1055 Kleffmann, J., Lörzer, J. C., Wiesen, P., Kern, C., Trick, S., Volkamer, R., Rodenas, M., and Wirtz, K.: Intercomparison of the DOAS and LOPAP techniques for the detection of nitrous acid (HONO), *Atmospheric Environment*, 40, 3640-3652, <https://doi.org/10.1016/j.atmosenv.2006.03.027>, 2006.
- 1060 Kramer, L. J., Crilley, L. R., Adams, T. J., Ball, S. M., Pope, F. D., and Bloss, W. J.: Nitrous acid (HONO) emissions under real-world driving conditions from vehicles in a UK road tunnel, *Atmos. Chem. Phys.*, 20, 5231-5248, <https://doi.org/10.5194/acp-20-5231-2020>, 2020.
- Kurtenbach, R., Becker, K. H., Gomes, J. A. G., Kleffmann, J., Lörzer, J. C., Spittler, M., Wiesen, P., Ackermann, R., Geyer, A., and Platt, U.: Investigations of emissions and heterogeneous formation of HONO in a road traffic tunnel, *Atmospheric Environment*, 35, 3385-3394, [https://doi.org/10.1016/S1352-2310\(01\)00138-8](https://doi.org/10.1016/S1352-2310(01)00138-8), 2001.
- 1065 Lammel, G., and Cape, J. N.: Nitrous acid and nitrite in the atmosphere, *Chemical Society Reviews*, 25, 361-369, <http://dx.doi.org/10.1039/CS9962500361>, 1996.
- Laufs, S., and Kleffmann, J.: Investigations on HONO formation from photolysis of adsorbed HNO₃ on quartz glass surfaces, *Phys Chem Chem Phys*, 18, 9616-9625, <https://doi.org/10.1039/C6CP00436A>, 2016.
- 1070 Laufs, S., Cazaunau, M., Stella, P., Kurtenbach, R., Cellier, P., Mellouki, A., Loubet, B., and Kleffmann, J.: Diurnal fluxes of HONO above a crop rotation, *Atmos. Chem. Phys.*, 17, 6907-6923, <https://doi.org/10.5194/acp-17-6907-2017>, 2017.
- Lee, J. D., Whalley, L. K., Heard, D. E., Stone, D., Dunmore, R. E., Hamilton, J. F., Young, D. E., Allan, J. D., Laufs, S., and Kleffmann, J.: Detailed budget analysis of HONO in central London reveals a missing daytime source, *Atmos. Chem. Phys.*, 16, 2747-2764, <https://doi.org/10.5194/acp-16-2747-2016>, 2016.
- 1075 Lelieveld, J., Gromov, S., Pozzer, A., and Taraborrelli, D.: Global tropospheric hydroxyl distribution, budget and reactivity, *Atmos. Chem. Phys.*, 16, 12477-12493, <https://doi.org/10.5194/acp-16-12477-2016>, 2016.

- Li, D., Xue, L., Wen, L., Wang, X., Chen, T., Mellouki, A., Chen, J., and Wang, W.: Characteristics and sources of nitrous acid in an urban atmosphere of northern China: Results from 1-yr continuous observations, *Atmospheric Environment*, 182, 296-306, <https://doi.org/10.1016/j.atmosenv.2018.03.033>, 2018a.
- Li, G., Lei, W., Zavala, M., Volkamer, R., Dusanter, S., Stevens, P., and Molina, L. T.: Impacts of HONO sources on the photochemistry in Mexico City during the MCMA-2006/MILAGO Campaign, *Atmos. Chem. Phys.*, 10, 6551-6567, <https://doi.org/10.5194/acp-10-6551-2010>, 2010.
- Li, H., Cheng, P., Yu, Y., and Yang, W.: Nitrous acid (HONO) budget analysis at a rural site in the North China Plain during snowy days, in preparation.
- Li, J., Lu, K., Lv, W., Li, J., Zhong, L., Ou, Y., Chen, D., Huang, X., and Zhang, Y.: Fast increasing of surface ozone concentrations in Pearl River Delta characterized by a regional air quality monitoring network during 2006–2011, *Journal of Environmental Sciences*, 26, 23-36, [https://doi.org/10.1016/S1001-0742\(13\)60377-0](https://doi.org/10.1016/S1001-0742(13)60377-0), 2014a.
- Li, L., Duan, Z., Li, H., Zhu, C., Henkelman, G., Francisco, J. S., and Zeng, X. C.: Formation of HONO from the NH₃ promoted hydrolysis of NO₂ dimers in the atmosphere, *Proceedings of the National Academy of Sciences*, 115, 7236-7241, <https://doi.org/10.1073/pnas.1807719115>, 2018b.
- Li, S., Matthews, J., and Sinha, A.: Atmospheric hydroxyl radical production from electronically excited NO₂ and H₂O, *Science*, 319, 1657-1660, <https://doi.org/10.1126/science.1151443>, 2008.
- Li, W., Tong, S., Cao, J., Su, H., Zhang, W., Wang, L., Jia, C., Zhang, X., Wang, Z., Chen, M., and Ge, M.: Comparative observation of atmospheric nitrous acid (HONO) in Xi'an and Xianyang located in the GuanZhong basin of western China, *Environmental Pollution*, 289, 117679, <https://doi.org/10.1016/j.envpol.2021.117679>, 2021.
- Li, X., Brauers, T., Häsel, R., Bohn, B., Fuchs, H., Hofzumahaus, A., Holland, F., Lou, S., Lu, K. D., Rohrer, F., Hu, M., Zeng, L. M., Zhang, Y. H., Garland, R. M., Su, H., Nowak, A., Wiedensohler, A., Takegawa, N., Shao, M., and Wahner, A.: Exploring the atmospheric chemistry of nitrous acid (HONO) at a rural site in Southern China, *Atmos. Chem. Phys.*, 12, 1497-1513, <https://doi.org/10.5194/acp-12-1497-2012>, 2012.
- Li, X., Rohrer, F., Hofzumahaus, A., Brauers, T., Häsel, R., Bohn, B., Broch, S., Fuchs, H., Gomm, S., Holland, F., Jäger, J., Kaiser, J., Keutsch, F. N., Lohse, I., Lu, K., Tillmann, R., Wegener, R., Wolfe, G. M., Mentel, T. F., Kiendler-Scharr, A., and Wahner, A.: Missing Gas-Phase Source of HONO Inferred from Zeppelin Measurements in the Troposphere, *Science*, 344, 292-296, <https://doi.org/10.1126/science.1248999>, 2014b.
- Li, Y., An, J., Min, M., Zhang, W., Wang, F., and Xie, P.: Impacts of HONO sources on the air quality in Beijing, Tianjin and Hebei Province of China, *Atmospheric Environment*, 45, 4735-4744, <https://doi.org/10.1016/j.atmosenv.2011.04.086>, 2011.
- Liao, B., Huang, J., Wang, C., Weng, J., Li, L., Cai, H., and D, W.: Comparative analysis on the boundary layer features of haze processes and cleaning process in Guangzhou, *China Environmental Science*, 38, 4432-4443, DOI:10.19674/j.cnki.issn1000-6923.2018.0496, 2018.
- Liao, W., Wu, L., Zhou, S., Wang, X., and Chen, D.: Impact of Synoptic Weather Types on Ground-Level Ozone Concentrations in Guangzhou, China, *Asia-Pacific Journal of Atmospheric Sciences*, <https://doi.org/10.1007/s13143-020-00186-2>, 2020.
- Lin, Y.-C., Cheng, M.-T., Ting, W.-Y., and Yeh, C.-R.: Characteristics of gaseous HNO₂, HNO₃, NH₃ and particulate ammonium nitrate in an urban city of Central Taiwan, *Atmospheric Environment*, 40, 4725-4733, <https://doi.org/10.1016/j.atmosenv.2006.04.037>, 2006.
- Liu, J., Deng, H., Li, S., Jiang, H., Mekic, M., Zhou, W., Wang, Y., Loisel, G., Wang, X., and Gligorovski, S.: Light-Enhanced Heterogeneous Conversion of NO₂ to HONO on Solid Films Consisting of Fluorene and Fluorene/Na₂SO₄: An Impact on Urban and Indoor Atmosphere, *Environ Sci Technol*, 54, 11079-11086, <https://doi.org/10.1021/acs.est.0c02627>, 2020a.
- Liu, J., Liu, Z., Ma, Z., Yang, S., Yao, D., Zhao, S., Hu, B., Tang, G., Sun, J., Cheng, M., Xu, Z., and Wang, Y.: Detailed budget analysis of HONO in Beijing, China: Implication on atmosphere oxidation capacity in polluted megacity, *Atmospheric Environment*, 244, 117957, <https://doi.org/10.1016/j.atmosenv.2020.117957>, 2021.
- Liu, Y.: Observations and parameterized modelling of ambient nitrous acid (HONO) in the megacity areas of the eastern China, Ph.D. thesis. College of Environmental Sciences and Engineering, Peking University, China, 2017.

- Liu, Y., Lu, K., Ma, Y., Yang, X., Zhang, W., Wu, Y., Peng, J., Shuai, S., Hu, M., and Zhang, Y.: Direct emission of nitrous acid (HONO) from gasoline cars in China determined by vehicle chassis dynamometer experiments, *Atmospheric Environment*, 169, 89-96, <https://doi.org/10.1016/j.atmosenv.2017.07.019>, 2017.
- 1130 Liu, Y., Lu, K., Li, X., Dong, H., Tan, Z., Wang, H., Zou, Q., Wu, Y., Zeng, L., Hu, M., Min, K. E., Kecorius, S., Wiedensohler, A., and Zhang, Y.: A Comprehensive Model Test of the HONO Sources Constrained to Field Measurements at Rural North China Plain, *Environ Sci Technol*, <https://doi.org/10.1021/acs.est.8b06367>, 2019a.
- Liu, Y., Nie, W., Xu, Z., Wang, T., Wang, R., Li, Y., Wang, L., Chi, X., and Ding, A.: Semi-quantitative understanding of source contribution to nitrous acid (HONO) based on 1 year of continuous observation at the SORPES station in eastern China, *Atmos. Chem. Phys.*, 19, 13289-13308, <https://doi.org/10.5194/acp-19-13289-2019>, 2019b.
- 1135 Liu, Y., Ni, S., Jiang, T., Xing, S., Zhang, Y., Bao, X., Feng, Z., Fan, X., Zhang, L., and Feng, H.: Influence of Chinese New Year overlapping COVID-19 lockdown on HONO sources in Shijiazhuang, *Science of The Total Environment*, 745, 141025, <https://doi.org/10.1016/j.scitotenv.2020.141025>, 2020b.
- 1140 Liu, Y., Zhang, Y., Lian, C., Yan, C., Feng, Z., Zheng, F., Fan, X., Chen, Y., Wang, W., Chu, B., Wang, Y., Cai, J., Du, W., Daellenbach, K. R., Kangasluoma, J., Bianchi, F., Kujansuu, J., Petäjä, T., Wang, X., Hu, B., Wang, Y., Ge, M., He, H., and Kulmala, M.: The promotion effect of nitrous acid on aerosol formation in wintertime in Beijing: the possible contribution of traffic-related emissions, *Atmos. Chem. Phys.*, 20, 13023-13040, <https://doi.org/10.5194/acp-20-13023-2020>, 2020c.
- Liu, Z., Wang, Y., Costabile, F., Amoroso, A., Zhao, C., Huey, L. G., Stickel, R., Liao, J., and Zhu, T.: Evidence of aerosols as a media for rapid daytime HONO production over China, *Environ Sci Technol*, 48, 14386-14391, <https://doi.org/10.1021/es504163z>, 2014.
- 1145 Lou, S., Holland, F., Rohrer, F., Lu, K., Bohn, B., Brauers, T., Chang, C. C., Fuchs, H., Häsel, R., Kita, K., Kondo, Y., Li, X., Shao, M., Zeng, L., Wahner, A., Zhang, Y., Wang, W., and Hofzumahaus, A.: Atmospheric OH reactivities in the Pearl River Delta – China in summer 2006: measurement and model results, *Atmos. Chem. Phys.*, 10, 11243-11260, <https://doi.org/10.5194/acp-10-11243-2010>, 2010.
- 1150 Lu, K. D., Rohrer, F., Holland, F., Fuchs, H., Bohn, B., Brauers, T., Chang, C. C., Häsel, R., Hu, M., Kita, K., Kondo, Y., Li, X., Lou, S. R., Nehr, S., Shao, M., Zeng, L. M., Wahner, A., Zhang, Y. H., and Hofzumahaus, A.: Observation and modelling of OH and HO₂ concentrations in the Pearl River Delta 2006: a missing OH source in a VOC rich atmosphere, *Atmos. Chem. Phys.*, 12, 1541-1569, <https://doi.org/10.5194/acp-12-1541-2012>, 2012.
- 1155 Lu, K. D., Hofzumahaus, A., Holland, F., Bohn, B., Brauers, T., Fuchs, H., Hu, M., Häsel, R., Kita, K., Kondo, Y., Li, X., Lou, S. R., Oebel, A., Shao, M., Zeng, L. M., Wahner, A., Zhu, T., Zhang, Y. H., and Rohrer, F.: Missing OH source in a suburban environment near Beijing: observed and modelled OH and HO₂ concentrations in summer 2006, *Atmos. Chem. Phys.*, 13, 1057-1080, <https://doi.org/10.5194/acp-13-1057-2013>, 2013.
- 1160 Lu, K. D., Rohrer, F., Holland, F., Fuchs, H., Brauers, T., Oebel, A., Dlugi, R., Hu, M., Li, X., Lou, S. R., Shao, M., Zhu, T., Wahner, A., Zhang, Y. H., and Hofzumahaus, A.: Nighttime observation and chemistry of HO_x in the Pearl River Delta and Beijing in summer 2006, *Atmos. Chem. Phys.*, 14, 4979-4999, <https://doi.org/10.5194/acp-14-4979-2014>, 2014.
- Lu, X., Hong, J., Zhang, L., Cooper, O. R., Schultz, M. G., Xu, X., Wang, T., Gao, M., Zhao, Y., and Zhang, Y.: Severe Surface Ozone Pollution in China: A Global Perspective, *Environmental Science & Technology Letters*, 5, 487-494, <https://doi.org/10.1021/acs.estlett.8b00366>, 2018.
- 1165 Maljanen, M., Yli-Pirilä, P., Hytönen, J., Joutsensaari, J., and Martikainen, P. J.: Acidic northern soils as sources of atmospheric nitrous acid (HONO), *Soil Biology and Biochemistry*, 67, 94-97, <https://doi.org/10.1016/j.soilbio.2013.08.013>, 2013.
- Malkin, T. L., Heard, D. E., Hood, C., Stocker, J., Carruthers, D., MacKenzie, I. A., Doherty, R. M., Vieno, M., Lee, J., Kleffmann, J., Laufs, S., and Whalley, L. K.: Assessing chemistry schemes and constraints in air quality models used to predict ozone in London against the detailed Master Chemical Mechanism, *Faraday Discuss*, 189, 589-616, <https://doi.org/10.1039/C5FD00218D>, 2016.
- 1170 Marion, A., Morin, J., Gandolfo, A., Ormeño, E., D'Anna, B., and Wortham, H.: Nitrous acid formation on Zea mays leaves by heterogeneous reaction of nitrogen dioxide in the laboratory, *Environmental Research*, 193, 110543, <https://doi.org/10.1016/j.envres.2020.110543>, 2021.
- 1175 Martinez, M., Harder, H., Kovacs, T. A., Simpas, J. B., Bassis, J., Leshner, R., Brune, W. H., Frost, G. J., Williams, E. J., Stroud, C. A., Jobson, B. T., Roberts, J. M., Hall, S. R., Shetter, R. E., Wert, B., Fried, A., Alicke, B., Stutz, J., Young, V. L.,

- White, A. B., and Zamora, R. J.: OH and HO₂ concentrations, sources, and loss rates during the Southern Oxidants Study in Nashville, Tennessee, summer 1999, *Journal of Geophysical Research: Atmospheres*, 108, <https://doi.org/10.1029/2003JD003551>, 2003.
- 1180 Mebel, A. M., Lin, M. C., and Melius, C. F.: Rate Constant of the HONO + HONO → H₂O + NO + NO₂ Reaction from ab Initio MO and TST Calculations, *The Journal of Physical Chemistry A*, 102, 1803-1807, <https://doi.org/10.1021/jp973449w>, 1998.
- Meng, F., Qin, M., Tang, K., Duan, J., Fang, W., Liang, S., Ye, K., Xie, P., Sun, Y., Xie, C., Ye, C., Fu, P., Liu, J., and Liu, W.: High-resolution vertical distribution and sources of HONO and NO₂ in the nocturnal boundary layer in urban Beijing, China, *Atmos. Chem. Phys.*, 20, 5071-5092, <https://doi.org/10.5194/acp-20-5071-2020>, 2020.
- 1185 Meusel, H., Kuhn, U., Reiffs, A., Mallik, C., Harder, H., Martinez, M., Schuladen, J., Bohn, B., Parchatka, U., Crowley, J. N., Fischer, H., Tomsche, L., Novelli, A., Hoffmann, T., Janssen, R. H. H., Hartogensis, O., Pikridas, M., Vrekoussis, M., Bourtsoukidis, E., Weber, B., Lelieveld, J., Williams, J., Pöschl, U., Cheng, Y., and Su, H.: Daytime formation of nitrous acid at a coastal remote site in Cyprus indicating a common ground source of atmospheric HONO and NO, *Atmos. Chem. Phys.*, 16, 14475-14493, <https://doi.org/10.5194/acp-16-14475-2016>, 2016.
- 1190 Meusel, H., Tamm, A., Kuhn, U., Wu, D., Leifke, A. L., Fiedler, S., Ruckteschler, N., Yordanova, P., Lang-Yona, N., Pöhlker, M., Lelieveld, J., Hoffmann, T., Pöschl, U., Su, H., Weber, B., and Cheng, Y.: Emission of nitrous acid from soil and biological soil crusts represents an important source of HONO in the remote atmosphere in Cyprus, *Atmos. Chem. Phys.*, 18, 799-813, <https://doi.org/10.5194/acp-18-799-2018>, 2018.
- 1195 Michoud, V., Kukui, A., Camredon, M., Colomb, A., Borbon, A., Miet, K., Aumont, B., Beekmann, M., Durand-Jolibois, R., Perrier, S., Zapf, P., Siour, G., Ait-Helal, W., Locoge, N., Sauvage, S., Afif, C., Gros, V., Furger, M., Ancellet, G., and Doussin, J. F.: Radical budget analysis in a suburban European site during the MEGAPOLI summer field campaign, *Atmos. Chem. Phys.*, 12, 11951-11974, <https://doi.org/10.5194/acp-12-11951-2012>, 2012.
- 1200 Michoud, V., Colomb, A., Borbon, A., Miet, K., Beekmann, M., Camredon, M., Aumont, B., Perrier, S., Zapf, P., Siour, G., Ait-Helal, W., Afif, C., Kukui, A., Furger, M., Dupont, J. C., Haefelin, M., and Doussin, J. F.: Study of the unknown HONO daytime source at a European suburban site during the MEGAPOLI summer and winter field campaigns, *Atmos. Chem. Phys.*, 14, 2805-2822, <https://doi.org/10.5194/acp-14-2805-2014>, 2014.
- Monge, M. E., D'Anna, B., Mazri, L., Giroir-Fendler, A., Ammann, M., Donaldson, D. J., and George, C.: Light changes the atmospheric reactivity of soot, *Proceedings of the National Academy of Sciences*, 107, 6605-6609, <https://doi.org/10.1073/pnas.0908341107>, 2010.
- 1205 Nakashima, Y., and Kajii, Y.: Determination of nitrous acid emission factors from a gasoline vehicle using a chassis dynamometer combined with incoherent broadband cavity-enhanced absorption spectroscopy, *Science of The Total Environment*, 575, 287-293, <https://doi.org/10.1016/j.scitotenv.2016.10.050>, 2017.
- 1210 Ndour, M., D'Anna, B., George, C., Ka, O., Balkanski, Y., Kleffmann, J., Stemmler, K., and Ammann, M.: Photoenhanced uptake of NO₂ on mineral dust: Laboratory experiments and model simulations, *Geophysical Research Letters*, 35, <https://doi.org/10.1029/2007GL032006>, 2008.
- Neuman, J. A., Trainer, M., Brown, S. S., Min, K.-E., Nowak, J. B., Parrish, D. D., Peischl, J., Pollack, I. B., Roberts, J. M., Ryerson, T. B., and Veres, P. R.: HONO emission and production determined from airborne measurements over the Southeast U.S, *Journal of Geophysical Research: Atmospheres*, 121, 9237-9250, <https://doi.org/10.1002/2016JD025197>, 2016.
- 1215 Nie, W., Ding, A. J., Xie, Y. N., Xu, Z., Mao, H., Kerminen, V. M., Zheng, L. F., Qi, X. M., Huang, X., Yang, X. Q., Sun, J. N., Herrmann, E., Petäjä, T., Kulmala, M., and Fu, C. B.: Influence of biomass burning plumes on HONO chemistry in eastern China, *Atmos. Chem. Phys.*, 15, 1147-1159, <https://doi.org/10.5194/acp-15-1147-2015>, 2015.
- 1220 Oswald, R., Behrendt, T., Ermel, M., Wu, D., Su, H., Cheng, Y., Breuninger, C., Moravek, A., Mougin, E., Delon, C., Loubet, B., Pommerening-Röser, A., Sörgel, M., Pöschl, U., Hoffmann, T., Andreae, M. O., Meixner, F. X., and Trebs, I.: HONO Emissions from Soil Bacteria as a Major Source of Atmospheric Reactive Nitrogen, *Science*, 341, 1233-1235, <https://doi.org/10.1126/science.1242266>, 2013.
- Pagsberg, P., Bjergbakke, E., Ratajczak, E., and Sillesen, A.: Kinetics of the gas phase reaction OH + NO(+M)→HONO(+M) and the determination of the UV absorption cross sections of HONO, *Chemical Physics Letters*, 272, 383-390, [https://doi.org/10.1016/S0009-2614\(97\)00576-9](https://doi.org/10.1016/S0009-2614(97)00576-9), 1997.

- 1225 Perner, D., and Platt, U.: Detection of nitrous acid in the atmosphere by differential optical absorption, *Geophysical Research Letters*, 6, 917-920, <https://doi.org/10.1029/GL006i012p00917>, 1979.
- Pitts, J. N., Biermann, H. W., Winer, A. M., and Tuazon, E. C.: Spectroscopic identification and measurement of gaseous nitrous acid in dilute auto exhaust, *Atmospheric Environment* (1967), 18, 847-854, [https://doi.org/10.1016/0004-6981\(84\)90270-1](https://doi.org/10.1016/0004-6981(84)90270-1), 1984.
- 1230 Porada, P., Tamm, A., Raggio, J., Cheng, Y., Kleidon, A., Pöschl, U., and Weber, B.: Global NO and HONO emissions of biological soil crusts estimated by a process-based non-vascular vegetation model, *Biogeosciences*, 16, 2003-2031, <https://doi.org/10.5194/bg-16-2003-2019>, 2019.
- Qin, M., Xie, P., Su, H., Gu, J., Peng, F., Li, S., Zeng, L., Liu, J., Liu, W., and Zhang, Y.: An observational study of the HONO-NO₂ coupling at an urban site in Guangzhou City, South China, *Atmospheric Environment*, 43, 5731-5742, <https://doi.org/10.1016/j.atmosenv.2009.08.017>, 2009.
- 1235 Rappenglück, B., Lubertino, G., Alvarez, S., Golovko, J., Czader, B., and Ackermann, L.: Radical precursors and related species from traffic as observed and modeled at an urban highway junction, *Journal of the Air & Waste Management Association*, 63, 1270-1286, <https://doi.org/10.1080/10962247.2013.822438>, 2013.
- Reisinger, A. R.: Observations of HNO₂ in the polluted winter atmosphere: possible heterogeneous production on aerosols, *Atmospheric Environment*, 34, 3865-3874, [https://doi.org/10.1016/S1352-2310\(00\)00179-5](https://doi.org/10.1016/S1352-2310(00)00179-5), 2000.
- 1240 Ren, X., Harder, H., Martinez, M., Leshner, R. L., Oligier, A., Simpas, J. B., Brune, W. H., Schwab, J. J., Demerjian, K. L., He, Y., Zhou, X., and Gao, H.: OH and HO₂ Chemistry in the urban atmosphere of New York City, *Atmospheric Environment*, 37, 3639-3651, [https://doi.org/10.1016/S1352-2310\(03\)00459-X](https://doi.org/10.1016/S1352-2310(03)00459-X), 2003.
- Ren, X., van Duin, D., Cazorla, M., Chen, S., Mao, J., Zhang, L., Brune, W. H., Flynn, J. H., Grossberg, N., Lefer, B. L., Rappenglück, B., Wong, K. W., Tsai, C., Stutz, J., Dibb, J. E., Thomas Jobson, B., Luke, W. T., and Kelley, P.: Atmospheric oxidation chemistry and ozone production: Results from SHARP 2009 in Houston, Texas, *Journal of Geophysical Research: Atmospheres*, 118, 5770-5780, <https://doi.org/10.1002/jgrd.50342>, 2013.
- 1245 Rohrer, F., and Berresheim, H.: Strong correlation between levels of tropospheric hydroxyl radicals and solar ultraviolet radiation, *Nature*, 442, 184-187, <https://doi.org/10.1038/nature04924>, 2006.
- 1250 Romanias, M. N., El Zein, A., and Bedjanian, Y.: Reactive uptake of HONO on aluminium oxide surface, *Journal of Photochemistry and Photobiology A: Chemistry*, 250, 50-57, <https://doi.org/10.1016/j.jphotochem.2012.09.018>, 2012.
- Saliba, N. A., Yang, H., and Finlayson-Pitts, B. J.: Reaction of Gaseous Nitric Oxide with Nitric Acid on Silica Surfaces in the Presence of Water at Room Temperature, *The Journal of Physical Chemistry A*, 105, 10339-10346, <https://doi.org/10.1021/jp012330r>, 2001.
- 1255 Sarwar, G., Roselle, S. J., Mathur, R., Appel, W., Dennis, R. L., and Vogel, B.: A comparison of CMAQ HONO predictions with observations from the Northeast Oxidant and Particle Study, *Atmospheric Environment*, 42, 5760-5770, <https://doi.org/10.1016/j.atmosenv.2007.12.065>, 2008.
- Seinfeld, J. H., and Pandis, S. N.: *Atmospheric chemistry and physics: from air pollution to climate change*, John Wiley & Sons, 2016.
- 1260 Shao, M., Ren, X., Wang, H., Zeng, L., Zhang, Y., and Tang, X.: Quantitative relationship between production and removal of OH and HO₂ radicals in urban atmosphere, *Chinese Science Bulletin*, 49, 2253-2258, <https://doi.org/10.1360/04wb0006>, 2004.
- Shi, X., Ge, Y., Zhang, Y., Ma, Y., and Zheng, J.: HONO observation and assessment of the effects of atmospheric oxidation capacity in Changzhou during the springtime of 2017, *Environmental Science*, v.41, 113-121, DOI: 10.13227/j.hjkx.201909032, 2020a.
- 1265 Shi, X., Ge, Y., Zheng, J., Ma, Y., Ren, X., and Zhang, Y.: Budget of nitrous acid and its impacts on atmospheric oxidative capacity at an urban site in the central Yangtze River Delta region of China, *Atmospheric Environment*, 238, 117725, <https://doi.org/10.1016/j.atmosenv.2020.117725>, 2020b.
- 1270 Slater, E. J., Whalley, L. K., Woodward-Massey, R., Ye, C., Lee, J. D., Squires, F., Hopkins, J. R., Dunmore, R. E., Shaw, M., Hamilton, J. F., Lewis, A. C., Crilley, L. R., Kramer, L., Bloss, W., Vu, T., Sun, Y., Xu, W., Yue, S., Ren, L., Acton, W. J. F., Hewitt, C. N., Wang, X., Fu, P., and Heard, D. E.: Elevated levels of OH observed in haze events during wintertime in central Beijing, *Atmos. Chem. Phys.*, 20, 14847-14871, <https://doi.org/10.5194/acp-20-14847-2020>, 2020.
- Song, L., Deng, T., and Wu, D.: Study on planetary boundary layer height in a typical haze period and different weather types over Guangzhou, *Acta Scientiae Circumstantiae*, 39(5), 1381-1391, DOI: 10.13671/j.hjkxxb.2019.0080, 2019.

- 1275 Sörgel, M., Regelin, E., Bozem, H., Diesch, J. M., Drewnick, F., Fischer, H., Harder, H., Held, A., Hosaynali-Beygi, Z., Martinez, M., and Zetzsch, C.: Quantification of the unknown HONO daytime source and its relation to NO₂, *Atmos. Chem. Phys.*, 11, 10433-10447, <https://doi.org/10.5194/acp-11-10433-2011>, 2011a.
- 1280 Sörgel, M., Trebs, I., Serafimovich, A., Moravek, A., Held, A., and Zetzsch, C.: Simultaneous HONO measurements in and above a forest canopy: influence of turbulent exchange on mixing ratio differences, *Atmos. Chem. Phys.*, 11, 841-855, <https://doi.org/10.5194/acp-11-841-2011>, 2011b.
- Sosedova, Y., Rouvière, A., Bartels-Rausch, T., and Ammann, M.: UVA/Vis-induced nitrous acid formation on polyphenolic films exposed to gaseous NO₂, *Photochemical & Photobiological Sciences*, 10, 1680-1690, <http://dx.doi.org/10.1039/C1PP05113J>, 2011.
- 1285 Spindler, G., Brüggemann, E., and Herrmann, H.: Nitrous acid (HNO₂) concentration measurements and estimation of dry deposition over grassland in eastern Germany, *Proceedings of the EUROTRAC Symposium 1998*, Vol. 2, WITpress, Southampton, UK, 218–222, 1999.
- Stemmler, K., Ammann, M., Donders, C., Kleffmann, J., and George, C.: Photosensitized reduction of nitrogen dioxide on humic acid as a source of nitrous acid, *Nature*, 440, 195-198, <https://doi.org/10.1038/nature04603>, 2006.
- 1290 Stutz, J., Kim, E. S., Platt, U., Bruno, P., Perrino, C., and Febo, A.: UV-visible absorption cross sections of nitrous acid, *Journal of Geophysical Research: Atmospheres*, 105, 14585-14592, <https://doi.org/10.1029/2000JD900003>, 2000.
- Stutz, J., Alicke, B., and Neftel, A.: Nitrous acid formation in the urban atmosphere: Gradient measurements of NO₂ and HONO over grass in Milan, Italy, *Journal of Geophysical Research: Atmospheres*, 107, 8192, <https://doi.org/10.1029/2001JD000390>, 2002.
- 1295 Stutz, J., Alicke, B., Ackermann, R., Geyer, A., Wang, S., White, A. B., Williams, E. J., Spicer, C. W., and Fast, J. D.: Relative humidity dependence of HONO chemistry in urban areas, *Journal of Geophysical Research: Atmospheres*, 109, <https://doi.org/10.1029/2003JD004135>, 2004.
- Su, H.: HONO: a study to its sources and impacts from field measurements at the sub-urban areas of PRD region, Ph.D. thesis, College of Environmental Sciences and Engineering, Peking University, China, 2008.
- 1300 Su, H., Cheng, Y. F., Cheng, P., Zhang, Y. H., Dong, S., Zeng, L. M., Wang, X., Slanina, J., Shao, M., and Wiedensohler, A.: Observation of nighttime nitrous acid (HONO) formation at a non-urban site during PRIDE-PRD2004 in China, *Atmospheric Environment*, 42, 6219-6232, <https://doi.org/10.1016/j.atmosenv.2008.04.006>, 2008a.
- Su, H., Cheng, Y. F., Shao, M., Gao, D. F., Yu, Z. Y., Zeng, L. M., Slanina, J., Zhang, Y. H., and Wiedensohler, A.: Nitrous acid (HONO) and its daytime sources at a rural site during the 2004 PRIDE-PRD experiment in China, *Journal of Geophysical Research*, 113, <https://doi.org/10.1029/2007JD009060>, 2008b.
- 1305 Su, H., Cheng, Y., Oswald, R., Behrendt, T., Trebs, I., Meixner, F. X., Andreae, M. O., Cheng, P., Zhang, Y., and Pöschl, U.: Soil Nitrite as a Source of Atmospheric HONO and OH Radicals, *Science*, 333, 1616-1618, <https://doi.org/10.1126/science.1207687>, 2011.
- Tan, Z., Fuchs, H., Lu, K., Hofzumahaus, A., Bohn, B., Broch, S., Dong, H., Gomm, S., Häsel, R., He, L., Holland, F., Li, X., Liu, Y., Lu, S., Rohrer, F., Shao, M., Wang, B., Wang, M., Wu, Y., Zeng, L., Zhang, Y., Wahner, A., and Zhang, Y.: Radical chemistry at a rural site (Wangdu) in the North China Plain: observation and model calculations of OH, HO₂ and RO₂ radicals, *Atmos. Chem. Phys.*, 17, 663-690, <https://doi.org/10.5194/acp-17-663-2017>, 2017.
- 1310 Tan, Z., Rohrer, F., Lu, K., Ma, X., Bohn, B., Broch, S., Dong, H., Fuchs, H., Gkatzelis, G. I., Hofzumahaus, A., Holland, F., Li, X., Liu, Y., Liu, Y., Novelli, A., Shao, M., Wang, H., Wu, Y., Zeng, L., Hu, M., Kiendler-Scharr, A., Wahner, A., and Zhang, Y.: Wintertime photochemistry in Beijing: observations of RO_x radical concentrations in the North China Plain during the BEST-ONE campaign, *Atmos. Chem. Phys.*, 18, 12391-12411, <https://doi.org/10.5194/acp-18-12391-2018>, 2018.
- 1315 Tan, Z., Lu, K., Hofzumahaus, A., Fuchs, H., Bohn, B., Holland, F., Liu, Y., Rohrer, F., Shao, M., Sun, K., Wu, Y., Zeng, L., Zhang, Y., Zou, Q., Kiendler-Scharr, A., Wahner, A., and Zhang, Y.: Experimental budgets of OH, HO₂, and RO₂ radicals and implications for ozone formation in the Pearl River Delta in China 2014, *Atmos. Chem. Phys.*, 19, 7129-7150, <https://doi.org/10.5194/acp-19-7129-2019>, 2019a.
- 1320 Tan, Z., Lu, K., Jiang, M., Su, R., Wang, H., Lou, S., Fu, Q., Zhai, C., Tan, Q., Yue, D., Chen, D., Wang, Z., Xie, S., Zeng, L., and Zhang, Y.: Daytime atmospheric oxidation capacity in four Chinese megacities during the photochemically polluted season: a case study based on box model simulation, *Atmos. Chem. Phys.*, 19, 3493-3513, <https://doi.org/10.5194/acp-19-3493-2019>, 2019b.

- 1325 Tang, X. Y.: The characteristics of urban air pollution in China, in *Urbanization, energy, and air pollution in China: The challenges ahead*, Proceedings of A Symposium, 47-54, DOI : 10.17226/11192, 2004.
- Tang, Y., An, J., Wang, F., Li, Y., Qu, Y., Chen, Y., and Lin, J.: Impacts of an unknown daytime HONO source on the mixing ratio and budget of HONO, and hydroxyl, hydroperoxyl, and organic peroxy radicals, in the coastal regions of China, *Atmos. Chem. Phys.*, 15, 9381-9398, <https://doi.org/10.5194/acp-15-9381-2015>, 2015.
- 1330 Tian, Z., Yang, W., Yu, X., Zhang, M., Zhang, H., Cheng, D., Cheng, P., and Wang, B.: HONO pollution characteristics and nighttime sources during autumn in Guangzhou, China *Environmental Science*, 39 (05), 2000-2009, DOI: 10.13227/j.hjckx.201709269, 2018.
- Tong, S., Hou, S., Zhang, Y., Chu, B., Liu, Y., He, H., Zhao, P., and Ge, M.: Comparisons of measured nitrous acid (HONO) concentrations in a pollution period at urban and suburban Beijing, in autumn of 2014, *Science China Chemistry*, 58, 1393-1402, <https://doi.org/10.1007/s11426-015-5454-2>, 2015.
- 1335 Tong, S., Hou, S., Zhang, Y., Chu, B., Liu, Y., He, H., Zhao, P., and Ge, M.: Exploring the nitrous acid (HONO) formation mechanism in winter Beijing: direct emissions and heterogeneous production in urban and suburban areas, *Faraday Discuss*, 189, 213-230, <https://doi.org/10.1039/C5FD00163C>, 2016.
- Trinh, H. T., Imanishi, K., Morikawa, T., Hagino, H., and Takenaka, N.: Gaseous nitrous acid (HONO) and nitrogen oxides (NO_x) emission from gasoline and diesel vehicles under real-world driving test cycles, *Journal of the Air & Waste Management Association*, 67, 412-420, <https://doi.org/10.1080/10962247.2016.1240726>, 2017.
- VandenBoer, T. C., Brown, S. S., Murphy, J. G., Keene, W. C., Young, C. J., Pszenny, A. A. P., Kim, S., Warneke, C., de Gouw, J. A., Maben, J. R., Wagner, N. L., Riedel, T. P., Thornton, J. A., Wolfe, D. E., Dubé, W. P., Öztürk, F., Brock, C. A., Grossberg, N., Lefter, B., Lerner, B., Middlebrook, A. M., and Roberts, J. M.: Understanding the role of the ground surface in HONO vertical structure: High resolution vertical profiles during NACHTT-11, *Journal of Geophysical Research: Atmospheres*, 118, 10,155-110,171, <https://doi.org/10.1002/jgrd.50721>, 2013.
- 1345 VandenBoer, T. C., Young, C. J., Talukdar, R. K., Markovic, M. Z., Brown, S. S., Roberts, J. M., and Murphy, J. G.: Nocturnal loss and daytime source of nitrous acid through reactive uptake and displacement, *Nature Geoscience*, 8, 55-60, <https://doi.org/10.1038/ngeo2298>, 2015.
- 1350 Villena, G., Kleffmann, J., Kurtenbach, R., Wiesen, P., Lissi, E., Rubio, M. A., Croxatto, G., and Rappenglück, B.: Vertical gradients of HONO, NO_x and O₃ in Santiago de Chile, *Atmospheric Environment*, 45, 3867-3873, <https://doi.org/10.1016/j.atmosenv.2011.01.073>, 2011.
- Voogt, J. A., and Oke, T. R.: Complete Urban Surface Temperatures, *Journal of Applied Meteorology*, 36, 1117-1132, [https://doi.org/10.1175/1520-0450\(1997\)036<1117:CUST>2.0.CO;2](https://doi.org/10.1175/1520-0450(1997)036<1117:CUST>2.0.CO;2), 1997.
- 1355 Wall, K. J., and Harris, G. W.: Uptake of nitrogen dioxide (NO₂) on acidic aqueous humic acid (HA) solutions as a missing daytime nitrous acid (HONO) surface source, *Journal of Atmospheric Chemistry*, 74, 283-321, <https://doi.org/10.1007/s10874-016-9342-8>, 2017.
- Wang, G., Zhang, R., Gomez, M. E., Yang, L., Levy Zamora, M., Hu, M., Lin, Y., Peng, J., Guo, S., Meng, J., Li, J., Cheng, C., Hu, T., Ren, Y., Wang, Y., Gao, J., Cao, J., An, Z., Zhou, W., Li, G., Wang, J., Tian, P., Marrero-Ortiz, W., Secret, J., Du, Z., Zheng, J., Shang, D., Zeng, L., Shao, M., Wang, W., Huang, Y., Wang, Y., Zhu, Y., Li, Y., Hu, J., Pan, B., Cai, L., Cheng, Y., Ji, Y., Zhang, F., Rosenfeld, D., Liss, P. S., Duce, R. A., Kolb, C. E., and Molina, M. J.: Persistent sulfate formation from London Fog to Chinese haze, *Proceedings of the National Academy of Sciences*, 113, 13630-13635, <https://doi.org/10.1073/pnas.1616540113>, 2016.
- 1360 Wang, G., Ma, S., Niu, X., Chen, X., Liu, F., Li, X., Li, L., Shi, G., and Wu, Z.: Barrierless HONO and HOS(O)₂-NO₂ Formation via NH₃-Promoted Oxidation of SO₂ by NO₂, *The Journal of Physical Chemistry A*, 125, 2666-2672, <https://doi.org/10.1021/acs.jpca.1c00539>, 2021a.
- 1365 Wang, J., Zhang, X., Guo, J., Wang, Z., and Zhang, M.: Observation of nitrous acid (HONO) in Beijing, China: Seasonal variation, nocturnal formation and daytime budget, *Science of The Total Environment*, 587-588, 350-359, <https://doi.org/10.1016/j.scitotenv.2017.02.159>, 2017a.
- 1370 Wang, S., Zhou, R., Zhao, H., Wang, Z., Chen, L., and Zhou, B.: Long-term observation of atmospheric nitrous acid (HONO) and its implication to local NO₂ levels in Shanghai, China, *Atmospheric Environment*, 77, 718-724, <https://doi.org/10.1016/j.atmosenv.2013.05.071>, 2013.

- 1375 Wang, T., Wei, X. L., Ding, A. J., Poon, C. N., Lam, K. S., Li, Y. S., Chan, L. Y., and Anson, M.: Increasing surface ozone concentrations in the background atmosphere of Southern China, 1994–2007, *Atmos. Chem. Phys.*, 9, 6217–6227, <https://doi.org/10.5194/acp-9-6217-2009>, 2009.
- Wang, T., Xue, L., Brimblecombe, P., Lam, Y. F., Li, L., and Zhang, L.: Ozone pollution in China: A review of concentrations, meteorological influences, chemical precursors, and effects, *Science of The Total Environment*, 575, 1582–1596, <https://doi.org/10.1016/j.scitotenv.2016.10.081>, 2017b.
- 1380 Wang, Y., Fu, X., Wu, D., Wang, M., Lu, K., Mu, Y., Liu, Z., Zhang, Y., and Wang, T.: Agricultural Fertilization Aggravates Air Pollution by Stimulating Soil Nitrous Acid Emissions at High Soil Moisture, *Environmental Science & Technology*, 55, 14556–14566, <https://doi.org/10.1021/acs.est.1c04134>, 2021b.
- 1385 Weber, B., Wu, D., Tamm, A., Ruckteschler, N., Rodriguez-Caballero, E., Steinkamp, J., Meusel, H., Elbert, W., Behrendt, T., Sorgel, M., Cheng, Y., Crutzen, P. J., Su, H., and Poschl, U.: Biological soil crusts accelerate the nitrogen cycle through large NO and HONO emissions in drylands, *Proceedings of the National Academy of Sciences*, 112, 15384–15389, <https://doi.org/10.1073/pnas.1515818112>, 2015.
- Wen, L., Chen, T., Zheng, P., Wu, L., Wang, X., Mellouki, A., Xue, L., and Wang, W.: Nitrous acid in marine boundary layer over eastern Bohai Sea, China: Characteristics, sources, and implications, *Science of The Total Environment*, 670, 282–291, <https://doi.org/10.1016/j.scitotenv.2019.03.225>, 2019.
- 1390 Wojtal, P., Halla, J. D., and McLaren, R.: Pseudo steady states of HONO measured in the nocturnal marine boundary layer: a conceptual model for HONO formation on aqueous surfaces, *Atmos. Chem. Phys.*, 11, 3243–3261, <https://doi.org/10.5194/acp-11-3243-2011>, 2011.
- Wolfe, G. M., Marvin, M. R., Roberts, S. J., Travis, K. R., and Liao, J.: The Framework for 0-D Atmospheric Modeling (F0AM) v3.1, *Geosci. Model Dev.*, 9, 3309–3319, <https://doi.org/10.5194/gmd-9-3309-2016>, 2016.
- 1395 Wong, K. W., Oh, H. J., Lefer, B. L., Rappenglück, B., and Stutz, J.: Vertical profiles of nitrous acid in the nocturnal urban atmosphere of Houston, TX, *Atmos. Chem. Phys.*, 11, 3595–3609, <https://doi.org/10.5194/acp-11-3595-2011>, 2011.
- Wong, K. W., Tsai, C., Lefer, B., Haman, C., Grossberg, N., Brune, W. H., Ren, X., Luke, W., and Stutz, J.: Daytime HONO vertical gradients during SHARP 2009 in Houston, TX, *Atmos. Chem. Phys.*, 12, 635–652, <https://doi.org/10.5194/acp-12-635-2012>, 2012.
- 1400 Wu, C., Wu, D., and Yu, J. Z.: Quantifying black carbon light absorption enhancement with a novel statistical approach, *Atmos. Chem. Phys.*, 18, 289–309, <https://doi.org/10.5194/acp-18-289-2018>, 2018.
- Wu, D., Horn, M. A., Behrendt, T., Muller, S., Li, J., Cole, J. A., Xie, B., Ju, X., Li, G., Ermel, M., Oswald, R., Frohlich-Nowoisky, J., Hoor, P., Hu, C., Liu, M., Andreae, M. O., Poschl, U., Cheng, Y., Su, H., Trebs, I., Weber, B., and Sorgel, M.: Soil HONO emissions at high moisture content are driven by microbial nitrate reduction to nitrite: tackling the HONO puzzle, *ISME J*, 13, 1688–1699, <https://doi.org/10.1038/s41396-019-0379-y>, 2019.
- 1405 Wu, Y., Li, S., and Yu, S.: Monitoring urban expansion and its effects on land use and land cover changes in Guangzhou city, China, *Environmental Monitoring and Assessment*, 188, 54, <https://doi.org/10.1007/s10661-015-5069-2>, 2015.
- Xia, D., Zhang, X., Chen, J., Tong, S., Xie, H.-b., Wang, Z., Xu, T., Ge, M., and Allen, D. T.: Heterogeneous Formation of HONO Catalyzed by CO₂, *Environmental Science & Technology*, 55, 12215–12222, <https://doi.org/10.1021/acs.est.1c02706>, 2021.
- 1410 Xing, L., Wu, J., Elser, M., Tong, S., Liu, S., Li, X., Liu, L., Cao, J., Zhou, J., El-Haddad, I., Huang, R., Ge, M., Tie, X., Prévôt, A. S. H., and Li, G.: Wintertime secondary organic aerosol formation in Beijing–Tianjin–Hebei (BTH): contributions of HONO sources and heterogeneous reactions, *Atmos. Chem. Phys.*, 19, 2343–2359, <https://doi.org/10.5194/acp-19-2343-2019>, 2019.
- 1415 Xu, W., Kuang, Y., Zhao, C., Tao, J., Zhao, G., Bian, Y., Yang, W., Yu, Y., Shen, C., Liang, L., Zhang, G., Lin, W., and Xu, X.: NH₃-promoted hydrolysis of NO₂ induces explosive growth in HONO, *Atmos. Chem. Phys.*, 19, 10557–10570, <https://doi.org/10.5194/acp-19-10557-2019>, 2019.
- Xu, Z., Wang, T., Xue, L. K., Louie, P. K. K., Luk, C. W. Y., Gao, J., Wang, S. L., Chai, F. H., and Wang, W. X.: Evaluating the uncertainties of thermal catalytic conversion in measuring atmospheric nitrogen dioxide at four differently polluted sites in China, *Atmospheric Environment*, 76, 221–226, <https://doi.org/10.1016/j.atmosenv.2012.09.043>, 2013.
- 1420 Xu, Z., Wang, T., Wu, J., Xue, L., Chan, J., Zha, Q., Zhou, S., Louie, P. K. K., and Luk, C. W. Y.: Nitrous acid (HONO) in a polluted subtropical atmosphere: Seasonal variability, direct vehicle emissions and heterogeneous production at ground surface, *Atmospheric Environment*, 106, 100–109, <https://doi.org/10.1016/j.atmosenv.2015.01.061>, 2015.

- Xue, C., Zhang, C., Ye, C., Liu, P., Catoire, V., Krysztofiak, G., Chen, H., Ren, Y., Zhao, X., Wang, J., Zhang, F., Zhang, C., Zhang, J., An, J., Wang, T., Chen, J., Kleffmann, J., Mellouki, A., and Mu, Y.: HONO Budget and Its Role in Nitrate Formation in the Rural North China Plain, *Environ Sci Technol*, 54, 11048-11057, <https://doi.org/10.1021/acs.est.0c01832>, 2020.
- Xue, L., Gu, R., Wang, T., Wang, X., Saunders, S., Blake, D., Louie, P. K. K., Luk, C. W. Y., Simpson, I., Xu, Z., Wang, Z., Gao, Y., Lee, S., Mellouki, A., and Wang, W.: Oxidative capacity and radical chemistry in the polluted atmosphere of Hong Kong and Pearl River Delta region: analysis of a severe photochemical smog episode, *Atmos. Chem. Phys.*, 16, 9891-9903, <https://doi.org/10.5194/acp-16-9891-2016>, 2016.
- Xue, L. K., Wang, T., Gao, J., Ding, A. J., Zhou, X. H., Blake, D. R., Wang, X. F., Saunders, S. M., Fan, S. J., Zuo, H. C., Zhang, Q. Z., and Wang, W. X.: Ground-level ozone in four Chinese cities: precursors, regional transport and heterogeneous processes, *Atmos. Chem. Phys.*, 14, 13175-13188, <https://doi.org/10.5194/acp-14-13175-2014>, 2014.
- Yabushita, A., Enami, S., Sakamoto, Y., Kawasaki, M., Hoffmann, M. R., and Colussi, A. J.: Anion-Catalyzed Dissolution of NO₂ on Aqueous Microdroplets, *The Journal of Physical Chemistry A*, 113, 4844-4848, <https://doi.org/10.1021/jp900685f>, 2009.
- Yang, J., Shen, H., Guo, M.-Z., Zhao, M., Jiang, Y., Chen, T., Liu, Y., Li, H., Zhu, Y., Meng, H., Wang, W., and Xue, L.: Strong marine-derived nitrous acid (HONO) production observed in the coastal atmosphere of northern China, *Atmospheric Environment*, 244, 117948, <https://doi.org/10.1016/j.atmosenv.2020.117948>, 2021a.
- Yang, Q.: Observations and sources analysis of gaseous nitrous acid — A case study in Beijing and Pearl River Delta area, Ph.D. thesis, College of Environmental Sciences and Engineering, Peking University, China, 2014.
- Yang, Q., Su, H., Li, X., Cheng, Y., Lu, K., Cheng, P., Gu, J., Guo, S., Hu, M., Zeng, L., Zhu, T., and Zhang, Y.: Daytime HONO formation in the suburban area of the megacity Beijing, China, *Science China Chemistry*, 57, 1032-1042, <https://doi.org/10.1007/s11426-013-5044-0>, 2014.
- Yang, W., Cheng, P., Tian, Z., Zhang, H., Zhang, M., and Wang, B.: Study on HONO pollution characteristics and daytime unknown sources during summer and autumn in Guangzhou, China., *China Environmental Science*, 37 (006), 2029-2039, DOI: 10.3969/j.issn.1000-6923.2017.06.005, 2017a.
- Yang, W., Han, C., Zhang, T., Tang, N., Yang, H., and Xue, X.: Heterogeneous photochemical uptake of NO₂ on the soil surface as an important ground-level HONO source, *Environmental Pollution*, 271, 116289, <https://doi.org/10.1016/j.envpol.2020.116289>, 2021b.
- Yang, W., You, D., Li, C., Han, C., Tang, N., Yang, H., and Xue, X.: Photolysis of Nitroaromatic Compounds under Sunlight: A Possible Daytime Photochemical Source of Nitrous Acid?, *Environmental Science & Technology Letters*, 8, 747-752, <https://doi.org/10.1021/acs.estlett.1c00614>, 2021c.
- Yang, Y., Shao, M., Keβel, S., Li, Y., Lu, K., Lu, S., Williams, J., Zhang, Y., Zeng, L., Nölscher, A. C., Wu, Y., Wang, X., and Zheng, J.: How the OH reactivity affects the ozone production efficiency: case studies in Beijing and Heshan, China, *Atmos. Chem. Phys.*, 17, 7127-7142, <https://doi.org/10.5194/acp-17-7127-2017>, 2017b.
- Yang, Y., Li, X., Zu, K., Lian, C., Chen, S., Dong, H., Feng, M., Liu, H., Liu, J., Lu, K., Lu, S., Ma, X., Song, D., Wang, W., Yang, S., Yang, X., Yu, X., Zhu, Y., Zeng, L., Tan, Q., and Zhang, Y.: Elucidating the effect of HONO on O₃ pollution by a case study in southwest China, *Science of The Total Environment*, 756, 144127, <https://doi.org/10.1016/j.scitotenv.2020.144127>, 2021d.
- Ye, C., Zhou, X., Pu, D., Stutz, J., Festa, J., Spolaor, M., Cantrell, C., Mauldin, R. L., Weinheimer, A., and Haggerty, J.: ATMOSPHERIC SCIENCE. Comment on "Missing gas-phase source of HONO inferred from Zeppelin measurements in the troposphere", *Science*, 348, 1326, DOI: 10.1126/science.aaa1992, 2015.
- Ye, C., Gao, H., Zhang, N., and Zhou, X.: Photolysis of Nitric Acid and Nitrate on Natural and Artificial Surfaces, *Environ Sci Technol*, 50, 3530-3536, <https://doi.org/10.1021/acs.est.5b05032>, 2016.
- Ye, C., Zhang, N., Gao, H., and Zhou, X.: Photolysis of Particulate Nitrate as a Source of HONO and NO_x, *Environmental Science & Technology*, 51, 6849-6856, <https://doi.org/10.1021/acs.est.7b00387>, 2017.
- Yu, Y., Galle, B., Panday, A., Hodson, E., Prinn, R., and Wang, S.: Observations of high rates of NO₂/HONO conversion in the nocturnal atmospheric boundary layer in Kathmandu, Nepal, *Atmos. Chem. Phys.*, 9, 6401-6415, <https://doi.org/10.5194/acp-9-6401-2009>, 2009.
- Yue, D. L., Hu, M., Wu, Z. J., Guo, S., Wen, M. T., Nowak, A., Wehner, B., Wiedensohler, A., Takegawa, N., Kondo, Y., Wang, X. S., Li, Y. P., Zeng, L. M., and Zhang, Y. H.: Variation of particle number size distributions and chemical

- compositions at the urban and downwind regional sites in the Pearl River Delta during summertime pollution episodes, *Atmos. Chem. Phys.*, 10, 9431-9439, <https://doi.org/10.5194/acp-10-9431-2010>, 2010.
- 1475 Yue, D. L., Zhong, L., Shen, J., Zhang, T., Zhou, Y., Zeng, L., and Dong, H.: Pollution properties of atmospheric HNO₂ and its effect on OH radical formation in the PRD region in autumn, *Environmental Science & Technology*, 162-166, DOI: 10.3969/j.issn.1003-6504.2016.02.030, 2016.
- 1480 Yun, H., Wang, Z., Zha, Q., Wang, W., Xue, L., Zhang, L., Li, Q., Cui, L., Lee, S., Poon, S. C. N., and Wang, T.: Nitrous acid in a street canyon environment: Sources and contributions to local oxidation capacity, *Atmospheric Environment*, 167, 223-234, <https://doi.org/10.1016/j.atmosenv.2017.08.018>, 2017.
- Yun, H.: Reactive nitrogen oxides (HONO, N₂O₅ and ClNO₂) in different atmospheric environment in China: concentrations formation and the impact on atmospheric oxidation capacity, Ph.D. thesis. Department of Civil and Environmental Engineering, The Hong Kong Polytechnic University, China, 2018.
- 1485 Zha, Q., Xue, L., Wang, T., Xu, Z., Yeung, C., Louie, P. K. K., and Luk, C. W. Y.: Large conversion rates of NO₂ to HNO₂ observed in air masses from the South China Sea: Evidence of strong production at sea surface?, *Geophysical Research Letters*, 41, 7710-7715, <https://doi.org/10.1002/2014GL061429>, 2014.
- Zhang, B., and Tao, F.-M.: Direct homogeneous nucleation of NO₂, H₂O, and NH₃ for the production of ammonium nitrate particles and HONO gas, *Chemical Physics Letters*, 489, 143-147, <https://doi.org/10.1016/j.cplett.2010.02.059>, 2010.
- 1490 Zhang, J., An, J., Qu, Y., Liu, X., and Chen, Y.: Impacts of potential HONO sources on the concentrations of oxidants and secondary organic aerosols in the Beijing-Tianjin-Hebei region of China, *Science of The Total Environment*, 647, 836-852, <https://doi.org/10.1016/j.scitotenv.2018.08.030>, 2019a.
- Zhang, L., Wang, T., Zhang, Q., Zheng, J., Xu, Z., and Lv, M.: Potential sources of nitrous acid (HONO) and their impacts on ozone: A WRF-Chem study in a polluted subtropical region, *Journal of Geophysical Research: Atmospheres*, 121, 3645-3662, <https://doi.org/10.1002/2015JD024468>, 2016.
- 1495 Zhang, N., Zhou, X., Shepson, P. B., Gao, H., Alaghmand, M., and Stirm, B.: Aircraft measurement of HONO vertical profiles over a forested region, *Geophysical Research Letters*, 36, <https://doi.org/10.1029/2009GL038999>, 2009.
- Zhang, S., Sarwar, G., Xing, J., Chu, B., Xue, C., Sarav, A., Ding, D., Zheng, H., Mu, Y., Duan, F., Ma, T., and He, H.: Improving the representation of HONO chemistry in CMAQ and examining its impact on haze over China, *Atmos. Chem. Phys.*, 21, 15809-15826, <https://doi.org/10.5194/acp-21-15809-2021>, 2021.
- 1500 Zhang, W., Tong, S., Ge, M., An, J., Shi, Z., Hou, S., Xia, K., Qu, Y., Zhang, H., Chu, B., Sun, Y., and He, H.: Variations and sources of nitrous acid (HONO) during a severe pollution episode in Beijing in winter 2016, *Science of The Total Environment*, 648, 253-262, <https://doi.org/10.1016/j.scitotenv.2018.08.133>, 2019b.
- Zhao, X., Shi, X., Ma, X., Wang, J., Xu, F., Zhang, Q., Li, Y., Teng, Z., Han, Y., Wang, Q., and Wang, W.: Simulation Verification of Barrierless HONO Formation from the Oxidation Reaction System of NO, Cl, and Water in the Atmosphere, *Environmental Science & Technology*, 55, 7850-7857, <https://doi.org/10.1021/acs.est.1c01773>, 2021.
- 1505 Zheng, J., Zhong, L., Wang, T., Louie, P. K. K., and Li, Z.: Ground-level ozone in the Pearl River Delta region: Analysis of data from a recently established regional air quality monitoring network, *Atmospheric Environment*, 44, 814-823, <https://doi.org/10.1016/j.atmosenv.2009.11.032>, 2010.
- Zheng, J., Shi, X., Ma, Y., Ren, X., Jabbour, H., Diao, Y., Wang, W., Ge, Y., Zhang, Y., and Zhu, W.: Contribution of nitrous acid to the atmospheric oxidation capacity in an industrial zone in the Yangtze River Delta region of China, *Atmos. Chem. Phys.*, 20, 5457-5475, <https://doi.org/10.5194/acp-20-5457-2020>, 2020.
- Zhong, L., Louie, P. K. K., Zheng, J., Yuan, Z., Yue, D., Ho, J. W. K., and Lau, A. K. H.: Science-policy interplay: Air quality management in the Pearl River Delta region and Hong Kong, *Atmospheric Environment*, 76, 3-10, <https://doi.org/10.1016/j.atmosenv.2013.03.012>, 2013.
- 1515 Zhou, X., Civerolo, K., Dai, H., Huang, G., Schwab, J., and Demerjian, K.: Summertime nitrous acid chemistry in the atmospheric boundary layer at a rural site in New York State, *Journal of Geophysical Research: Atmospheres*, 107, ACH 13-11-ACH 13-11, <https://doi.org/10.1029/2001JD001539>, 2002a.
- Zhou, X., He, Y., Huang, G., Thornberry, T. D., Carroll, M. A., and Bertman, S. B.: Photochemical production of nitrous acid on glass sample manifold surface, *Geophysical Research Letters*, 29, 26-21-26-24, <https://doi.org/10.1029/2002GL015080>, 2002b.
- 1520

Zhou, X., Gao, H., He, Y., Huang, G., Bertman, S. B., Civerolo, K., and Schwab, J.: Nitric acid photolysis on surfaces in low-NO_x environments: Significant atmospheric implications, *Geophysical Research Letters*, 30, <https://doi.org/10.1029/2003GL018620>, 2003.

1525 Zhou, X., Huang, G., Civerolo, K., Roychowdhury, U., and Demerjian, K. L.: Summertime observations of HONO, HCHO, and O₃ at the summit of Whiteface Mountain, New York, *Journal of Geophysical Research: Atmospheres*, 112, <https://doi.org/10.1029/2006JD007256>, 2007.

Zhou, X., Zhang, N., TerAvest, M., Tang, D., Hou, J., Bertman, S., Alaghmand, M., Shepson, P. B., Carroll, M. A., Griffith, S., Dusanter, S., and Stevens, P. S.: Nitric acid photolysis on forest canopy surface as a source for tropospheric nitrous acid, *Nature Geoscience*, 4, 440-443, <https://doi.org/10.1038/ngeo1164>, 2011.

1530 Ziemba, L. D., Dibb, J. E., Griffin, R. J., Anderson, C. H., Whitlow, S. I., Lefer, B. L., Rappenglück, B., and Flynn, J.: Heterogeneous conversion of nitric acid to nitrous acid on the surface of primary organic aerosol in an urban atmosphere, *Atmospheric Environment*, 44, 4081-4089, <https://doi.org/10.1016/j.atmosenv.2008.12.024>, 2010.

Budget of nitrous acid (HONO) ~~and its impacts on atmospheric oxidation capacity~~ at an urban site in the fall season of Guangzhou, China

5 Yihang Yu^{1,2,†}, Peng Cheng^{1,2,5,*†}, Huirong Li^{1,2}, Wenda Yang^{1,2}, Baobin Han^{1,2}, Wei Song³, Weiwei Hu³, Xinming Wang³, Bin Yuan^{4,5}, Min Shao^{4,5}, Zhijiong Huang⁴, Zhen Li⁴, Junyu Zheng^{4,5}, Haichao Wang⁶ and Xiaofang Yu^{1,2}

¹Institute of Mass Spectrometry and Atmospheric Environment, Jinan University, Guangzhou 510632, China

10 ²Guangdong Provincial Engineering Research Center for Online Source Apportionment System of Air Pollution, Guangzhou 510632, China

³State Key Laboratory of Organic Geochemistry, Guangzhou Institute of Geochemistry, Chinese Academy of Sciences, Guangzhou 510640, China

⁴Institute for Environmental and Climate Research, Jinan University, Guangzhou 511443, China

15 ⁵Guangdong-Hongkong-Macau Joint Laboratory of Collaborative Innovation for Environmental Quality, Guangzhou 511443, China

⁶School of Atmospheric Sciences, Sun Yat-Sen University, Zhuhai, China.

~~†These authors contribute equally to this paper.~~

*Correspondence to: Peng Cheng (chengp@jnu.edu.cn)

The introduction of our custom-built LOPAP

The LOPAP instrument was first developed by Heland et al. (2001), which is based on wet chemical sampling and photometric detection. Ambient air is sampled into an external sampling unit consisting of two similar stripping coils in series. Almost all the HONO and a small fraction of interfering substances (PAN, HNO₃, NO₂, etc.) are absorbed in solution in the first stripping coil, while in the second stripping coil only the interfering species are absorbed. To minimize the potential interferences, we assume the interferences absorbed in the first and the second coil are the same, so the real HONO concentration in the atmosphere is determined by subtracting the measured signal of the second coil from the measured signal of the first coil. The absorption solution R1 is a mixture reagent of 1 L hydrochloric acid (HCl) (37% volume fraction) and 100 g sulfanilamide dissolved in 9 L pure water. The dye solution R2, 2 g n-(1-naphtyl)-ethylenediamine-dihydrochloride (NEDA) dissolved in 10 L pure water, is then reacted with the absorption solution from two stripping coils pumped by a peristaltic pump to form colored azo dye. The light-absorbing colored azo dye is then pumped through a debubbler by the peristaltic pump and flows into the detection unit, which consists of two liquid waveguide capillary cells (World Precision Instrument, LWCC), one LED light source (Ocean Optics), two miniature spectrometers (Ocean Optics, Maya2000Pro) and several optical fibers. To correct for the small zero-drifts in the instrument's baseline, the zero measurements were conducted every 12 h by introducing zero air (highly pure nitrogen). During the instrument's operation, the instrument calibration was performed every week using the standard sodium nitrite (NaNO₂) solution.

Detection limit is defined as 3σ of HONO concentration measured in zero air measurement. The detection limit of 5 pptv for this campaign was determined by zero air measurement. This 5 pptv also serves as the precision of the instrument. Time resolution is defined as the time interval between HONO signal decreases from 90% of the signal when start zero air running to 10% higher than the zero signal. It also relates to the liquid flow. The determined time resolution during the campaign is about 15 min considering the air flow of 1 L min⁻¹ and liquid flow of 0.4 mL min⁻¹. Measurement error is the sum of statistic error and systematic error. Statistic error is defined as 1σ of HONO signal in zero air measurement. Systematic error is coming from the uncertainties of air flow rate, liquid flow rate and calibration factor, and is about 8% of measured HONO by applying "Gaussian Error Propagation" method (Trebs et al., 2004). The instrument parameters are listed in Table S1.

A commercial LOPAP (QUMA, Germany) operated by the Guangzhou Institute of Geochemistry Chinese Academy of Sciences (GIGCAS) also measured HONO during the observation. Unfortunately, only less than 10 days data were obtained by the commercial LOPAP due to malfunction. Our custom-built LOPAP was validated against the commercial LOPAP instrument with good agreement ($R^2 = 0.910$) (see Fig. S2), which further demonstrated the reliability of our instrument.

Evaluation of model performance

The index of agreement (IOA) can be calculated by E-S1 to further evaluate the performance of O₃ simulation against the measurement.

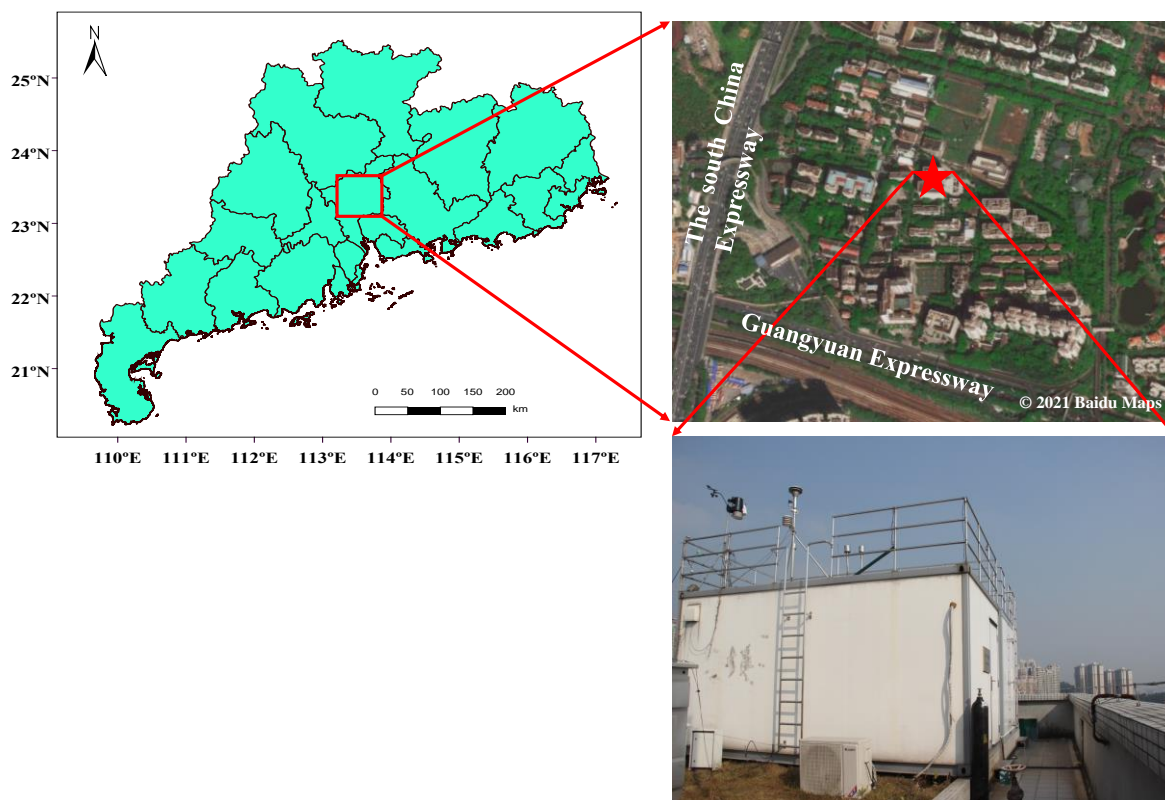
55

$$IOA = 1 - \frac{\sum_{i=1}^n (O_i - S_i)^2}{\sum_{i=1}^n (|O_i - \bar{O}| + |S_i - \bar{O}|)^2} \quad (E-S1)$$

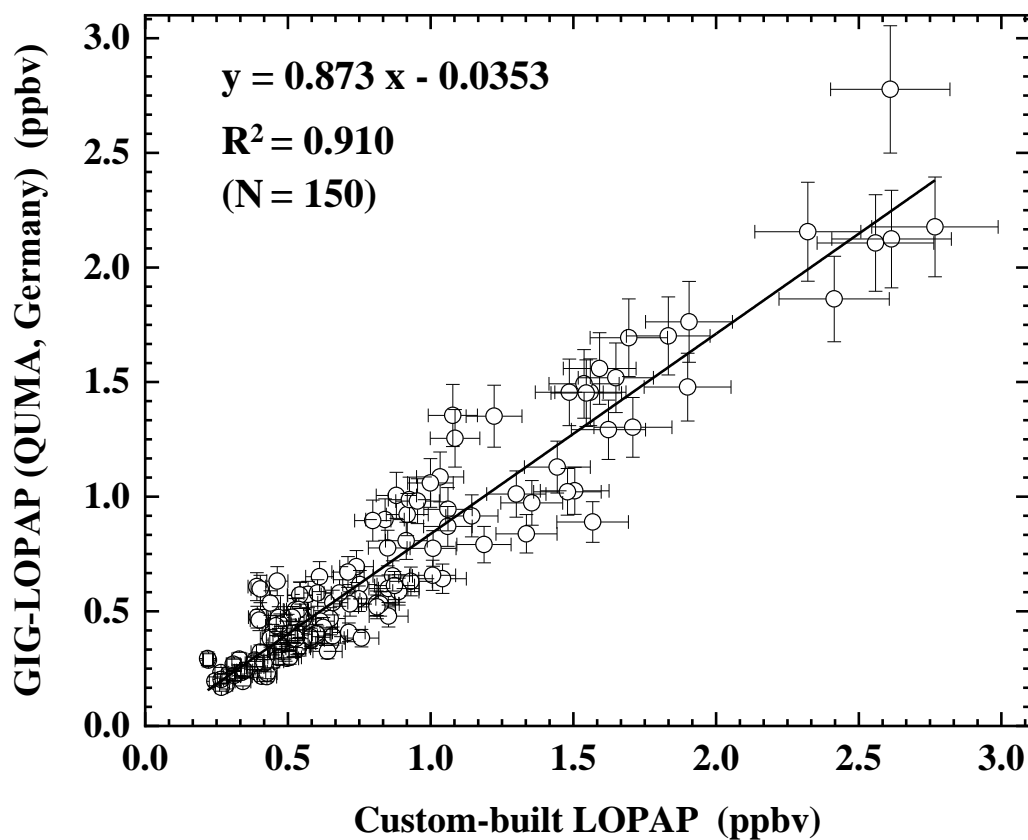
where n is a number of data points, and S_i and O_i denote box model simulated and observed concentrations, respectively.

The IOA ranges from 0 to 1, and a larger IOA value suggests better agreement between model and observation. The IOA of

60 O₃ simulation is 0.78, showing the good performance of model in this study.



65 Figure S1. Schematic map of the measurement site in Guangzhou. The red star represents specimen building of the Guangzhou Institute of Geochemistry, Chinese Academy of Sciences (GIGCAS).



70 Figure S2. Intercomparison between the custom-built LOPAP with the commercial LOPAP (QUMA, Germany). The linear fitting line has an intercept of $A = -0.035 \pm 0.022$, a slope of $B = 0.873 \pm 0.023$ and $R^2 = 0.910$ ($N = 150$). The error bars represent the uncertainties of our custom-built LOPAP (8%) and commercial LOPAP data (QUMA, Germany) (10%). The data from October 15-18 and November 1-6, 2018 was used for comparison.

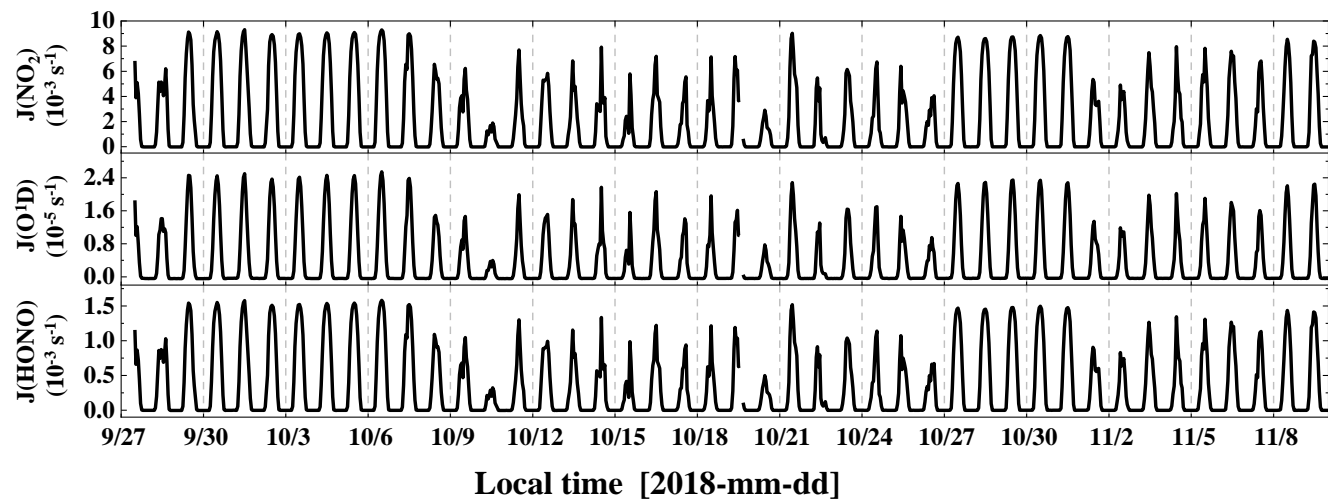
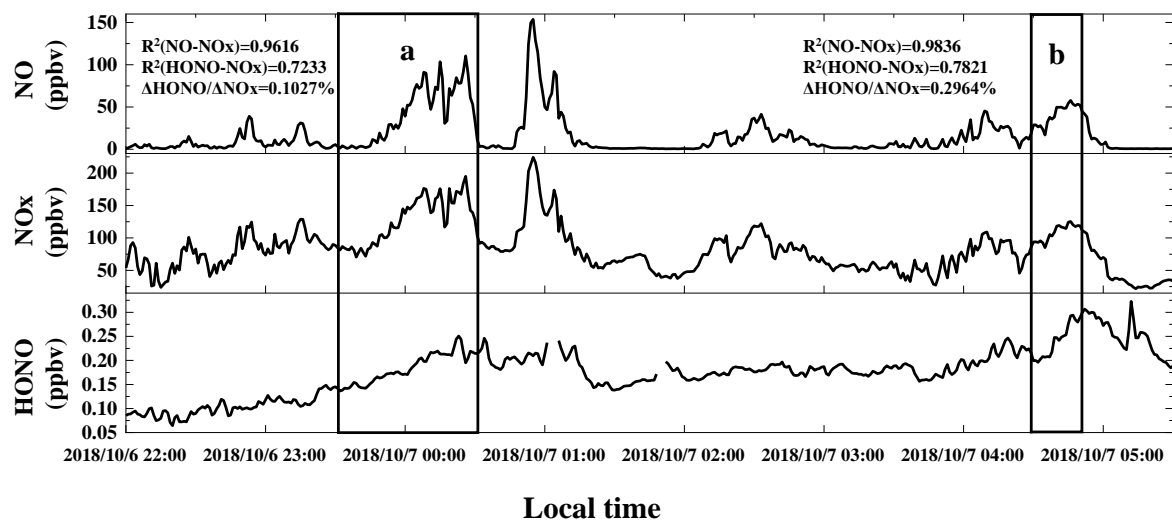


Figure S3. Temporal variations of photolysis rates $J(\text{HONO})$, $J(\text{O}^1\text{D})$ and $J(\text{NO}_2)$ during the observation period.



80 Figure S4. Temporal variations of nocturnal HONO, NO_x and NO on October 6–7, 2018. The HONO emission factors were obtained according to the data in the black frames a and b.

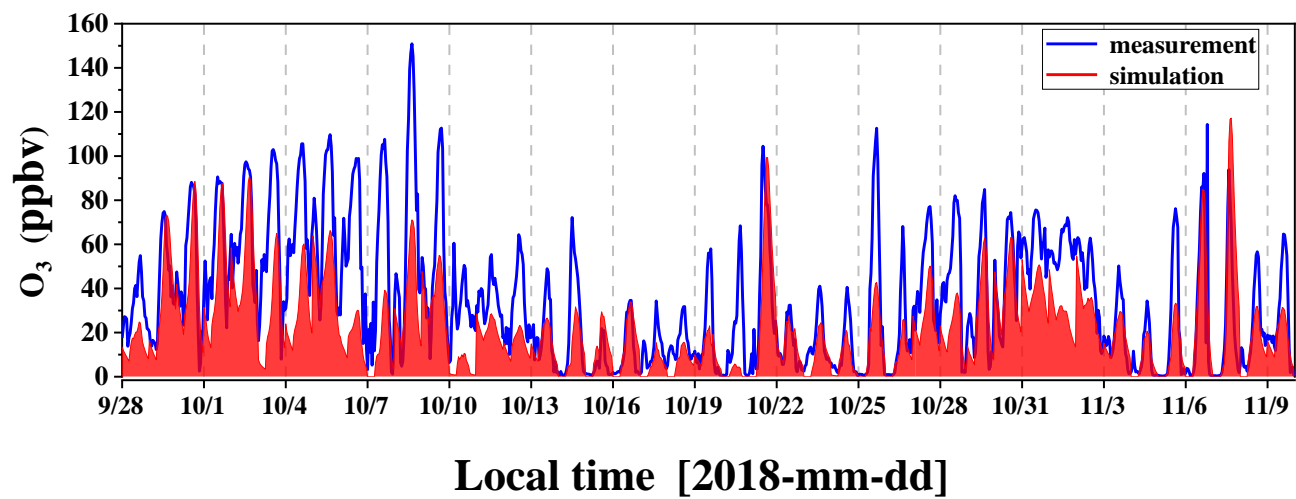
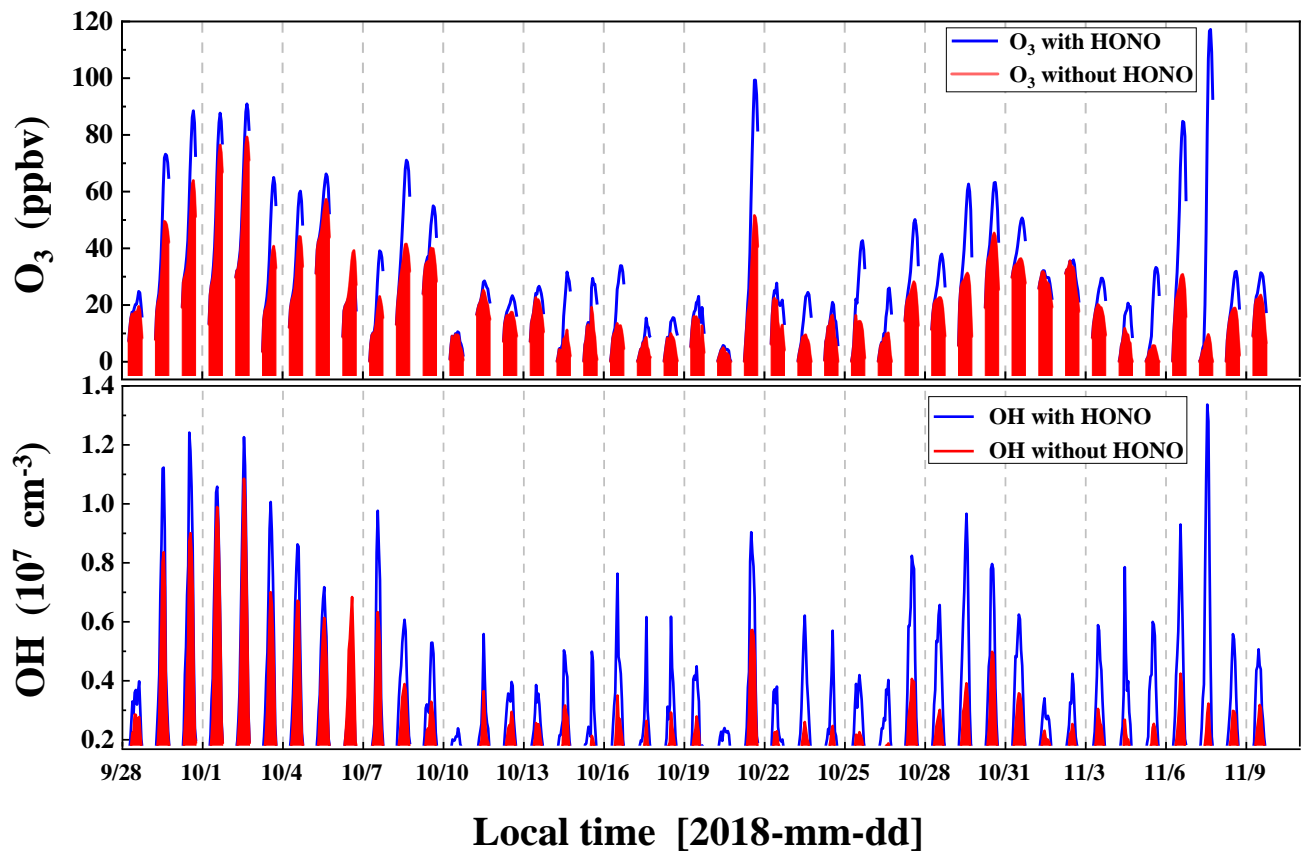


Figure S5. The time series of measured and simulated O_3 values.



85

Figure S6. The time series of simulation results of O₃ and OH.

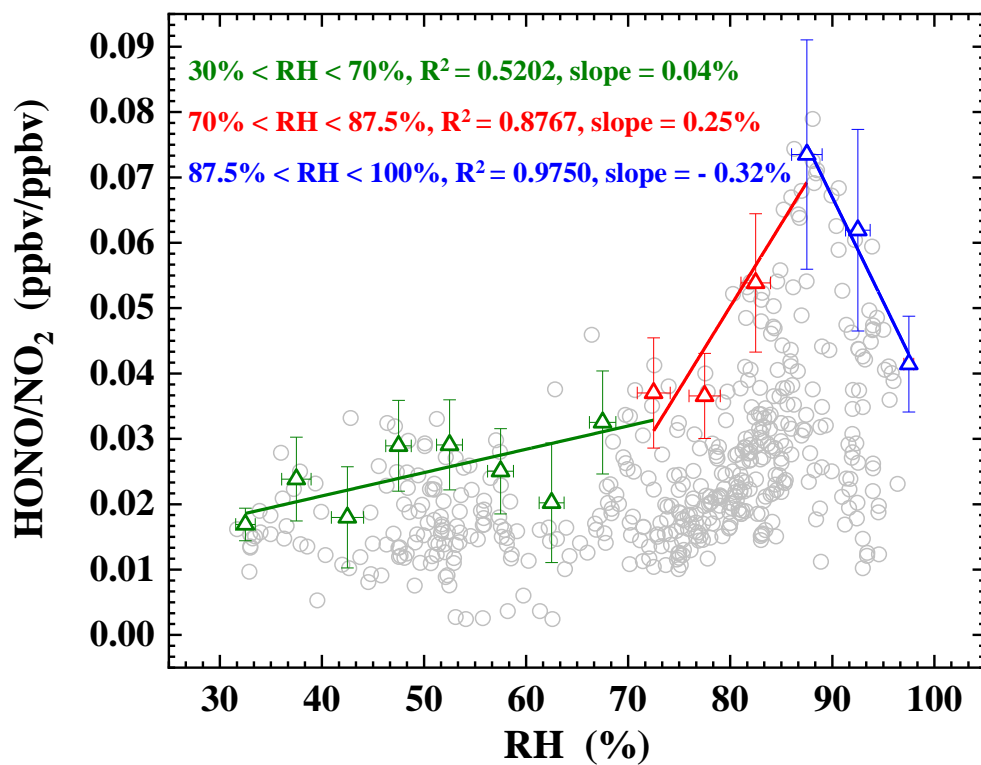
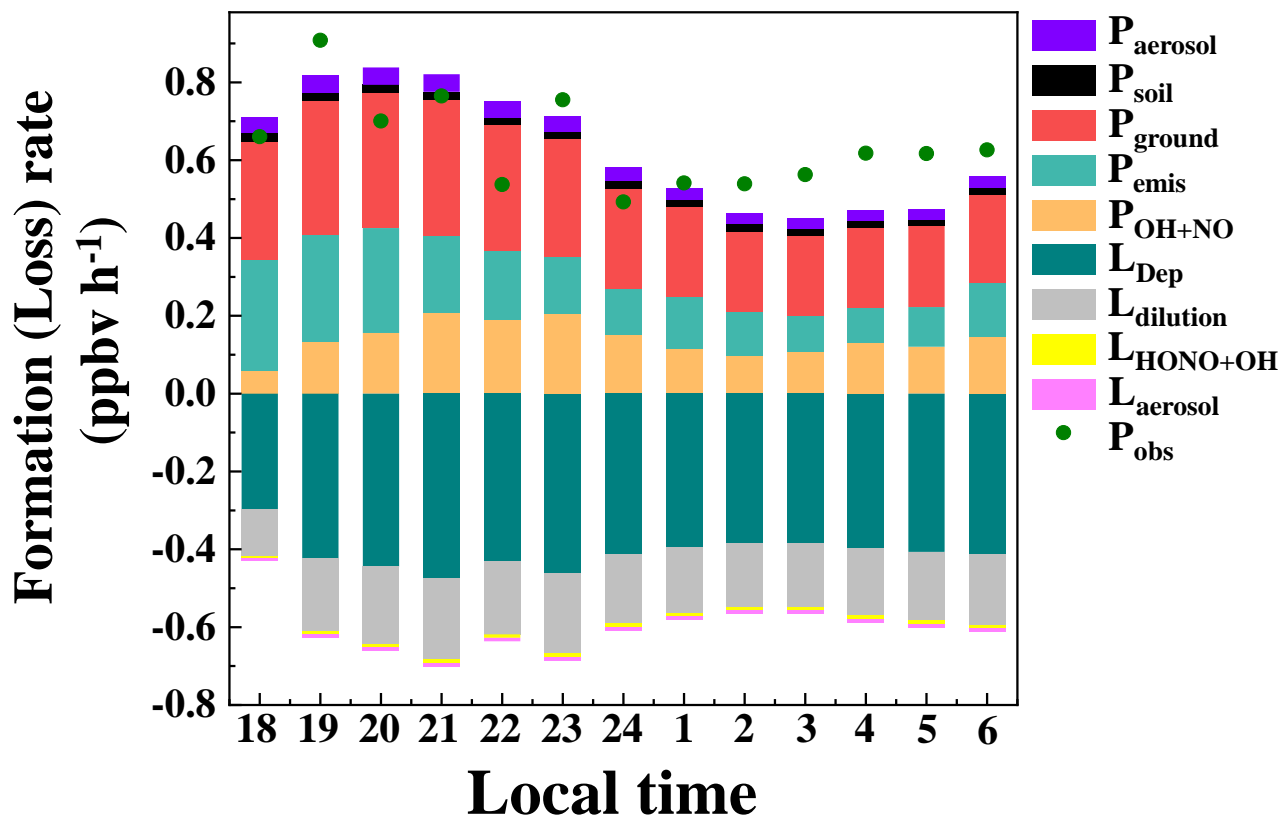


Figure S5. Scatter plot of HONO/NO₂ ratio against RH during nighttime from 18:00 to 6:00. Triangles are the average of top-5 HONO/NO₂ values in each 5% RH interval.



90

Figure S6. Nighttime HONO budget in Guangzhou during the observation period.

95 **Table S1. The parameters of ~~our~~the custom-built LOPAP.**

Parameters	Values
Air flow	1 L min ⁻¹
Liquid flow	0.4 mL min ⁻¹
Length of LWCC	100 cm
Detection limit	5 pptv
Detection range	5 pptv–10 ppbv
Time resolution	15 min
Uncertainty	8%

Table S2. The VOCs species constrained in the F0AM model.

Classification	Measured hydrocarbons
Alkane	CYCLOHEXANE, ETHANE, N-BUTANE, N-DECANE, N-NONANE, N-OCTANE, PROPANE, 2-METHYLHEXANE, 2-METHYLPENTANE, 3-METHYLHEXANE, 3-METHYLPENTANE, 2-METHYLPROPANE, 2-METHYLBUTANE, PENTANE, HEXANE, HEPTANE, HENDECANE
Alkene	PROPENE, TRANS-2-BUTENE, TRANS-2-PENTENE, 1-BUTENE, 1-PENTENE, 1-HEXENE, CIS-2-BUTENE, CIS-2-PENTENE, STYRENE
ISO	ISOPRENE
Alkyne	ETHYNE
Aromatic	BENZENE, N-PROPYLBENZENE, 1-2-3-TRIMETHYLBENZENE, 1-2-4-TRIMETHYLBENZENE, 1-3-5-TRIMETHYLBENZENE, METHYLBENZENE, ETHYLBENZENE, 1,4-DIMETHYLBENZENE, 1,2-DIMETHYLBENZENE, 1-PROPYLBENZENE, 1-ETHYL-3-METHYLBENZENE, 1-ETHYL-4-METHYLBENZENE, 1-ETHYL-2-METHYLBENZENE

Table S23. Emission factors ($\Delta\text{HONO}/\Delta\text{NO}_x$) and other information in 11 fresh plumes.

Starting time	Duration (min)	$R^2(\text{NO}-\text{NO}_x)$	$R^2(\text{HONO}-\text{NO}_x)$	$\Delta\text{NO}/\Delta\text{NO}_x$	HONO/NO_x	$\Delta\text{HONO}/\Delta\text{NO}_x$
2018/10/6 23:29	62	0.9616	0.7233	0.90	0.002	0.001
2018/10/7 4:29	22	0.9836	0.7821	0.97	0.002	0.003
2018/10/7 20:44	34	0.9559	0.7054	0.88	0.011	0.010
2018/10/7 22:49	22	0.9904	0.8051	1.05	0.013	0.008
2018/10/20 0:33	24	0.9621	0.7826	0.96	0.020	0.007
2018/10/21 6:28	40	0.9959	0.9403	0.89	0.021	0.014
2018/10/25 6:55	20	0.9615	0.7291	1.04	0.024	0.014
2018/11/4 19:04	22	0.9761	0.8148	1.05	0.022	0.011
2018/11/4 22:01	78	0.9892	0.7684	1.02	0.016	0.007
2018/11/6 7:31	29	0.9835	0.7902	1.03	0.029	0.009
2018/11/7 4:56	30	0.9750	0.7007	0.93	0.027	0.015

100 **Table S34. The overview of percentage of nighttime primary emissions of HONO from urban sites in China.**

Location	Date	Nighttime NOx (ppbv)	[HONO] _{emis} /[HONO] (%)	Emission ratio HONO/NO _x (%)	Reference
Guangzhou	Oct 2015	57.9	15.1	0.65	1
Guangzhou	Sep–Nov 2018	47.7	47	0.9	2
Shanghai	May 2016	–	12.5	0.65	3
Changzhou	Apr 2017	–	31.4	0.69	4
		41	17 ^a		
Zhengzhou	Jan 2019	68.7	16 ^b	0.65	5
		107.3	16 ^c		
Ji'nan	Nov 2013–Jan 2014	–	42	0.58	6
	Sep–Nov 2015	38	18		
Ji'nan	Dec 2015–Feb 2016	78.5	21	0.53	7
	Mar–May 2016	47.3	12		
	Jun–Aug 2016	29.1	15		
Beijing	Jan–Feb 2007	–	20.59		
	Aug 2007	–	11.68	0.65	8
Beijing	Oct–Nov 2014	94.5	39.6	0.65	9
Beijing	Dec 2015	–	48.8	0.8	10
		–	52 ^b		
Beijing	Dec 2015	–	40 ^c	1.3	11
Beijing	Dec 2016	–	29.3	0.78	12
Beijing	Aug–Sep 2018	–	17.6	0.8	13
Beijing	May–Jul 2018	–	14.21		
	Nov 2018–Jan 2019	–	30.79	0.78	13 14

^a: clean; ^b: polluted; ^c: severely polluted. Reference: 1: Tian et al. (2018); 2: This work; 3: Cui et al. (2018); 4: Shi et al. (2020); 5: Hao et al. (2020); 6: Wang et al. (2015); 7: Li et al. (2018); 8: Spataro et al. (2013); 9: Tong et al. (2015); 10: Tong et al. (2016); 11: Zhang et al. (2019); 12: Meng et al. (2020); 13: [Jia et al. \(2020\)](#); 14: Liu et al. (2021).

105 Table S45. The OH concentration is assumed of ~~1.0~~ 0.5×10^6 molecules cm^{-3} . The integrated ~~P_{net}~~ $P_{\text{net}}^{\text{net}}$ of homogeneous reaction of $\text{NO} + \text{OH}$ from 18:00 to 6:00.

OH/molecules cm^{-3}	Integrated $P_{\text{net}}^{\text{net}}$ /ppbv	Measured HONO/ppbv
1×10^5	0.32	0.26
5×10^5	1.62	
1×10^6	3.24	
2×10^6	6.48	

110 ~~Table S6. Ozonolysis reaction rate constants and OH formation yields of the volatile organic compounds (VOC) used in the calculation.~~

VOC	$k(298\text{ K})/(\times 10^{-18}\text{-cm}^3\text{ molec.}^{-1}\text{-s}^{-1})^{\text{a}}$	OH yield
PROPENE	10.1	0.34 ^b
TRANS 2 BUTENE	190	0.59 ^b
TRANS 2 PENTENE	160	0.47 ^e
1 BUTENE	9.64	0.41 ^b
1 HEXENE	11.3	0.32 ^b
1 PENTENE	10.6	0.37 ^b
CIS 2 BUTENE	125	0.37 ^b
CIS 2 PENTENE	130	0.3 ^e
STYRENE	17	0.07 ^e
ISOPRENE	12.8 ^e	0.13 ± 0.03 ^e

^aAtkinson and Arey (2003); ^bRickard et al. (1999); ^eAlicke et al. (2002)

Table S5. Parameterisations of HONO production and loss mechanisms.

Mechanism	Parameterisation			Reference	
	HONO formation/loss reactions	Median	Lower		Upper
Primary emission		$P_{\text{emis}} = 0.16 \text{ ppbv h}^{-1}$	Emission source inventory 1	Emission source inventory 2	1
NO + OH	$\text{NO} + \text{OH} \rightarrow \text{HONO}$	$\text{OH} = 0.5 \times 10^6 \text{ cm}^{-3}$	$1.0 \times 10^5 \text{ cm}^{-3}$	$1.0 \times 10^6 \text{ cm}^{-3}$	2
NO ₂ on aerosol	$\text{NO}_2 + \text{aerosol} \rightarrow \text{HONO}$	$\gamma_{\text{NO}_2 \rightarrow \text{ground}} = 4 \times 10^{-6}$	2×10^{-7}	1×10^{-5}	3, 4, 5
NO ₂ on ground	$\text{NO}_2 + \text{ground} \rightarrow \text{HONO}$	$\gamma_{\text{NO}_2 \rightarrow \text{aerosol}} = 4 \times 10^{-6}$	2×10^{-7}	1×10^{-5}	3, 4, 5
Soil emission		water content: 35%–45%	45%–55%	25%–35%	6, 7, 8
Deposition		$V_d = 2.5 \text{ cm s}^{-1}$	0.077 cm s^{-1}	3 cm s^{-1}	9, 10, 11, 12
Vertical transport		$k_{(\text{dilution})} = 0.23 \text{ h}^{-1}$	0.1 h^{-1}	0.44 h^{-1}	13, 14, 15
HONO on aerosol		$\gamma_{\text{HONO} \rightarrow \text{aerosol}} = 4 \times 10^{-5}$	3×10^{-7}	5×10^{-4}	16, 17, 18
HONO + OH	$\text{HONO} + \text{OH} \rightarrow \text{NO}_2 + \text{H}_2\text{O}$	$\text{OH} = 0.5 \times 10^6 \text{ cm}^{-3}$	$1.0 \times 10^5 \text{ cm}^{-3}$	$1.0 \times 10^6 \text{ cm}^{-3}$	2

Emission source inventory 1 denotes the 2017 NO_x emission source inventory of Guangzhou city; Emission source inventory 2 denotes the 2017 NO_x emission source inventory of the 3 km × 3 km grid cell centred on the Guangzhou Institute of Geochemistry. Reference: 1: Huang et al. (2021); 2: Tan et al. (2019); 3: Li et al. (2018); 4: Liu et al. (2019); 5: Zhang et al. (2021); 6: Oswald et al. (2013); 7: Liu et al. (2020a); 8: Liu et al. (2020b); 9: Stutz et al. (2002); 10: Harrison and Kitto (1994); 11: Harrison et al. (1996); 12: Spindler et al. (1999); 13: Dillon et al. (2002); 14: Lin et al. (1996); 15: Kalthoff et al. (2000); 16: El Zein et al. (2013); 17: El Zein and Bedjanian (2012); 18: Romanias et al. (2012).

References

- Alicke, B., Platt, U., and Stutz, J.: Impact of nitrous acid photolysis on the total hydroxyl radical budget during the Limitation of Oxidant Production/Pianura Padana Produzione di Ozono study in Milan, *Journal of Geophysical Research: Atmospheres*, 107, 8196, <https://doi.org/10.1029/2000JD000075>, 2002.
- 5 Atkinson, R., and Arey, J.: Atmospheric Degradation of Volatile Organic Compounds, *Chemical Reviews*, 103, 4605-4638, <https://doi.org/10.1021/cr0206420>, 2003.
- Cui, L., Li, R., Zhang, Y., Meng, Y., Fu, H., and Chen, J.: An observational study of nitrous acid (HONO) in Shanghai, China: The aerosol impact on HONO formation during the haze episodes, *Science of The Total Environment*, 630, 1057-1070, <https://doi.org/10.1016/j.scitotenv.2018.02.063>, 2018.
- 10 Dillon, M. B., Lamanna, M. S., Schade, G. W., Goldstein, A. H., and Cohen, R. C.: Chemical evolution of the Sacramento urban plume: Transport and oxidation, *Journal of Geophysical Research: Atmospheres*, 107, ACH 3-1-ACH 3-15, <https://doi.org/10.1029/2001JD000969>, 2002.
- El Zein, A., and Bedjanian, Y.: Reactive Uptake of HONO to TiO₂ Surface: “Dark” Reaction, *The Journal of Physical Chemistry A*, 116, 3665-3672, <https://doi.org/10.1021/jp300859w>, 2012.
- 15 El Zein, A., Romanias, M. N., and Bedjanian, Y.: Kinetics and Products of Heterogeneous Reaction of HONO with Fe₂O₃ and Arizona Test Dust, *Environmental Science & Technology*, 47, 6325-6331, <https://doi.org/10.1021/es400794c>, 2013.
- Hao, Q., Jiang, N., Zhang, R., Yang, L., and Li, S.: Characteristics, sources, and reactions of nitrous acid during winter at an urban site in the Central Plains Economic Region in China, *Atmos. Chem. Phys.*, 20, 7087-7102, <https://doi.org/10.5194/acp-20-7087-2020>, 2020.
- 20 Harrison, R. M., and Kitto, A.-M. N.: Evidence for a surface source of atmospheric nitrous acid, *Atmospheric Environment*, 28, 1089-1094, [https://doi.org/10.1016/1352-2310\(94\)90286-0](https://doi.org/10.1016/1352-2310(94)90286-0), 1994.
- Harrison, R. M., Peak, J. D., and Collins, G. M.: Tropospheric cycle of nitrous acid, *Journal of Geophysical Research: Atmospheres*, 101, 14429-14439, <https://doi.org/10.1029/96JD00341>, 1996.
- Heland, J., Kleffmann, J., Kurtenbach, R., and Wiesen, P.: A New Instrument To Measure Gaseous Nitrous Acid (HONO) in the Atmosphere, *Environmental Science & Technology*, 35, 3207-3212, <https://doi.org/10.1021/es000303t>, 2001.
- 25 Huang, Z., Zhong, Z., Sha, Q., Xu, Y., Zhang, Z., Wu, L., Wang, Y., Zhang, L., Cui, X., Tang, M., Shi, B., Zheng, C., Li, Z., Hu, M., Bi, L., Zheng, J., and Yan, M.: An updated model-ready emission inventory for Guangdong Province by incorporating big data and mapping onto multiple chemical mechanisms, *Science of The Total Environment*, 769, 144535, <https://doi.org/10.1016/j.scitotenv.2020.144535>, 2021.
- 30 Jia, C., Tong, S., Zhang, W., Zhang, X., Li, W., Wang, Z., Wang, L., Liu, Z., Hu, B., Zhao, P., and Ge, M.: Pollution characteristics and potential sources of nitrous acid (HONO) in early autumn 2018 of Beijing, *Science of The Total Environment*, 735, 139317, <https://doi.org/10.1016/j.scitotenv.2020.139317>, 2020.
- Kalthoff, N., Horlacher, V., Corsmeier, U., Volz-Thomas, A., Kolahgar, B., Geiß, H., Möllmann-Coers, M., and Knaps, A.: Influence of valley winds on transport and dispersion of airborne pollutants in the Freiburg-Schauinsland area, *Journal of Geophysical Research: Atmospheres*, 105, 1585-1597, <https://doi.org/10.1029/1999JD900999>, 2000.
- 35 Li, D., Xue, L., Wen, L., Wang, X., Chen, T., Mellouki, A., Chen, J., and Wang, W.: Characteristics and sources of nitrous acid in an urban atmosphere of northern China: Results from 1-yr continuous observations, *Atmospheric Environment*, 182, 296-306, <https://doi.org/10.1016/j.atmosenv.2018.03.033>, 2018.
- Lin, X., Roussel, P. B., Laszlo, S., Taylor, R., Meld, O. T., Shepson, P. B., Hastie, D. R., and Niki, H.: Impact of Toronto urban emissions on ozone levels downwind, *Atmospheric Environment*, 30, 2177-2193, [https://doi.org/10.1016/1352-2310\(95\)00130-1](https://doi.org/10.1016/1352-2310(95)00130-1), 1996.
- 40 Liu, J., Liu, Z., Ma, Z., Yang, S., Yao, D., Zhao, S., Hu, B., Tang, G., Sun, J., Cheng, M., Xu, Z., and Wang, Y.: Detailed budget analysis of HONO in Beijing, China: Implication on atmosphere oxidation capacity in polluted megacity, *Atmospheric Environment*, 244, 117957, <https://doi.org/10.1016/j.atmosenv.2020.117957>, 2021.
- 45 Liu, Y., Lu, K., Li, X., Dong, H., Tan, Z., Wang, H., Zou, Q., Wu, Y., Zeng, L., Hu, M., Min, K. E., Kecorius, S., Wiedensohler, A., and Zhang, Y.: A Comprehensive Model Test of the HONO Sources Constrained to Field Measurements at Rural North China Plain, *Environ Sci Technol*, <https://doi.org/10.1021/acs.est.8b06367>, 2019.

- 50 Liu, Y., Ni, S., Jiang, T., Xing, S., Zhang, Y., Bao, X., Feng, Z., Fan, X., Zhang, L., and Feng, H.: Influence of Chinese New Year overlapping COVID-19 lockdown on HONO sources in Shijiazhuang, *Science of The Total Environment*, 745, 141025, <https://doi.org/10.1016/j.scitotenv.2020.141025>, 2020a.
- Liu, Y., Zhang, Y., Lian, C., Yan, C., Feng, Z., Zheng, F., Fan, X., Chen, Y., Wang, W., Chu, B., Wang, Y., Cai, J., Du, W., Daellenbach, K. R., Kangasluoma, J., Bianchi, F., Kujansuu, J., Petäjä, T., Wang, X., Hu, B., Wang, Y., Ge, M., He, H., and Kulmala, M.: The promotion effect of nitrous acid on aerosol formation in wintertime in Beijing: the possible contribution of traffic-related emissions, *Atmos. Chem. Phys.*, 20, 13023-13040, <https://doi.org/10.5194/acp-20-13023-2020>, 2020b.
- 55 Meng, F., Qin, M., Tang, K., Duan, J., Fang, W., Liang, S., Ye, K., Xie, P., Sun, Y., Xie, C., Ye, C., Fu, P., Liu, J., and Liu, W.: High-resolution vertical distribution and sources of HONO and NO₂ in the nocturnal boundary layer in urban Beijing, China, *Atmos. Chem. Phys.*, 20, 5071-5092, <https://doi.org/10.5194/acp-20-5071-2020>, 2020.
- Oswald, R., Behrendt, T., Ermel, M., Wu, D., Su, H., Cheng, Y., Breuninger, C., Moravek, A., Mougín, E., Delon, C., Loubet, B., Pommerening-Röser, A., Sörgel, M., Pöschl, U., Hoffmann, T., Andreae, M. O., Meixner, F. X., and Trebs, I.: HONO Emissions from Soil Bacteria as a Major Source of Atmospheric Reactive Nitrogen, *Science*, 341, 1233-1235, <https://doi.org/10.1126/science.1242266>, 2013.
- 60 Rickard, A. R., Johnson, D., McGill, C. D., and Marston, G.: OH Yields in the Gas-Phase Reactions of Ozone with Alkenes, *The Journal of Physical Chemistry A*, 103, 7656-7664, <https://doi.org/10.1021/jp9916992>, 1999.
- Romanias, M. N., El Zein, A., and Bedjanian, Y.: Reactive uptake of HONO on aluminium oxide surface, *Journal of Photochemistry and Photobiology A: Chemistry*, 250, 50-57, <https://doi.org/10.1016/j.jphotochem.2012.09.018>, 2012.
- 65 Shi, X., Ge, Y., Zheng, J., Ma, Y., Ren, X., and Zhang, Y.: Budget of nitrous acid and its impacts on atmospheric oxidative capacity at an urban site in the central Yangtze River Delta region of China, *Atmospheric Environment*, 238, 117725, <https://doi.org/10.1016/j.atmosenv.2020.117725>, 2020.
- Spataro, F., Ianniello, A., Esposito, G., Allegrini, I., Zhu, T., and Hu, M.: Occurrence of atmospheric nitrous acid in the urban area of Beijing (China), *Science of The Total Environment*, 447, 210-224, <https://doi.org/10.1016/j.scitotenv.2012.12.065>, 2013.
- Spindler, G., Brüggemann, E., and Herrmann, H.: Nitrous acid (HNO₂) concentration measurements and estimation of dry deposition over grassland in eastern Germany, *Proceedings of the EUROTRAC Symposium 1998*, Vol. 2, WITpress, Southampton, UK, 218-222, 1999.
- 75 Stutz, J., Alicke, B., and Neftel, A.: Nitrous acid formation in the urban atmosphere: Gradient measurements of NO₂ and HONO over grass in Milan, Italy, *Journal of Geophysical Research: Atmospheres*, 107, 8192, <https://doi.org/10.1029/2001JD000390>, 2002.
- Tan, Z., Lu, K., Hofzumahaus, A., Fuchs, H., Bohn, B., Holland, F., Liu, Y., Rohrer, F., Shao, M., Sun, K., Wu, Y., Zeng, L., Zhang, Y., Zou, Q., Kiendler-Scharr, A., Wahner, A., and Zhang, Y.: Experimental budgets of OH, HO₂, and RO₂ radicals and implications for ozone formation in the Pearl River Delta in China 2014, *Atmos. Chem. Phys.*, 19, 7129-7150, <https://doi.org/10.5194/acp-19-7129-2019>, 2019.
- 80 Tian, Z., Yang, W., Yu, X., Zhang, M., Zhang, H., Cheng, D., Cheng, P., and Wang, B.: HONO pollution characteristics and nighttime sources during autumn in Guangzhou, China *Environmental Science*, 39 (05), 2000-2009, DOI: 10.13227/j. hjkx. 201709269, 2018.
- 85 Tong, S., Hou, S., Zhang, Y., Chu, B., Liu, Y., He, H., Zhao, P., and Ge, M.: Comparisons of measured nitrous acid (HONO) concentrations in a pollution period at urban and suburban Beijing, in autumn of 2014, *Science China Chemistry*, 58, 1393-1402, <https://doi.org/10.1007/s11426-015-5454-2>, 2015.
- Tong, S., Hou, S., Zhang, Y., Chu, B., Liu, Y., He, H., Zhao, P., and Ge, M.: Exploring the nitrous acid (HONO) formation mechanism in winter Beijing: direct emissions and heterogeneous production in urban and suburban areas, *Faraday Discuss*, 189, 213-230, <https://doi.org/10.1039/C5FD00163C>, 2016.
- 90 Trebs, I., Meixner, F. X., Slanina, J., Otjes, R., Jongejan, P., and Andreae, M. O.: Real-time measurements of ammonia, acidic trace gases and water-soluble inorganic aerosol species at a rural site in the Amazon Basin, *Atmos. Chem. Phys.*, 4, 967-987, <https://doi.org/10.5194/acp-4-967-2004>, 2004.
- 95 Wang, L., Wen, L., Xu, C., Chen, J., Wang, X., Yang, L., Wang, W., Yang, X., Sui, X., Yao, L., and Zhang, Q.: HONO and its potential source particulate nitrite at an urban site in North China during the cold season, *Science of The Total Environment*, 538, 93-101, <https://doi.org/10.1016/j.scitotenv.2015.08.032>, 2015.

- 100 Zhang, S., Sarwar, G., Xing, J., Chu, B., Xue, C., Sarav, A., Ding, D., Zheng, H., Mu, Y., Duan, F., Ma, T., and He, H.: Improving the representation of HONO chemistry in CMAQ and examining its impact on haze over China, *Atmos. Chem. Phys.*, 21, 15809-15826, <https://doi.org/10.5194/acp-21-15809-2021>, 2021.
- Zhang, W., Tong, S., Ge, M., An, J., Shi, Z., Hou, S., Xia, K., Qu, Y., Zhang, H., Chu, B., Sun, Y., and He, H.: Variations and sources of nitrous acid (HONO) during a severe pollution episode in Beijing in winter 2016, *Science of The Total Environment*, 648, 253-262, <https://doi.org/10.1016/j.scitotenv.2018.08.133>, 2019.